INVESTIGATION ON FRACTURE BEHAVIOUR OF FIBROUS SELF COMPACTING CONCRETE

Submitted in partial fulfilment of the requirement for the award of the degree of

Doctor of Philosophy

by

B. RAJA RAJESHWARI

Roll No. 715007

Supervisor

Dr. M.V.N. SIVAKUMAR

DEPARTMENT OF CIVIL ENGINEERING

NATIONAL INSTITUTE OF TECHNOLOGY

WARANGAL

DECEMBER - 2021

NATIONAL INSTITUE OF TECHNOLOGY

WARANGAL

CERTIFICATE

This is to certify that the thesis entitled "**Investigation on Fracture Behaviour of Fibrous Self Compacting Concrete**" being submitted by Ms. B. Raja Rajeshwari for the award of the degree of doctor of philosophy to the faculty of Engineering and Technology of National Institute of Technology, Warangal is a record of bonafide research work carried out by her under my supervision and it has not been submitted elsewhere for award of my degree.

Dr. M.V.N. Sivakumar

Thesis supervisor
Assistant Professor
Department of Civil Engineering
NIT Warangal

NATIONAL INSTITUE OF TECHNOLOGY

WARANGAL

DECLARATION

This is to certify that the work presented in the thesis entitled **"Investigation on Fracture Behaviour of Fibrous Self Compacting Concrete"** is a bonafide work done by me under the supervision of Dr. M.V.N. Sivakumar and was not submitted elsewhere for the award of any degree.

I declare that this written submission represented my ideas in my own words and where others ideas or words have been included, I have adequately cited and referenced the original sources. I also declare that I have adhered to all principles of academic honesty and integrity and have not misrepresented or fabricated or falsified any idea / data / fact / source in my submission. I understand that any violation of the above will be a cause for disciplinary action by the Institute and can also evoke penal action from the sources which have thus not been properly cited or from whom proper permission has not been taken when needed.

_____
(Signature)

_____
(Name of the student)

_____
(Roll No.)

Date: _____

Dedicated to

My

Beloved Parents

&

Gurus

ACKNOWLEDGEMENTS

From the bottom my heart I express my sincere gratitude to my research supervisor, **Dr. M.V.N. Sivakumar**, Assistant Professor, Department of Civil Engineering, National Institute of Technology, Warangal, for his valuable guidance and continuous support during the period of my research work. He delivered a constant motivation, positive thoughts and creative ideas in different stages of this research work. His patience, enthusiasm, suggestions made me to produce my research work in the present form. I thankfully acknowledge him for giving me an opportunity to work under his guidance.

I am deeply grateful to Prof. C.B. Kameshwar Rao, Chairman, Doctoral Scrutiny Committee, Civil Engineering Department for immense support in bringing out this research work.

I would like to extend my sincere gratitude to Doctoral Scrutiny Committee members, Prof. D. Ramaseshu, Professor in Civil Engineering Department, Prof. P. Rathish Kumar, Professor and Head in Civil Engineering Department, Dr. G. Raghavendra, Assistant Professor in Mechanical Engineering Department, for their insightful comments and suggestions throughout my research work.

I am thankful to Prof. G. Rajesh Kumar, Prof. T.D. Gunneswara Rao, Dr. S. Venkateswara Rao, Dr. T.P. Tezeswi, Dr. D. Ravi Prasad, Dr. K. Gopi Krishna, Dr. S. Anitha Priyadharshani, Dr. B. Kavitha, Dr. B. Umesh, the faculty members of Structure Division, NITW for giving me constant encouragement during my research work.

I would like to thank my senior research scholars Dr. M. Sri Rama Chand, Dr. Y. Shudheer Kumar, Dr. P. Harsha Praneeth, Dr. Ch. Rama Vara Prasad, Dr. P. Swamy Naga Ratna Giri, Dr. G. Mallikarjuna Rao, for their motivation and scholarly advices during my research work.

I’m blessed to have Mrs. G. Pallavi as my friend for her constant support and motivation when things would get a bit discouraging. Thank you for being with me in all stages.

I express my gratitude to my friends Mr. Oggu Praveen, Mr. Emmadi Srikanth, Mr. T. Suman, Mrs. J. Vani, Mr. V. Guru Pratap Reddy, Mr. K. Shriram Tej, Dr. B. Murali Krishna, Mrs. D. Madhu Malini, Mrs. R. Chandana, Mrs. K. Vineela, Mrs. K. Preethi, Mrs. G. Siva Sree who always encouraged and supported me during my tough times. I am thankful to my fellow scholars Mr. P. Ravi Teja, Mr. B. Sagar, Mr. Y. Subba Rao, Ms. Saraswathi, Mr. M. Teja for their help during my research work. I would like to thank all my co-research scholars who helped me directly and indirectly for my research work.

I would like to thank laboratory technician Mr. M. Naresh for helping out in doing the laboratory work. I would like to thank Sri A. Chandranarayana, Sri A. Laxmana, Late. Sri P. Palaiah, the technicians from concrete and material testing laboratory for smooth functioning of the experiments. I am thankful to Sri Md. Hussain and administrative staff for the help done during the research period.

I would like to thank RADAR diagnosis centre, Hanamkonda, Warangal, India for allowing me to perform scanning of the specimens despite of their busy schedule.

I am grateful to have Mr. Md. Ziauddin, founder of Suswara Music Academy, Hanamkonda as my guru in transforming me to better person and guiding me in all aspects.

Last but not the least I take immense pleasure to be thankful to my parents Dr. B. Keshavulu and Dr. G. Thirupathamma (B. Padmavathi) because of whom for what I'm today. I thank my brother Mr. B. Rajendra Kumar for being protective and encouraging all the time.

Finally, I acknowledge help given by all the persons either directly or indirectly in support of my research work.

-Ms. B. Raja Rajeshwari

ABSTRACT

Concrete, by the virtue of its inherent properties, turned out to be inevitable material in the field of construction and resulted being the second largest consuming material in the world. Over a past few decades, many researchers were in the process of enhancing the concrete properties. One such research outcome was self compacting concrete (SCC), a special concrete which resolves the in-situ issues related with compaction of the concrete. SCC was designed based on the higher finer particles making a highly workable concrete with intrinsic properties like flowability, passing ability, filling ability and resistance to segregation. The higher fines and lower coarse reduces the voids and increases the quality of interfacial transition zone (ITZ) resulting in a densified concrete. Therefore, the change in coarse aggregate properties, mix proportions and improved quality of ITZ influence the fracture behaviour and hence, there is a need to study the failure criteria of the self compacting concrete. The fracture properties are effected by the material properties, geometry of the specimen, size of the specimen and type of the testing method. Coming to material influence on fracture properties, aggregates play a vital role for changes in the fracture behaviour of concrete as they constitute about 60-75 % of the total volume of the concrete. The present study deals with the effect of size and quantity of coarse aggregate on the fracture behaviour of non-fibrous and fibrous self-compacting concrete.

Usually, fracture properties for Mode I (opening type i.e., the plane splits apart) type of failure are evaluated by Three Point Bend Test, Compact Tension Test, Wedge Split Test and Uniaxial Tensile Test. Among all these tests, three point bend test is the most widely used method for determining fracture properties on notched beams (RILEM FMC 50, 1985). On the other side, Wedge splitting test is a most stable test to determine the fracture properties of the material that involves standard cubes used for laboratory purpose or core samples obtained from existing structures. Wedge splitting test method has been extensively used for fracture and fatigue studies of conventional and fiber reinforced concretes. Present research work constituted the experimentation on fracture behaviour of non-fibrous and fibrous self compacting concrete based on three point bend test and wedge splitting test methods considering the parameters as three varying coarse aggregate sizes (20mm, 16mm and 12.5mm) and coarse to fine aggregate quantities (50-50, 45-55 and 40-60). Based on the size effect method analysis for three point bend test for both non fibrous and fibrous self compacting concrete, it reveals that the smaller coarse aggregate size with higher coarse to fine aggregate quantities, showed better fracture

properties as it was considering only peak load for evaluating fracture properties. And coming to wedge splitting test, the fracture properties were prominent in higher coarse aggregate size and higher coarse to fine aggregate quantities. In case of fibrous self compacting concrete, due to the presence of fiber energy dissipation was higher compared to non fibrous self compacting concrete.

The crack proliferation path is greatly influenced by the bridging material which results in effecting fracture behaviour. Digital image processing technique, an image based study to access the behaviour of the concrete can be used. There are many image based methods such as digital image correlation, scanning electron microscopy, optical microscopy, to access the behaviour of concrete. Often these methods are limited to surface studies i.e., 2D, smaller specimen or sample size and repeatability. All these limitations can be overcome by an advanced image technique naming Computed Tomography. Computed tomography helps in analysing the internal behaviour of the concrete. For the present study internal failure behaviour was studied by scanning the wedge splitting test specimen. Through the high resolution computed tomography study, it is evident from images that the aggregate properties play a major role in evaluating the fracture energy. Through the high resolution computed tomography study, it is evident that the energy dissipation in the hardened concrete was transgranular failure for smaller size coarse aggregate and intergranular failure for larger sized coarse aggregate in case of both non fibrous and fibrous self compacting concrete.

Fracture properties are evaluated experimentally considering the size effect of specimen and notch length. With the variation of parameters the experimental specimens required for testing are more in number. To reduce this casting procedure for various parameters influencing the concrete behaviour, numerical modelling was considered. Numerical modelling reduces the number of physical prototypes and experiments and optimize components in their design phase to develop better products faster. Numerical modelling helps in validating the experimental results and also to develop a constitute behaviour of the concrete. Many researchers develop numerical modelling using FEM based software's to predict the concrete behaviour. Numerical modelling on wedge splitting test specimen using ABAQUS software and considering the specimen depth and notch length variation was studied. From the fracture curve, it was evident that for all the specimen and notch depth combinations the failure was quasi brittle in nature following non-linear elastic fracture mechanics.

CONTENTS

LIST OF TABLES

LIST OF FIGURES

ABBREVIATIONS

SCC	: Self Compacting Concrete
ITZ	: Interfacial Transition Zone
FPZ	: Fracture Process Zone
CT	: Computed Tomography
FEM	: Finite Element Method
CA	: Coarse Aggregate
FA	: Fine Aggregate
TPBT	: Three Point Bend Test
WST	: Wedge Splitting Test
CMOD	: Crack Mouth Opening Displacement
DIC	: Digital Image Correlation
DICOM	: Digital Imaging and Communication in Medicine
ROI	: Region of Interest
LEFM	: Linear Elastic Fracture Mechanics
NLEM	: Nonlinear Elastics Fracture Mechanics
OPC	: Ordinary Portland Cement

NOTATIONS

F_{st}	: Split tensile strength test
G_F	: Fracture Energy
C_f	: Effective length of process zone
l_{ch}	: Characteristic length
σ_n	: Nominal Stress at failure
F_t'	: Tensile strength
β	: Brittleness number
δc	: Effective crack tip opening displacement
d or W	: Depth of the specimen
a	: Crack length
B	: Thickness of the specimen
α	: Wedge angle in wedge splitting test
μ	: Coefficient of friction for the roller bearing
F_v	: Vertical Force
F_{sp}	: Splitting Force
K_{IC}	: Critical stress intensity factor
G_{FCMOD}	: Fracture Energy for Wedge splitting test
W_{FCMOD}	: Area under the curve for Wedge splitting test
A_{lig}	: Area of the ligament
f_c'	: Compressive strength
E	: Young's Modulus
a_e	: Equivalent crack
a_0	: Crack length in BEM
a_∞*	: Characteristics Crack

CHAPTER 1

INTRODUCTION

CHAPTER 1
INTRODUCTION

1.0. General

Concrete, the second largest consuming material in the world next to water. The usage of concrete was about 3ton per person per year in the world. This is due to the rapid increase in urbanisation and infrastructure development. Constructing massive structures like dams, bridges, tall structures etc., requires superior quality concrete in order to achieve desired strength and durability. These constructions often requires less manual errors and easy with the construction. The most common in-situ problem with concrete is compaction and the most effected members would be deep sections and slender members. There comes a novel concrete resolving these problems i.e., self compacting concrete. The fresh and hardened properties of self compacting concrete differ from the conventional concrete. Self compacting concrete is a highly workable and densely packed concrete. Due to this difference the failure characteristics play an important role in predicting the behaviour of concrete.

1.1. Self Compacting Concrete

SCC was first developed by Okamura in 1986, further investigations and developments were carried out by several researchers, incorporating mineral admixtures, recycled aggregates and fibers for superior performance in several applications. As SCC was designed to compact on its own weight, finer particles concentrations are on the higher side in SCC mix, which results in high workability in fresh concrete and rich ITZ interface in harder concrete, than conventional concrete. SCC is suitable for casting in congested areas, because it is designed to have high flow, passing and filling ability, without the need for external compaction. Similar to conventional concrete, SCC is also a heterogeneous and quasi brittle material with multiple phase characterisation (Okamura and Ouchi, 2003). The failure mechanism taking place in concrete in general, is often influenced by the material properties and their proportions adopted during the mix design. In order to reduce the brittle nature of SCC, the ductility property needs to be enhanced, which is achieved by adding varying concentration of fiber in the SCC mix. Improving the mechanical properties of SCC, in turn enhances serviceability aspects also. With the inclusion of minimum concentration of fiber content, arresting the micro and macro cracks present in SCC specimens at various length scales can be achieved.

1.2. Need For Fracture Studies For SCC

The mix proportions of SCC are different from the conventional concrete i.e., higher finer particles content in the ingredients used. This variation influences the hardened properties more precisely the microstructure of the concrete varies. The interfacial transition zone is much stronger than conventional concrete. Consequently there is an increase in compressive and tensile strength in the concrete. With the increase in finer particles there is a decrease in coarse aggregate content resulting in a decrease in stiffness. This variation makes the change in the failure behaviour of the hardened SCC. Fracture behaviour of the SCC depends on the strength of the matrix and size and location of the coarse aggregate. Aggregates play a major role in crack bridging and branching (Amparano, Xi and Roh, 2000). With these variations, starting from the design considerations to properties of hardened concrete there is a need to study the fracture behaviour in concrete.

1.3. Fracture Mechanism in Concrete

Concrete being a composite, heterogeneous and quasi-brittle material with multiphase characterisation, the study of failure mechanism of concrete is complex nature. The failure behaviour of concrete is neither brittle as glass nor ductile as steel. The common defect in concrete is forming of micro cracks due to the loss of moisture, these micro cracks formed prior to loading extend further to form macro cracks (Shah S.P. 1990, 1997; Giaccio and Zerbino 1998). Often these cracks proliferates either through the matrix or aggregates or interfacial transition zone (ITZ). Proliferation depends on the type of loading condition, specimen type and size. In addition concrete behaviour also varies with the additives that are used in concrete like fibers, type of aggregate and many more resulting a novel concrete.

Fracture mechanics studies about the measure of consumption of energy for unit area of crack growth. The study depends on the plane in which the crack proliferation occurs. Usually crack proliferation occurs in three different planes depending on type of loading applied, they are (i) opening mode, a mode I type in which plane splits apart (ii) sliding mode, a mode II type in which plane slides over each other (iii) tearing mode, a mode III type in which plane moves against each.

The fracture properties viz., fracture toughness, fracture energy, fracture process zone (FPZ) and characteristic length are influenced by material properties, specimen size, test method and test control parameters i.e., displacement or deformation control. The fracture mechanism in concrete was explained based on the experimental graphs. Micro cracks starts growing to

macro cracks when the applied load increases. From the schematic diagram figure 1. load vs deformation in concrete the failure mechanism was explained as the crack starts growing at the interface between the cement paste and aggregate i.e., at the point ‘A’ and further propagates into the mortar reaching ‘B’. When the peak load is reached i.e., point ‘C’ where the micro cracks propagates in an unstable manner resulting into a macro cracks. Micro crack propagates through the specimen leading to the stress drop at ‘D’. The portion C-E is due to crack bridging and branching. In case of fiber reinforced concrete, from figure 2. the combined effect of aggregate and fibre plays a major role in fracture process of concrete. The portion from C-D have a small crack opening which is less than 0.1mm, fiber bridging increases gradually depending on the characteristic of fibre. The curve will slowly decrease for increase in fibre slip or crack opening until it becomes zero. Therefore, bridging material in concrete influences the fracture properties of concrete.

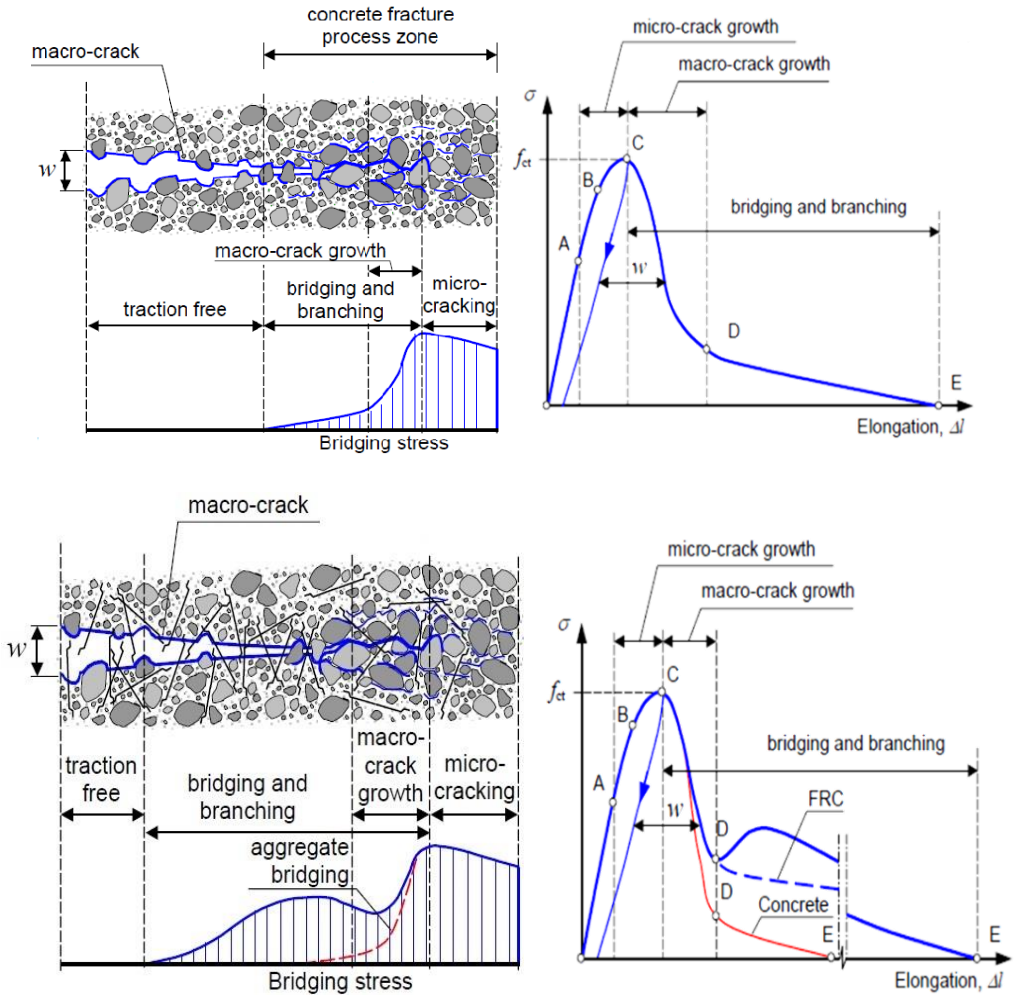

Figure 1.1. Schematic description of the stress-crack opening relationship for (a) concrete and (b) fiber reinforced concrete [Löfgren, I., 2005]

In order to evaluate the fracture properties of concrete, the fracture parameters such as critical stress intensity factor, crack mouth opening displacement, crack tip opening displacement, fracture energy are determined used three point bend test, four point bend test, compact tension test, wedge splitting test, uniaxial tensile test (Østergaard and Olesen, 2004; Xiao *et al.*, 2004; Skarżyński and Tejchman, 2016). All these methods are mode I type of fracture testing. The most common method used was three point bend test. Three point bend test was performed on a beam element with a central notch at the bottom of the specimen and central point loading. Four point bend test was similar to three point bend test with additional loading at the top. In four point bend test, the area between two loading point is under pure bending and crack proliferation due to pure bending is much higher than the shear failure. The specimens for three point bend test and four point bend test have a central notch at the bottom of the specimen. The uniaxial tension test was direct tension test which requires highly sophisticated equipment for testing. Wedge splitting test is a stable fracture testing performed on a cubic shaped specimens and core samples from existing structures. Wedge splitting test was first performed by the Linsbauer and Tschegg in 1986 and later developed by the Bruhwiler and Wittmann (Brühwiler and Wittmann, 1990). Figure 1.2 shows the mode I type of fracture testing methods.

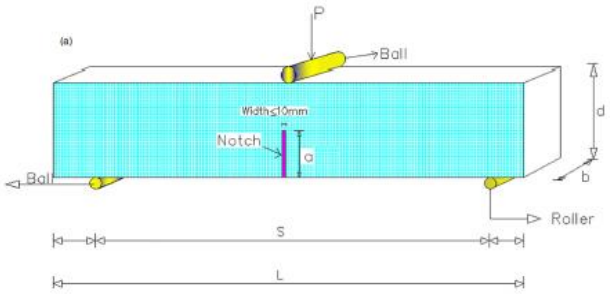

(a) Three Point Bend Test

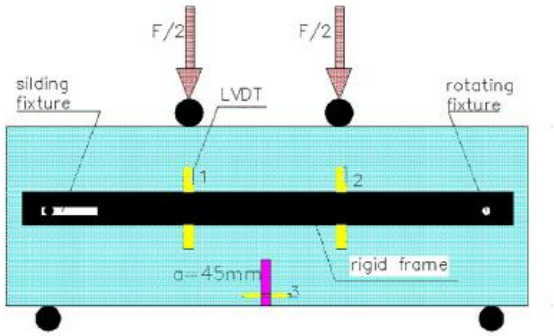

(b) Four Point Bend Test

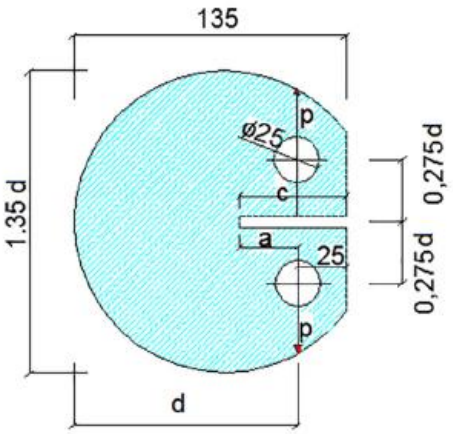

(c) Compact Tension Test

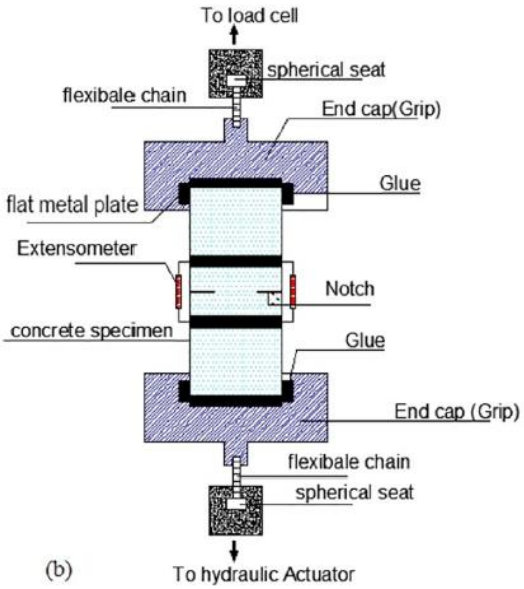

(d) Uniaxial Tension Test

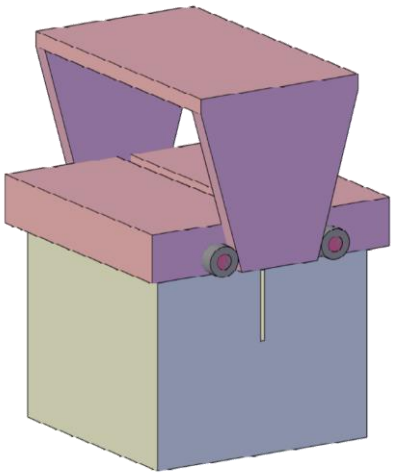

(e) Wedge Splitting Test

Figure 1.2 Fracture testing methods under Mode I

1.4. Digital Image Processing Technique

To understand the failure mechanism in concrete digital image processing technique was used. Digital image processing is an image based study which involves processing if image with some operations in order to extract some useful information. Techniques such as scanning electron microscopy, digital image correlation, and optical microscopy were used for analysing concrete (Haach V.G. *et al.*, 2016). Often these methods are limited to surface studies, smaller specimens, disturbing the test specimens. With these limitations to understand the failure behaviour of concrete computed tomography was used. CT scan helps in testing smaller and larger specimens across the depth i.e., 3D. Besides the conventional use of CT scan in medicine,

it is currently being used widely in concrete research. Computed Tomography technique is a non-destructive technique used for analysing the internal microstructure of the materials. Usage of computed tomography technique was widely used in determining the pores, cracks, fiber orientation, damage mechanism and aggregate particle quantification. Concrete under extreme loading conditions are prone to cracking, these cracks nucleate depending on the strength of paste, aggregate and interfacial transition zone. The physical changes taking place in the specimens due to the crack propagation needs to be investigated. This is essential to know which materials present in concrete are able to absorb most of the energy during the testing process.

1.5. Numerical Modelling

In order to evaluate the fracture properties of concrete, conducting tests at laboratory requires various parameters to be considered viz: specimen depth variation, notch length variation and other material parameters. To reduce these many number of physical prototypes and experiments, numerical modeling comes in handy which can optimize components in their design phase and develop better products at faster rate. Numerical modeling further benefits in reducing issues related to inadequacy of lab resources. Numerical simulation mathematically represents a physical or any other behavior, based on compatible hypotheses and simplifying assumptions. One of the numerical simulation method is finite element method (FEM), which estimates a certain behavior of the investigated component under a given load by computing relevant quantities of a structure (like stresses, strains, etc.,).

1.6. Concluding Remarks

The present introduction chapter dealt with the self compacting concrete and its importance in the field of construction in various applications. The need for study of failure mechanism of self compacting concrete was well explained. In-detailed literature was studied to identify the internal failure behaviour of self compacting concrete. The detailed literature is presented in chapter 2.

CHAPTER 2

LITERATURE REVIEW

CHAPTER 2
LITERATURE REVIEW

2.0. General

The previous chapter dealt with the introduction of self compacting concrete and the need to study the failure mechanism in concrete and fiber reinforced concrete. Also the test methods to assess the fracture properties were discussed. Furthermore, digital image processing technique was introduced to study the internal behaviour of the concrete. A brief study on numerical modelling for evaluating fracture properties were also discussed. Based on these topics of interest a detailed literature survey was conducted and presented in this present chapter.

2.1. Literature Review on Self Compacting Concrete

Self compacting concrete, a novel concrete that is used in the present era for the development of infrastructure. SCC was first conceptualized by Okamura, H. in 1986 and later in 1988 test methods and rational mix design for self compacting concrete was carried out to SCC has a standard concrete. Furthermore, Okamura, H. et al in 1994 developed a mix design for self compacting concrete confining coarse aggregate and fine aggregate contents has 50% and 40% to the total volume of solids with water cement 0.9 to 1.0. Later in 2001 Su, N., et al developed a simple mix design for SCC based on packing factor i.e., to fill the paste of binder into voids of the aggregate framework, which effects the content of aggregates in SCC. Incorporating fly ash has a replacement of cement in 40%, 50% and 60% volumes showed an economical SCC as studied by Bouzoubaa, N et al., 2001. The increase in water/powder ratio and slump increased the settlement of fresh self compacting concrete and also nature of stand influences the settlement of SCC as concluded by Sonebi, M. et al., 2002. Variation of water/cement ratio influences the fresh and hardened properties of SCC, the study result from Felekoglu, B. et al., 2007 revealed an optimum w/c ratio for producing SCC is in the range of 0.84-1.07 by volume. The use of mineral admixtures limestone powder (LP), basalt powder (BP) and marble powder (MP) as partial replacement of Portland cement enhanced the mechanical properties and improved the economical feasibility of SCC production on a unit strength basis as revealed by Uysal, M. et al., 2011. Replacement of Portland cement with fly ash (FA), granulated blast furnace slag (GBFS), limestone powder (LP), basalt powder (BP) and marble powder (MP) in various proportioning rates reveals that the flyash and GBFS significantly increased the workability and compressive strength. Mineral admixtures

helps in resisting against sodium and magnesium sulphate attacks and research reveals that best was obtained with 40% GBFS with 60% PC (Uysal, M. et al., 2011). Kanellopoulos, A. et al., 2012 studied on durability of self compacting concrete by sorptivity, porosity and chloride ion permeability tests enhanced the durability of SCC compared to normal vibrated concrete with the inclusion of silica fumes. There will be significant improvement in the micro structure due to the better packing of particles with the reaction of the pozzolanic materials.

In developing sustainable concrete various materials were used in developing SCC (Grdic Z.J., et al 2010). Recycled tyre rubber waste was incorporated in concrete by Bignozzi, M.C. et al 2006 with the 0, 22, 33 volume % of grinded tyre rubber was used as substitute to fine aggregate and resulted that the obtained compressive strength helps in binding rubber phase. For developing a sustainable SCC, coarse aggregate was substituted by recycled aggregate, the investigation by Zoran Jure et al., 2010 with substitution of recycled aggregate by 0, 50 and 100% indicate that the properties of these concretes have only a slight difference and that the recycled coarse aggregate can successfully be used for making self compacting concrete. Usage of waste plastic fibers in self compacting concrete to enhance the properties of SCC was studied by Al-Hadithi, A.I. et al., 2016 showed an adverse effect on fresh properties of self compacting concrete and enhanced the hardened properties of the concrete.

As the concrete is weak in tension and further coming to SCC, it is much more brittle than normal vibrated concrete. In order to enhance the ductility of SCC, fibers were incorporated in the concrete. Addition of different types of fibers like glass fibers, steel fibers, polypropylene fibers, polyester fibers, carbon fibers etc., enhanced various properties like strength and durability of the concrete. Rheology of paste model was applied by Ferrara, L. et al., 2007 to the mix design of steel fiber reinforced self compacting concrete. Fibers are included in the particle size distribution of the solid skeleton through the concept of an equivalent diameter, defined on the basis of the specific surface. The influence of fibers (type and quantity) on the grading of solid skeleton, minimum content and rheological properties of the paste required to achieve the required self-compactability and rheological stability were studied. The flexural behaviour of SCC for straight and hooked end steel fibers for volume fractions of 0.5%, 1.0% and 1.5% and to that of normal vibrated concrete resulted that SCC achieves the maximum crack mouth opening displacement for lower deflections than normal vibrated concrete as studied by Pajak, M. et al., 2013. Mechanical

properties splitting tensile strength, flexural strength and flexural toughness was increased with increase in percentage of fibers and compressive strength decreased with increase in the percentage of fibers as studied by Khaloo, A., et al., 2014. Factors effecting the mechanical properties of steel fiber reinforced self compacting concrete with volume fractions of 0%, 0.38%, 0.64% and 1% for maximum aggregate sizes of 10mm and 20mm with varying cement content of 400, 450 and 500 kg/m3 was studied by Madandoust, R. et al., 2015 the research reveals that the material characteristics and volume fraction of steel fibers can significantly affect the major properties of the SCC. Yehia, S. et al., 2016 studied the mechanical and durability aspects of steel, synthetic and hybrid fiber reinforced self compacting concrete based on the micro structure study using scanning electron microscopy concludes that the ITZ depended on the mixture composition. Steel fiber exhibited a wall effect with the surrounding cement paste, while synthetic fiber did not. For both fiber types, there was some interlock observed with the surrounding mortar, with a more pronounced interlock observed between concrete and steel fibers. Ductility index evaluation for steel fiber reinforced beams of self compacting concrete by Aldeen odaa, S. et al 2021 concluded that flexural stiffness improved to overcome beam deformation and constrained cracking. Increase in energy dissipation, flexural capacity and ductility index was increased with fibrous material.

2.2. Literature Review on Fracture Properties of Concrete

Failure study for elements made up of any material due to growing crack is known as fracture mechanics. Cracks starts growing when the tensile strength of the material reaches its maximum level. Depending on the tensile strength for each of the material, resistance against crack growing is dependent leading to fracture of the member (Khalilpouur S, et al 2019). There are many fracture mechanics theories developed by many researchers to enhance the study of fracture mechanics. Non linear fracture mechanics theory was formulated by Brogerg 1971 for crack growth criteria to investigate the post peak behaviour of the concrete curve. Fictitious crack model based on cohesive crack model (Dugdale 1960) for nonlinear fracture mechanics was developed by Hillerborg et al. 1976 for the crack propagation study. There are many other nonlinear models are crack band model (Bažant and Oh 1983), two-parameter fracture model, size-effect model, effective crack model, double-K fracture model (Xu and Reinhardt 1999), and double-G fracture model (Xu and Zhang 2008). The two parameter fracture model (Jenq and Shah 1985) includes the effect of pre peak behaviour of a real structure concrete structure. The model cannot predict the post peak response, characteristics of real concrete structure, if the condition $K_I = K_{IC}$ is

assumed to hold through out the post peak regime. Similar to two parameter fracture model effective crack model follows the same principle. The effective crack length is calculated not from the unloading compliance but from the secant stiffness of the real structure (Nallathambi and Karihaloo 1986). Size effect model (Bažant 1984, Bažant et al. 1986) defines the fracture energy and fracture process zone length with respect to an infinitely large specimen of any shape.

The fracture properties are evaluated based on the testing methods and analysis method that are chosen. Fracture energy varies with the size and geometry of the specimen and also local variation of fracture energy leads to a size dependent of the global specific fracture energy as concluded by Hu, X Z et al., 1992. The size independent specific fracture energy can also be obtained by testing a single size specimen with only two notch to depth ratios for both three point bend test and wedge splitting test method H.M. Abdalla et al., 2003. Ostergaard L et al., 2004 stress crack opening relationships using wedge splitting test and cracked non-linear hinge model based on the fictitious crack model resulted that fracture energy was found to increase with the age and characteristic length was decreasing. I. Lofgren et al., 2004 used WST method for assessment of fracture behaviour of FRC for different specimen geometry, fiber geometry to develop a tension softening relationship. Lofgren I et al., 2005 through inverse analysis fracture properties if steel fiber reinforced concrete using wedge splitting test and three point bend test determined stress crack relationship and resulted that variation of fiber content in stress crack relationship gives slightly higher post cracking stresses in three point bend test and no systematic difference in wedge splitting test. Korte S et al., 2014 studied the fracture properties of self compacting concrete and vibrated concrete using three point test and wedge splitting test under static and dynamic loading conditions reveals that the SCC is brittle concrete and performs worst under cyclic experiments whereas vibrated concrete is toughest and has the best fatigue resistance. Steel fibers also influence the fracture properties of high strength concrete as studied by Kazemi M.T. et al., 2017 using work of fracture method and size effect method. G_F/G_f increased from about 2.5 for high strength concrete to around 10.5 for steel fiber reinforced high strength concrete.

Aggregates play a major role in failure mechanism of concrete. Several researchers worked on the influence of aggregate particles on fracture behaviour of concrete using different test methods and loading conditions. In 1997 as studied by G.Giaccio et al., revealed that increase in compressive strength was observed for crushed aggregate and for high strength concrete the failure mechanism

was observed to be through coarse aggregate. The variation of volume fraction from 45-75% of aggregate varies the fracture behaviour of the concrete as studied by Felix E. Amparano et al., 2000 using size effect method and the fracture fracture energy varied within 25%. A meso mechanical approach was adopted by Tasdemir M.A. et al., 2001 to study the effect of aggregate volume fraction on fracture parameters of concrete, meso mechanical modelling approach gives a clear quantitative picture of how a brittle matrix transforms into a tougher, stiffer and more ductile composite as volume fraction of fine and coarse aggregate is increased without altering grading. Xiao J et al 2004 concluded that fracture parameters crack opening displacement, characteristics length and critical stress intensity factor tested under wedge splitting test method for ultra high strength concrete improved with the coarse aggregate contribution. With the variation of coarse aggregate sizes, the fracture parameters evaluated by Zhang J et al., 2010 using inverse analysis approach, the results concluded that small aggregate size lead to a high tensile strength and a sharp post peak stress drop. Using work of fracture method and size effect method, decrease in coarse aggregate from 60 to 30 % in SCC, fracture energy decreased. With the variation of coarse aggregate percentage as 30, 40, 50 and 60 for determining the fracture behaviour of self compacting concrete using work of fracture method and size effect method there was a decrease in fracture energy from both the method with the decrease in coarse aggregate from 60 to 30% as studied by Nikbin I.M. et al., 2014. A similar observation regarding the change in aggregate property was made by Beygi M.H. 2014, with the increase in maximum coarse aggregate size increase the fracture energy in work of fracture method and size effect method. Alyhya W. S. et al., 2016 concluded that the variation of mix proportions with respect to aggregate volume varies the fracture properties based on study performed on self compacting beam for varying notch to depth ratio of 0.1 and 0.6. The study reveals that the larger coarse aggregate volume larger is the toughness and critical crack opening and higher mix grade larger toughness and lower is critical crack opening. Karamloo M et al., 2016 stated that as coarse aggregate size increases, fracture toughness increases and increased ductile by means of effective length if fracture zone. The influence of aggregate size distribution on fracture behaviour of high strength concrete on performed on 63 notched beams by Siregar A.P.N. et al., 2017 resulted a decrease in fracture energy with the increase in coarseness of aggregate grain structure and also increase of stress intensity factor with reducing w/b ratio. Ghasemi M et al., 2018, 2019 considered steel fiber content of 0.1, 0.3 and 0.5% and aggregate sizes of 9.5mm, 12.5mm and 19mm to study the effect

of aggregate size and fiber content using work of fracture and size effect method. Work of fracture method performed better in energy absorption with the increase of aggregate size and steel fiber % and in size effect in such concrete with different fiber % was anticipated; G_F/G_f was 8.89. Prediction of structural fracture and fracture parameters evaluation for specimen types like three point bend test and wedge splitting test were considered by Guan J et al., 2019. The evaluating process includes the maximum aggregate size and a safe design diagram helps in predicting the structural failure using independent material constants.

Fracture and acoustic emission analysis show that increasing the volume of paste tends to make SCC more brittle (Al-Yousuf A., et al. 2007). Use of nano silica increased the mechanical, permeability and fracture properties of self compacting concrete with replacement of nano silica from 0 to 4% and 0.7% glass fiber. Use of nano silica made the concrete more ductile (Atewi Y.R., et al. 2019). Afzali-Naniz O., et al 2021 states that the use of micro silica and colloidal nano silica enhanced the fracture energy. 3% Colloidal nano silica was on higher side of fracture energy than the micro silica. The experimental and numerical study of fracture energy by wedge splitting test with the combined effect of flyash and slag of normal and high strength concrete reveals that the fracture energy decreased when FA and slag were added at all ages compared to the pure cement mix (Al-Yousuf A., et al. 2020). From the study of various steel fibers and volcanic pumice powder on fracture characteristic of self compacting concrete by Magbool H.M. et al 2021 reveals that the hybrid fibers attained highest fracture energy than the single fiber self compacting concrete. Also reduced length of hooded end fibers increased the total area under the curve. Gültekin A., et al 2021 study, fracture energies of glass and basalt fiber mixtures were up to 55.1% and 30.4% higher than that of the control mixture, respectively.

2.3. Literature Review on Image Processing Technique Using Computed Tomography

The usage of digital imaging in various fields made life easier for numerous reasons in various applications. One such growing field is construction industry. As discussed in introduction many imaging techniques like scanning electron microscope, digital image correlation, etc., were limited to surface studies or two dimensional studies. Computed tomography (CT) technique allows in predicting the internal behaviour across the depth. Usage of computed tomography for understanding the behaviour of concrete was performed by the Morgan I.L, et al in 1980 (Du Plessis A, et al 2019). CT scan was popularly used in predicting the failure patterns, pores network

and its changes due to chemical effects, thermal effects and hydration process. CT studies have gained popularity in the recent decade for visualizing parameters such as pore network, hydration process, permeability, chemical effects, thermal effects, carbonation, failure patterns etc. under different test conditions.

Experimental findings by Yun T.S., et al 2012 reveals that the quantification and distribution of paste void spacing based X-ray computed tomography scan images helped in developing a statistical approach for the assessment of the durability due to freeze – thaw of cement based materials. The water evaporation rate was investigated using X-ray micro CT for porous asphalt concrete. A quantitative and qualitative determination of pore network caused due to rain water on aging was determined by I. Jerjen et al 2015. The change in micro structure of the deteriorated specimens was investigated using X-ray micro CT by Ramaswamy K.P. et al. 2017 based on the image analysis that was carried out on cement paste specimens of 10 ×10 × 60mmwith w/c ration 0.4 in various acid solutions like 1% hydrochloric acid, 0.5M acetic acid, 0.5M citric acid, 1% sulfuric acid for 6 weeks and the primary attack indicators were variations of depth and area which was clearly observed through CT images. Micro CT scan was applied by Yang S et al 2018 to determine porosity for both wet and dry mix of glass concrete and also investigate the cracks formed due to alkali silica reaction. The study concluded that the measured porosity of dry mix glass concrete decreased after alkali silica reaction test further through the insitu observation of micro CT formation of new cracks was not observed in dry mix glass concrete with further development of alkali silica reaction. Internal microstructure and structural behaviour of fiber reinforced concrete under static and cyclic flexural loading using CT scan was studied by Vicente M.A., et al 2019 and a numerical equation was given to determine the residual tensile strength using crack width, damage, fiber content and orientation.

In concrete, damage caused due to various reasons was quantified using computed tomography technique. One such similar study was studied by Suzuki T et al 2010. The study emphasized on evolution of damage quantification using acoustic emission and X-ray CT under freeze- thawed condition of concrete. The durability index was calculated based in the initial damage of core samples estimated form acoustic emission data. The damage is evaluated by comparing the average CT number affected due to the internal cracks that are formed. Yujie huang et al 2015 examined on 3D meso scale damage plasticity model of concrete based on insitu X-ray CT was developed

for accurate understanding of damage initiation, evolution of failure in concrete under compression and tension were investigated using CT. The damage caused due to fire was determined using CT image analysis for a core sample of concrete by Lubloy E., et al 2017, the image analysis revealed that they was a decrease in porosity due to fire and analysis was quite well practically evident with the change in colour from gray to pink. X-ray micro Compute tomography for detection and segregation of 3D cracks by Loeffler C.M., et al 2018 aimed for finding the most effective technique for identifying cracks and damage in concrete subjected to dynamic loading and suggested a 3D geometric segmentation technique performed well across crack length scales.

The fiber properties influences the structural behaviour of concrete, many researchers used Computed Tomography technique to study the internal behaviour of fiber reinforced concrete. In 2014 synthetic fiber distribution and quantification was studied by Boredelon A.C. et al., 2014 using X-ray CT and concluded that the actual volume fractions of fiber samples correlated the measured total fracture energy. Ponikiewski T., et al 2015 focused on distribution and orientation of steel fiber in SCC slabs by CT scan, determined the angle between the fibers and the beam axis from images obtained from CT. The steel fiber observation, distribution and orientation in concrete was investigated by Balazs G.L., et al 2017 using CT scan on a beam specimen of 150 × 150 × 600 mm and concluded that average steel fibers distribution and homogenous mix was observed in 30min mixing than in 5min mixing for 0.5% fiber content. Also, it was observed that highest fibre content was at the bottom of the specimen and orientation was clearly visualized by CT scan images. Orientation of steel fiber reinforced concrete using wedge splitting test and CT scanning was studied by Gonzalez D.C., 2018 on specimens of sizes 50 × 50 × 150mm resulting a correlation between fiber orientation and residual tensile strength and fracture energy and higher orientation and residual strength and fracture energy was observed with better orientation of fibers.

Another application of the computed tomography is to understand fracture behaviour of concrete. Erdem S., et al 2014 studied on 3D X ray and fractal analysis by digital image analysis technique for quantitative analysis of resistance to segregation, static strength and corrosion induced cracking in SCC and light weight SCC specimens and results reveal that the light weight SCC was weaker in compression than normal SCC due to less homogeneity in internal structure. Yang Z., et al 2017 studied on Insitu X ray CT for characterisation of 3D fracture evolution with the image based evolution by digital volume correlation to observe complicated 3D fracture paths in multi phase

materials like concrete. Fracture process mechanism with different ITZ properties were studied on concrete considering 3D numerical study using X-ray CT by Yu Q., et al 2018 and proposed 3D realistic fracture process analysis using numerical modelling at meso/micro scopic levels under complex loading conditions. Considering compressive cyclic and monotonic loading for evolution of fracture in concrete by Skarzynski L., et al 2019 reveals that the evolution of cracking volume quantitative with increasing fatigue damage showed strong nonlinear shape with an increase by 30% compared to monotonic fatigue loading.

2.4. Literature Review on Numerical Modelling of Concrete

Numerical method for obtaining key fracture parameters describing the softening behaviour of quasi brittle materials in mode I failure for wedge splitting test was studied by Que, N.S. et al., 2002, and results revealed that the linear laws were computationally more tractable. Numerical simulation of a Wedge Splitting test for High-Strength Concrete was focused by Sitel, M et.al, 2014 using Simulia Abaqus software for developing a numerical model. And the result concluded that Model slightly over estimated the value of fracture energy established in the experiment. Klon J et.al, 2017 studied on spatial modeling of wedge-splitting test on cylindrical specimens using FEM Software to predict the crack/damage propagation to evaluate the fracture parameters using ATENA and the modelling resulted that the variant with loading wedge directly, propagation of cracks from the initial notch was noted. The crushing above the support block is negligible for this variant. Furthermore in 2017 Sucharda, O. et al., worked on mechanical and fracture properties of self compacting concrete beams with different types of steel fibers based on numerical approach, Trend lines for the material parameters and steel fibers fraction dependence are showed.

2.5. Concluding Remarks

From the detailed literature review, the following are the gist of the study:

- SCC requires more amount of powder content to achieve the distinct fresh properties and could be the future gen concrete.
- Experimental testing procedure, specimen size and the material properties influences the fracture parameters.
- Fibers enhanced the energy dissipation in the concrete. Limited study has been reported regarding fracture parameters of Fibrous SCC.
- For better understanding of internal failure behaviour can be studied using Computed Tomography a digital image processing technique.

- ❖ Numerical studies can be carried for validating the experimental results.

Based on detailed literature survey on self compacting concrete and failure behavior mechanism of hardened concrete, it is identified that there is an ample requisite to explore the fracture behavior of fibrous self compacting concrete. The next chapter presents the objectives of the research work along with the scope of the investigation.

CHAPTER 3

SCOPE AND OBJECTIVES OF RESEARCH WORK

CHAPTER 3
SCOPE AND OBJECTIVES OF RESEARCH WORK

3.0 General

For the present research work, a gap was identified from a detailed literature survey and was aimed to study the fracture properties of the self compacting concrete. Few points were observed from the literature and are as follows

- The test method has much effect on fracture behaviour of concrete.
- Material properties and proportions affect the fracture parameters.
- The internal behaviour study helps in identifying the crack path that makes the crack path tortuous.

3.1. Scope and Objective of the Research Work

Objectives of Research work

- ❖ To investigate the physical and mechanical properties of non-fibrous and fibrous self compacting concrete with different sizes of coarse aggregate and dissimilar volume proportions of aggregates.
- ❖ To evaluate the fracture parameters of non-fibrous and fibrous self compacting concrete.
- ❖ To compute the internal failure behavior of non-fibrous and fibrous SCC using digital image processing technique.
- ❖ To conduct the numerical modelling of wedge splitting test method for validating the results.

The scope of the research work are as follows

- ❖ Determine the physical and mechanical properties of non-fibrous and fibrous self compacting concrete with three different sizes of coarse aggregate and dissimilar volume proportions of aggregates.
- ❖ Comprehend the fracture parameters of non-fibrous and steel fibrous SCC under three point bend test and wedge splitting test method.
- ❖ Examine the internal failure behavior of non-fibrous and steel fibrous SCC using computed tomography.
- ❖ Numerical modelling of wedge splitting test method using FEM based software-ABAQUS.

3.2. Research Methodology

From the above objectives and scope of the work, a detailed research methodology is developed by dividing the work in to four phases.

Phase-1:

Mechanical and fracture properties for non-fibrous and fibrous self compacting concrete using size effect method for three point bend test method were evaluated.

Phase-2:

Fracture properties were assessed for non-fibrous and fibrous self compacting concrete using wedge splitting test method for without and with guide notch specimens

Phase-3:

Internal failure behaviour of non fibrous and fibrous self compacting concrete for wedge splitting test specimens was assessed based on image analysis of computed tomography

Phase-4:

The fracture behaviour of wedge splitting test specimen for a varying specimen depth and notch depth using ABAQUS software was evaluated.

The parameters for the research work include

- Size of Coarse aggregate - 20mm, 16mm, 12.5mm
- Coarse to fine aggregate quantities (CA-FA) - 50-50, 45-55, 40-60
- Size of specimens for three point bend test - L/d - 2.5, d_1:d_2:d_3: 1:2:4, Notch to depth ratio-0.15
  100mm × 100mm × 267mm
  100mm × 200mm × 534mm
  100mm × 400mm × 1068mm
- Size of specimens for Wedge splitting test - 150mm × 150mm × 150mm (with and without guide notch)

The size of cast specimens and details of tests conducted

S.No.	Name of test	Dimensions of specimen	Total
1.	Compressive Strength test	150 mm × 150mm × 150mm	18 × 3 = 54
2.	Split tensile strength test	100mm diameter,300mm height	18 × 3 = 54
3.	Flexure test on notched beams	Size 1 Size 2 Size 3 (d1:d2:d3 1:2:4) L/d = 2.5	18 × 3 = 54 18 × 3 = 54 18 × 3 = 54
4.	Wedge splitting test	150mm ×150mm × 150mm	18 × 3 = 54

* For each test 3 specimens were cast.

A schematic diagram of the research methodology adopted along with the variables considered in each phase is shown in **Fig 3.1**.

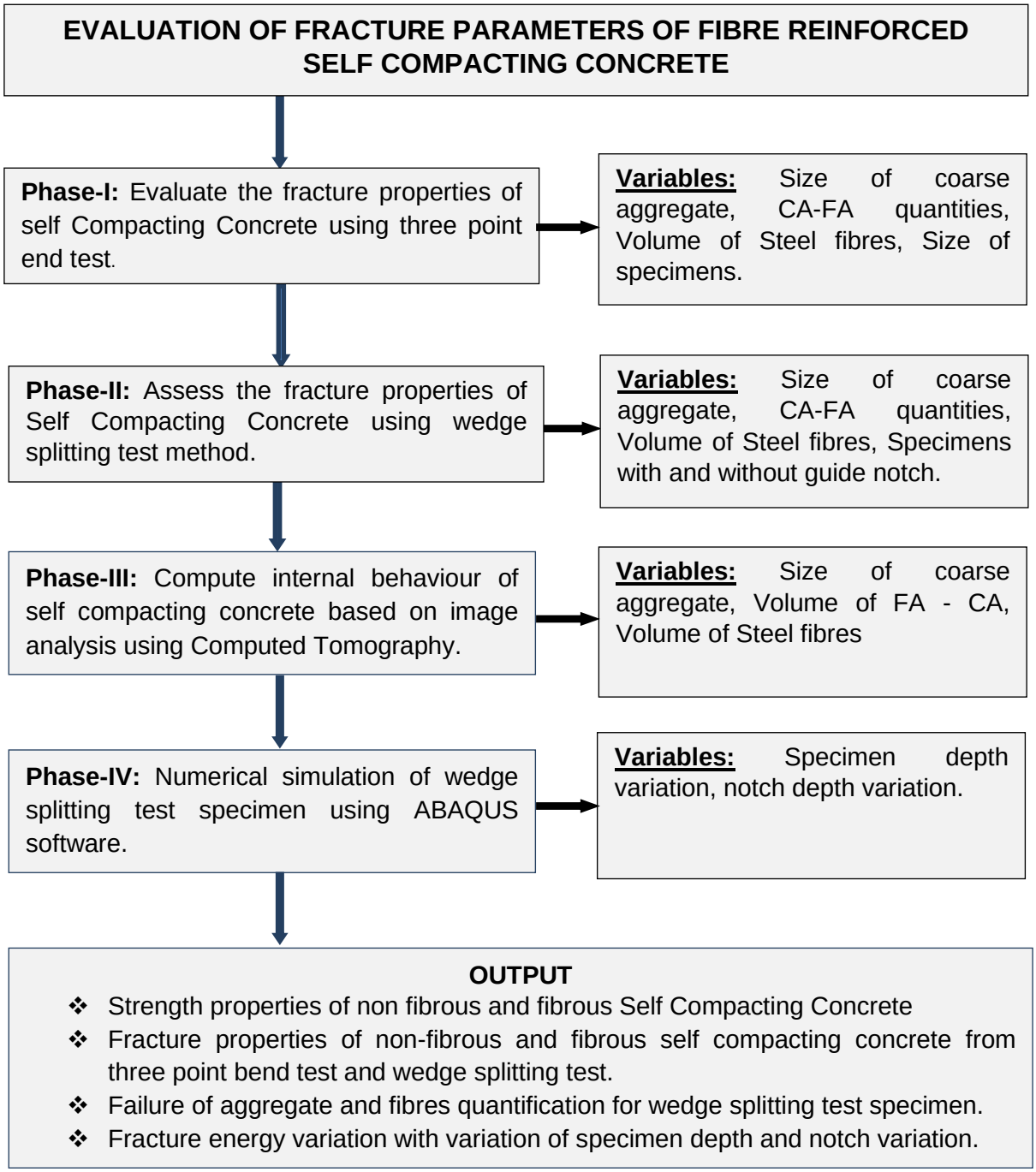

Fig. 3.1 Schematic Diagram of the Research work

CHAPTER 4

PHYSICAL, MECHANICAL AND FRACTURE PROPERTIES OF SELF COMPACTING CONCRETE

CHAPTER 4

PHYSICAL, MECHANICAL AND FRACTURE PROPERTIES OF SELF COMPACTING CONCRETE

4.0 General

Based on the objectives framed in chapter 3, the experimental work is planned accordingly to find out the physical, mechanical and fracture parameters of non-fibrous and fibrous self compacting concrete. The present chapter explains the fresh, mechanical and fracture behaviour of non-fibrous and fibrous self compacting concrete. The research work was carried out based on the strength criteria considering the parameters as coarse to fine aggregate quantity, coarse aggregate size and dosage of fibers in self compacting concrete. Three coarse aggregate sizes of 20mm, 16mm and 12.5mm were considered as maximum nominal size of the coarse aggregate. Three coarse to fine aggregate quantity ratios 50-50, 45-55, 40-60 were considered in the study. For fibrous self compacting concrete, steel fibers of 0.5% by volume of concrete were considered. The fracture parameters of non fibrous and fibrous SCC were evaluated using three point bend test and wedge splitting test methods. A thorough explanation of these test methods and evaluation of fracture parameters is done in the following sections.

4.1 Materials – physical properties

Self compacting concrete was prepared using the materials according to the Bureau of Indian standards. The following are the materials used for the research work.

4.1.1 Cement

The binding material, Ordinary Portland cement of 53 grade according to IS: 12269 (BIS, 2013) was used. The specific surface area was 300 m^2/Kg and specific gravity was 3.11 with initial setting time of 68min and final setting time of 510min.

4.1.2 Fine aggregate

Fine aggregate was procured from a nearby river source conforming to zone II as per IS 383 (BIS, 2016) to carry out the research work. The physical properties of fine aggregate such as sieve analysis, bulk density and specific gravity were performed as per IS: 2386 (BIS, 1997) and the details are tabulated in Table 4.1. Figure 4.1 shows the gradation curve for fine aggregate.

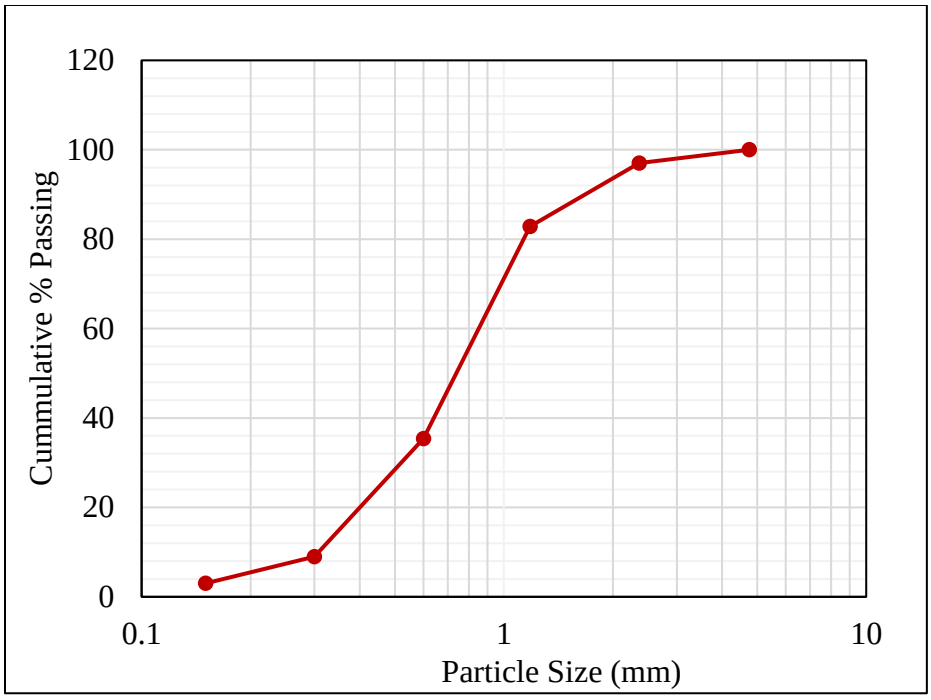

Figure 4.1. Gradation curve for Fine aggregate

Table 4.1 Properties of Fine aggregate

Properties	Fine Aggregate
Bulk Density (g/cm^3)	1.45
% of Voids	54.66
Void Ratio	0.98
Specific Gravity	2.65
Fineness Modulus	2.63
Water absorption (%)	1.81

4.1.3 Coarse aggregate

Granite stone procured from a local crushing unit of nominal size 20mm was used as a coarse aggregate. A well graded aggregate as per IS 383 (BIS 2016) segregated as 20mm, 16mm and 12.5mm as nominal sizes were used for the present research work. The gradation curve for each of the coarse aggregate size were shown in figure 4.2.

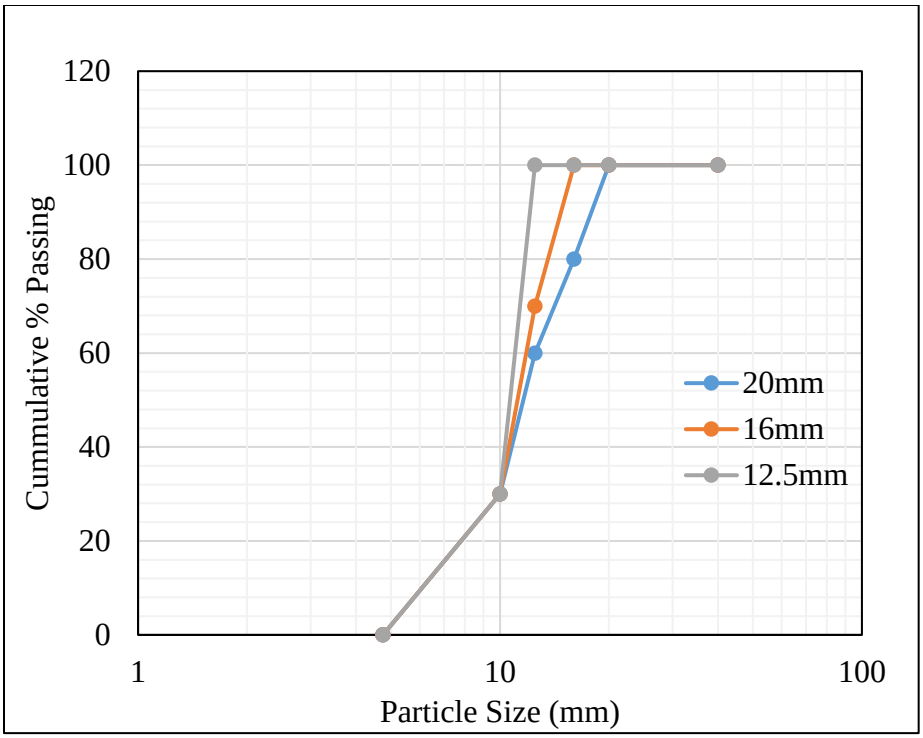

Figure 4.2. Gradation curve for coarse aggregate

4.1.4 Fly ash

Cementitious material, fly ash procured from a nearby National Thermal Power station was used as a mineral admixture for enhancing the fresh and hardened properties of self compacting concrete. The specific gravity of the fly ash was 2.11. Chemical properties of fly ash are tabulated in table 4.2.

Table 4.2 Chemical properties of Fly ash

Silica content	63.99
Silica + alumina + iron oxide	92.7%
Water and soluble salts	0.04%
pH	10
Loss on ignition	2.12%

4.1.5 Water

For mixing and curing of the concrete and concrete specimens, potable water was used for the experimental work.

4.1.6 Super plasticizer

High range water reducing chemical admixture, Chryso Fluid Optima S612, a polycarboxylic ether based on super plasticizer conforming to ASTM C494 (ASTM, 2016) was used as a super plasticiser. All the specifications as per EFNARC for a self compacting concrete are achieved using super plasticiser. The properties of Chryso Fluid Optima S612 were presented in table 4.3.

Table 4.3 Properties of Super Plasticizer

Form	Light Amber Liquid
Specific Gravity	1.10 ± 0.02
Air entrainment	≤ 1.5% over control mix
pH	≥ 6
Chloride content	Nil, as per BS-5075 (Part –I)

4.1.7 Fiber

Steel fibers of hooked end type was used in the present study. 0.5% by volume of concrete were added during dry mixing of the concrete ingredients. The properties of steel fiber are tabulated in the Table 4.4.

Table 4.4 Properties of hooked end steel fiber

Length (mm)	35
Diameter (mm)	0.5
Aspect Ratio (l/d)	70
Density (kg/m^3)	7850
Tensile Strength (MPa)	1100
% Elongation	2

4.2 Mix Proportions

The mix proportions for self compacting concrete were designed as per Nansu method of mix design (Nansu 2001). The material mix proportions were fixed to study the effect of fracture parameters with the variations of the coarse aggregate size and coarse to fine aggregate ratios variations. Cement, fine aggregate, fly ash and water were kept constant and aggregate properties were varied to study the true effect of aggregates in terms of fracture properties. The variations of aggregate proportions are tabulated in the table 4.5. As the study aims for the fracture properties

of non-fibrous and fibrous self compacting concrete with the variation of aggregate properties, the ingredients viz: cement, fly ash and water were kept constant for varying aggregate size and quantities. All the mixes were carried out as per EFNARC specifications (EFNARC, 2005) to ensure the fresh properties of the self compacting concrete for both non-fibrous and fibrous self compacting concrete.

Table 4.5 Quantities of materials

Constituents	C50F50			C45F55			C40F60		
	20mm	16mm	12.5mm	20mm	16mm	12.5mm	20mm	16mm	12.5mm
Cement (kg/m^3)	450	450	450	450	450	450	450	450	450
Fly ash (kg/m^3)	150	150	150	150	150	150	150	150	150
Water (l/m^3)	190	190	190	190	190	190	190	190	190
FA (kg/m^3)	771	771	771	835	835	835	945	945	945
CA (kg/m^3)	(800)	(800)	(800)	(710)	(710)	(710)	(630)	(630)	(630)
20-16mm	160	-	-	142	-	-	126	-	-
16-12.5mm	160	240	-	142	213	-	126	189	-
12.5-10mm	240	320	560	213	284	497	189	252	441
10-4.75mm	240	240	240	213	213	213	189	189	189
Admixture (l/m^3)	4.6								

4.3. Fresh properties

To ensure the fresh properties of the self compacting concrete, the concrete has to satisfy few properties as per EFNARC specifications. The important properties viz: flowability, filling ability, passing ability and resistance to segregation are to be tested for fresh concrete to call it as self compacting concrete. To determine the fresh properties of non-fibrous and fibrous self compacting concrete, the following tests were conducted.

4.3.1. Test for flowability – Slump flow test and T_{50cm} Slump Flow Test

Slump flow test and T_{50cm} are the tests conducted to identify the flowability of concrete. Slump flow test is the measure of flow diameter and flow time. The test was conducted on a smooth flat and non-absorbent surface. The top surface has two concentric circles having the diameters 200 and 500mm. The dimensions of slump cone are of height 300mm with top and bottom diameters

as 100 and 200mm respectively as shown in figure 4.3. The slump cone is placed on the first circle and the fresh concrete is poured up to top of the cone. The cone is lifted up and the time taken for concrete to spread 500mm diameter circle is noted as T50cm time and the maximum spread diameter is noted as the slump flow.

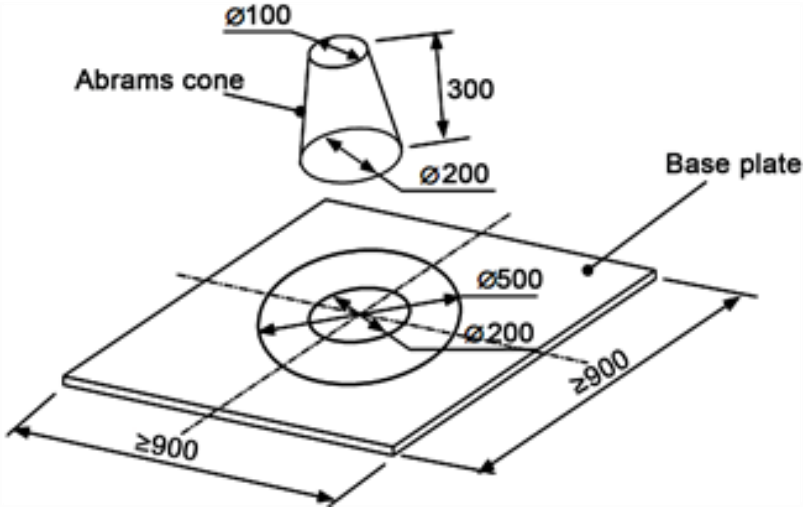

Figure 4.3 Slump flow test apparatus as per EFNARC 2005

4.3.2. Test method for filling ability - V funnel Test

V-funnel test was conducted to test the filling ability of concrete. The test also determines the resistance to segregation. The apparatus is a V shaped funnel as shown in figure 4.4. The fresh concrete is filled into the funnel with hinge trap door closed and the time taken to empty the funnel as soon as the hinge trap door is released is recorded as V funnel flow time. And for V-funnel T5minutes, the hinge trap door is closed for 5min with concrete remaining in the funnel. At the end of 5minutes the time taken for the concrete to empty the funnel is recorded as T_{5min}.

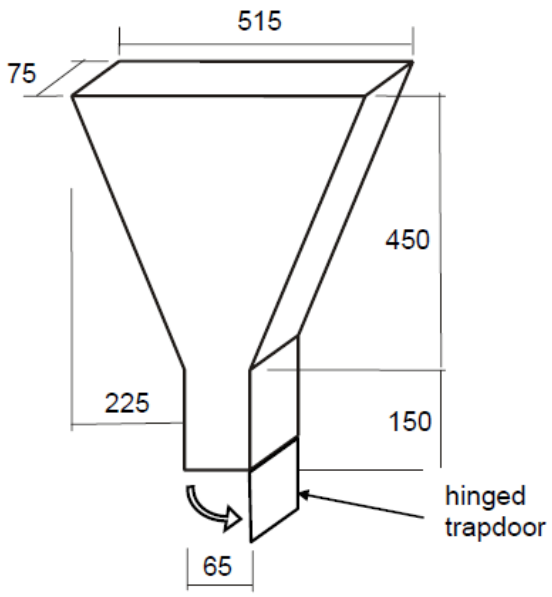

Figure 4.4 V funnel apparatus for testing filling ability as per EFNARC 2005

4.3.3. Test for Filling and/or passing ability – L Box Test

The passing and filling ability of self compacting concrete is determined by L box test. The equipment is a rectangular cross section of L shape. As shown in figure, at the junction of vertical and horizontal sections, the reinforcement bars are placed vertically. Once the vertical section is filled with concrete, sliding gate is lifted vertically up and the concrete is allowed to flow horizontally into the horizontal section. After the flow gets stabilized, the height of the concrete near the reinforcement (h_1) and height at the end of horizontal section (h_2) is measured. The ratio of h_2 and h_1 is calculated and referred to as L box value or blocking ratio value. The higher the number is better the passing ability. Figure 4.5. shows the L box test apparatus for conducting the fresh properties of SCC.

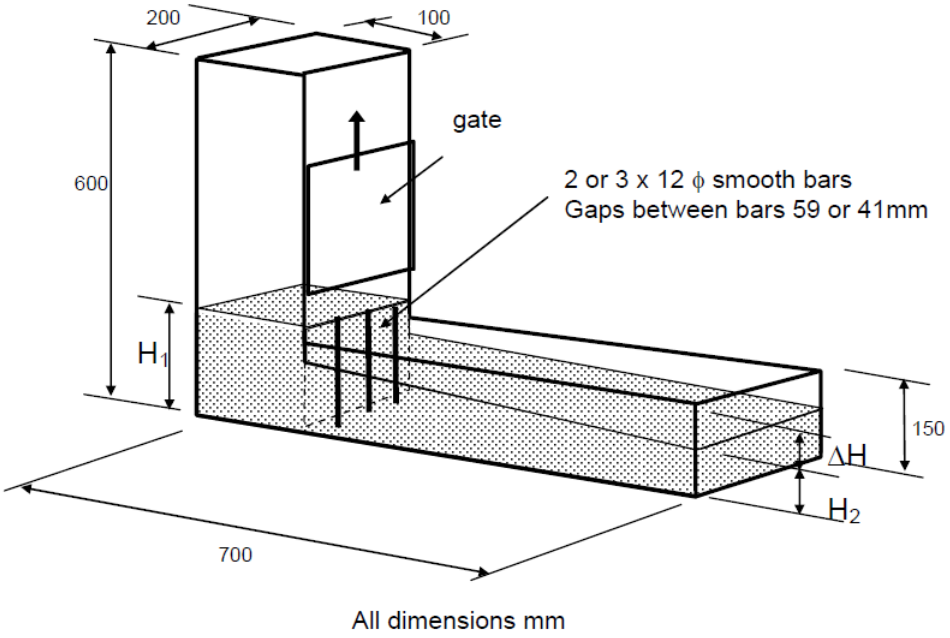

Figure 4.5. L Box test apparatus as per EFNARC 2005

4.3.4. Test for Filling and/or passing ability – J Ring Test

J ring test is a test to determine the passing ability of self compacting concrete. J ring consists of a circular ring of diameter 300mm with vertical reinforcing bars of 10mm diameter, length 100mm and spaced at 48mm as shown in figure 4.6. The steel ring is placed around the slump cone and the fresh concrete is poured into the slump cone up to the top surface of the cone. After clearing the excess concrete, the cone is lifted up vertically. The concrete passes through the spacing of the reinforcement of J ring apparatus. After the flow gets stabilized, concrete height inside the J ring and outside the J ring is measured. The difference between the two heights is reported as the J ring value.

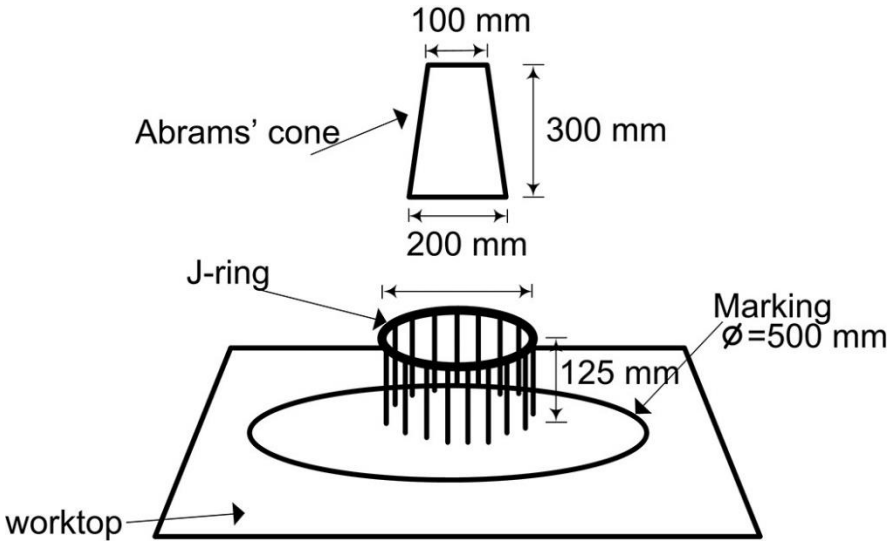

Figure 4.6. J Ring test apparatus as per EFNARC 2005

4.4. Experimental Work

The present study investigates the mechanical and fracture properties of non-fibrous and steel fibrous self compacting concrete for varying coarse aggregate size and coarse to fine aggregate quantity. The experimental program was divided into two stages. One evaluating the fracture properties based on three point bend test method and the other one consisted of determining the fracture parameters with wedge splitting test method. Table 4.6 shows the details of the specimens cast for determining mechanical and fracture properties of self compacting concrete.

4.5. Nomenclature of specimens

The mix designations for specimens with non-fibrous and fibrous self compacting concrete were assigned based on the aggregate quantity and coarse aggregate size. Three coarse to fine aggregate quantities (CA-FA) 50-50, 45-55 and 40-60. Typically, C50F50 represents 50-50 Coarse to fine aggregate quantity where C denotes coarse aggregate and F as fine aggregate. Three coarse aggregate sizes of 20mm, 16mm and 12.5mm were represented with the aggregate size. Non-fibrous self compacting concrete was represented with P and fibrous self compacting concrete with F'. The representation for non-fibrous and fibrous self compacting concrete was followed by the aggregate size.

4.5.1. Nomenclature for non-fibrous SCC

C50F50-20P - Non-fibrous SCC mix with CA-FA quantity 50-50 having aggregate size 20mm

C50F50-16P - Non-fibrous SCC mix with CA-FA quantity 50-50 having aggregate size 16mm

C50F50-12.5P - Non-fibrous SCC mix with CA-FA quantity 50-50 having aggregate size 12.5mm

C45F55-20P - Non-fibrous SCC mix with CA-FA quantity 45-55 having aggregate size 20mm

C45F55-16P - Non-fibrous SCC mix with CA-FA quantity 45-55 having aggregate size 16mm

C45F55-12.5P - Non-fibrous SCC mix with CA-FA quantity 45-55 having aggregate size 12.5mm

C40F60-20P - Non-fibrous SCC mix with CA-FA quantity 40-60 having aggregate size 20mm

C40F60-16P - Non-fibrous SCC mix with CA-FA quantity 40-60 having aggregate size 16mm

C40F60-12.5P - Non-fibrous SCC mix with CA-FA quantity 40-60 having aggregate size 12.5mm

4.5.2. Nomenclature for fibrous SCC

C50F50-20F’ - Fibrous SCC mix with CA-FA quantity 50-50 having aggregate size 20mm

C50F50-16F’ - Fibrous SCC mix with CA-FA quantity 50-50 having aggregate size 16mm

C50F50-12.5F’ - Fibrous SCC mix with CA-FA quantity 50-50 having aggregate size 12.5mm

C45F55-20F’ - Fibrous SCC mix with CA-FA quantity 45-55 having aggregate size 20mm

C45F55-16F’ - Fibrous SCC mix with CA-FA quantity 45-55 having aggregate size 16mm

C45F55-12.5F’ - Fibrous SCC mix with CA-FA quantity 45-55 having aggregate size 12.5mm

C40F60-20F’ - Fibrous SCC mix with CA-FA quantity 40-60 having aggregate size 20mm

C40F60-16F' - Fibrous SCC mix with CA-FA quantity 40-60 having aggregate size 16mm

C40F60-12.5F' - Fibrous SCC mix with CA-FA quantity 40-60 having aggregate size 12.5mm

4.6. Casting and Curing

The materials required to cast the specimens are weighed and batched for each mix. The materials are added to the drum mixer and allowed for dry mixing of the ingredients. After thorough dry mixing of all the ingredients, water mixed with super plasticizer was added and mixing was done for about 10min. Then the fresh concrete was tested to determine the fresh properties of SCC. The prepared fresh concrete mix was placed into greased moulds of specified dimensions. Demoulding of the specimens was done after 24hrs of casting. Further demoulded specimens were water cured for a specific age of curing i.e. 28days.

4.7. Sample details and preparation

In case of three point bend test, three geometrically similar specimens with loaded span to depth ratio of 2.5 with three varying depth ratios of 1:2:4 were cast for each mix. Three depths for three geometrically similar specimens were 100mm, 200m and 400mm with span length 250mm, 500mm and 1000mm, respectively. The width of the specimen was kept constant for all the depths i.e., 100mm. For each size of the specimens, three samples were cast. The schematic diagram for 200mm depth specimen was shown in figure 4.7. Subsequently the specimens were cast and cured for 28days. After curing specimens were sawed for a notch having notch to depth ratio of 0.15. Figure 4.8 shows the cutting of the beam specimen for providing notch at the soffit of the beam. Figure 4.9 shows the experimental test setup of three point bend test for depths 100mm, 200mm and 400mm.

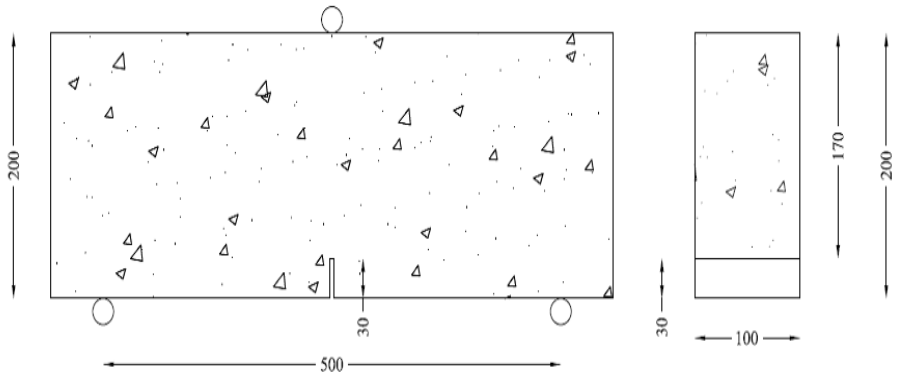

Figure 4.7. Three point bend test specimen details for 200mm depth specimen

Figure 4.8. Notch cutting of beam specimen

(a) d=100mm

(b) d=200mm

(c) d=400mm

Figure 4.9. Experimental Test setup for depth sizes (a) 100mm (b) 200mm (c) 400mm

Another method used in the study was wedge splitting test method, where the specimens are usually cubical or cylindrical in shape. In this method, the size of the specimen depends on the maximum fiber length or maximum size of the aggregate used. Recommended specimen dimensions should be at least 3.5 times larger than the maximum fiber length. In case of short fibers with 35mm long length, specimens of 150 mm ×150 mm ×150mm were used. The specimens were cast with a cast groove of 30mm wide and 22mm deep using a wooden piece placed on one of the faces of the cube. The schematic diagram of test specimens for wedge splitting test are shown in Figure 4.10. The specimens are provided with a starter notch and guided notch. The picture represents front view and top view of without and with guide notch specimens. A starter notch and a guide notch were sawed to the cast groove using concrete cutter. The depth of starter notch shall be half of the height of the specimen depth. The guide notch minimises the influence of wall effect at the formwork surfaces. The effect of change in area of ligament differs in the energy consumption to split the specimen into two parts (change in ligament dimensions can change the crack propagation direction). Figure 4.11 (a) shows the specimen with cast groove, (b) shows the cutting of the wedge splitting specimen using concrete cutter, (c) and (d) shows without and with guide notch specimens, respectively.

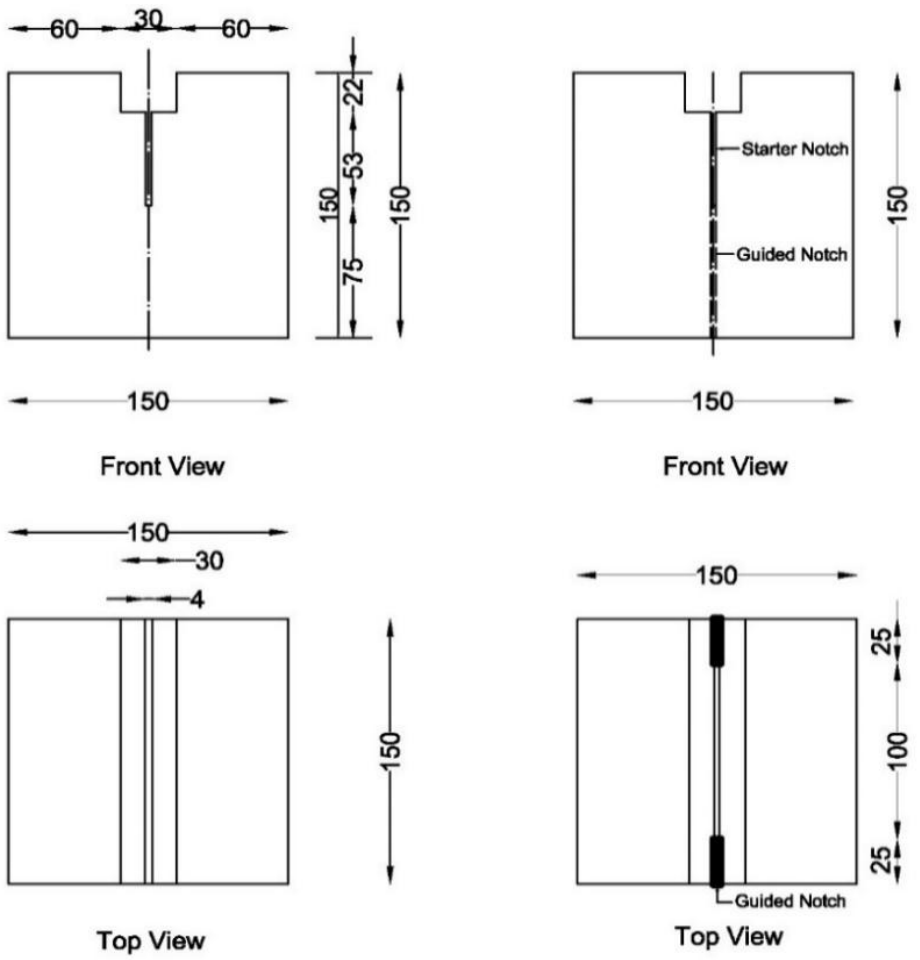

Figure 4.10. Specimen details for without and with guided notch wedge splitting test

(a) Specimen with cast groove

(b) Cutting of the wedge splitting test using concrete cutter

(c) Without guide notch specimen

(d) With guide notch specimen

Figure 4.11. Wedge Splitting Test Specimen

Table 4.6 Size of cast specimens and details of tests conducted

S.No.	Name of test	Dimensions of specimen	Total
1.	Compressive Strength test	150 mm × 150mm × 150mm	18 × 3 = 54
2.	Split tensile strength test	100mm diameter and 300mm height cylinder	18 × 3 = 54
3.	Flexure test on notched beams (d1:d2:d3 1:2:4) l/d = 2.5	Size 1 (d=100) Size 2 (d=200) Size 3 (d=400)	18 × 3 = 54 18 × 3 = 54 18 × 3 = 54
4.	Wedge splitting test	150mm ×150mm × 150mm	18 × 3 = 54

* For each test 3 specimens were cast.

4.8. Hardened properties

4.8.1. Compressive strength

The cube specimens of dimensions 150 × 150 × 150 mm were tested for compressive strength after conventional water curing. The testing was done as per IS 516-1956 on Tinius Olsen Testing machine of 2000kN capacity. The loading was applied on the other side of casting face of the cube. Compressive loading at the rate of 140 kg/cm^2/min was applied at the centre until the failure load was occurred. The compressive strength was recorded by taking the average of three specimens with the variation not more than ±15% of the average.

4.8.2. Split tensile strength

The split tensile strength test was done on the cylindrical specimen of height 300mm and 150mm diameter as per IS 5816 (BIS, 1999). Compressive load was applied axially on the line which is diametrically opposite. The load was applied constantly until the breakage of the specimen. The ultimate load was noted and the split tensile strength was calculated as per the Equation 4.1. The average of three specimens was recorded as the split tensile strength.

$$F_{st} = \frac{2P}{\Pi dl} \qquad \text{Eq. (4.1)}$$

Where, P – Maximum Load applied on to the specimen (Newton)

l- Height of the specimen (mm)

d- Diameter of the specimen (mm)

4.8.3. Three point bend test

The fracture parameters are analysed by three point bend test method on a beam type specimen. The beam was subjected to a central point load on top with a notch at the soffit of the beam. The fracture properties are evaluated from the size effect method as per RILEM TC-89 specification. Size effect method is applicable on the geometrically similar specimens. The specimen geometry and evaluation of the fracture properties are done according to the RILEM TC-89. The evaluation of fracture properties as per RILEM is as follows:

4.8.3(a). Calculation procedure

(a) The maximum load values $P_1,\ldots P_n$ for specimen with varying depth $d_1,\ldots d_n$. The corrected maximum loads, $P^0_1, P^0_2,\ldots.. P^0_n$, it takes the weight of the specimen into account

$$P_j{}^0 = P_j + \frac{1}{2} m_j g \quad (j = 1,2,\ldots. n)$$

Eq. (4.2)

$$P_j{}^0 = P_j + \frac{2S_j - L_j}{2S_j} m_j g \quad (j = 1,2,\ldots.. n)$$

Where, m_j – mass of the specimen j ; g- acceleration due to gravity ; n - number of tests conducted.

(b) The linear regression for the plot of ordinates Y_j and abscissae X_j

Where, $X_j = d_j$, $Y_j = \left[\frac{bd_j}{P_j{}^0}\right]^2$ Eq. (4.3)

Where, d_j – depth of the specimen; b – breadth of the specimen; $P_j{}^0$ – corrected maximum load

Determine the slope and intercept of the regression line: Y=AX+C

$$A = \frac{\sum_J (X_j - \bar{X})(Y_j - \bar{Y})}{\sum_J [X_j - \bar{X}]^2} \text{ , C} = \bar{Y} - A\bar{X} \quad \text{Eq. (4.4)}$$

Where,

$$\bar{X} = \frac{1}{n}\sum_j X_j \text{ , } \quad \bar{Y} = \frac{1}{n}\sum_j Y_j \quad \text{Eq. (4.5)}$$

$(\bar{X}, \bar{Y})$ is the centroid of all data points.

(c) Calculate auxiliary values for the extrapolation to very large specimen sizes for which liner elastic fracture mechanics applies.

For defining relative crack length α=a/d, where a= crack length, for l/d=2.5

$$F_{2.5}(\alpha) = \frac{1 - 2.5\alpha + 4.49\alpha^2 - 3.98\alpha^3 + 1.33\alpha^4}{(1-\alpha)^{3/2}} \quad \text{Eq. (4.6)}$$

The non-dimensional energy release rate is $g(\alpha) = \left[\frac{l}{d}\right]^2 \pi \alpha [1.5 F(\alpha)]^2$ Eq. (4.7)

The fracture energy G_f is given by: $G_f = \frac{g(\alpha)}{AE}$ Eq. (4.8)

Critical stress intensity factor: $K_{IC}{}^2 = G_f E$ Eq. (4.9)

Where, E is young's modulus

Effective length of process zone $C_f = \frac{g(\alpha)}{g'(\alpha)} \times \frac{C}{A}$ Eq. (4.10)

The size effect law as per RILEM is given by

$$\sigma_n = \frac{B f_t{}'}{(1+\beta)^{0.5}} \text{ , } \beta = \frac{d}{d_0} \quad \text{Eq. (4.11)}$$

Where, σ_n - nominal stress at failure, $f_t{}'$ - tensile strength, B and d_0 are empirical constants, β is brittleness number.

The above size effect law depicts the structural behaviour based on the brittleness number. For $\beta < 0.1$ the behaviour is ductile and follows strength criterion and when $\beta > 10$ the nature is brittle and structure follows linear elastic fracture mechanics. For $0.1 \leq \beta \leq 10$ the behaviour is nonlinear elastic fracture mechanic. With the increase in depth of the specimen, the failure nature changes from ductile to brittle.

The effective crack tip opening displacement (δ_c) at the peak load was determined by

$$\delta c = \frac{8K_{IC}}{E} \times \sqrt{\frac{C_f}{2\pi}} \qquad \text{Eq. (4.12)}$$

Where,

K_{IC} – critical stress intensity factor; E- young's modulus; C_f – effective length of process zone.

4.8.4. Wedge splitting Test

Wedge splitting test is one of the modes I type of fracture testing where the specimens are in cubical or cylindrical shape. The advantage of wedge splitting test method is that it can also be conducted on existing structures by taking the core sample which are cylindrical in shape while laboratory samples are cubical in shape. The specimens are provided with a starter notch and a guide notch, the guide notch is provided as shown in the Figure 4.12. The starter notch is provided to ensure the crack propagation and guide notch is provided to prevent the horizontal cracking. The guide notch also minimises the influence of wall effect at the formwork surfaces. The vertical compressive force is applied on top of the wedge plate and the load is transferred through the bearing attached to the two steel plates. The transferred load acts as a splitting force on to the face of the cube. A roller support is provided at the bottom of the cube which acts as a hinge support. The rate of loading applied should be less than or equal to 0.25 mm/min for crack mouth opening displacement (CMOD) between 0.2-2mm and for CMOD greater than 2mm, the rate of loading may be increased to 0.5mm/min. In the present experimentation, WST was conducted on a displacement controlled testing machine with a constant rate of loading of 0.2mm/min. The linearly varying displacement transducers (LVDTs) were attached horizontally to measure the horizontal deformation i.e., CMOD. The Splitting force (F_{sp}) was calculated from compression load (F_v) using Eq. (12) and F_{sp} vs CMOD graphs were plotted by considering the average of three specimens. The splitting force F_{sp} is calculated using the formula in Eq. (4.13). The specific

fracture energy G_F is calculated from the area under Load - CMOD curve and area of the ligament. The splitting force F_{sp} is given by

$$F_{sp} = \frac{F_V}{2tan(\alpha)}\left[\frac{1-\mu\, tan(\alpha)}{1+\mu\, tan(\alpha)}\right] \quad \text{Eq. (4.13)}$$

Where,

α - wedge angle (here α =15º)

μ - coefficient of friction for the roller bearing. μ varies from 0.1% to 0.5%.

If friction is ignored $F_{sp} = \frac{F_V}{2\tan(\alpha)} = 1.866 \times Fv$ Eq. (4.14)

The specific fracture energy, G_F CMOD is determined from the load-CMOD curves obtained from test results.

$$G_{FCMOD} = \frac{W_{FCMOD}}{A_{lig}} \quad \text{Eq. (4.15)}$$

Where,

$W_{F\,CMOD}$ is the area under the curve the F_{split} load- CMOD curve

A_{lig} is the area of the ligament

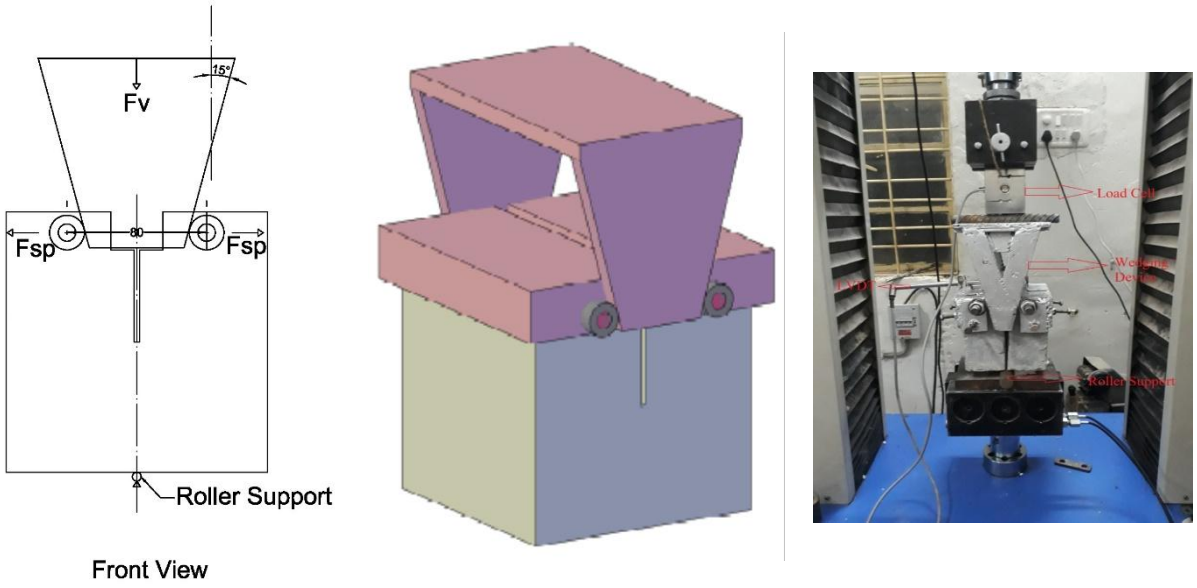

Figure 4.12. Experimental test setup for Wedge Splitting Test

4.9. Results and Discussions

4.9.1. Fresh properties of self compacting concrete

The mix design was based on the fresh properties of self compacting concrete i.e., filling ability, passing ability and resistance to segregation along with the reproducibility and repeatability. The tests that are conducted on fresh concrete are slump flow, L-box, J-ring and V-funnel as per EFNARC 2005 specifications.

Tables 4.7 and 4.8 presents the fresh property values of slump flow test, T50cm, V funnel test, T 5min, L box and J ring test for non-fibrous and steel fibrous self compacting concrete respectively. All the test results are in acceptance with EFNARC guidelines.

4.9.1. (a) Fresh properties of non-fibrous self compacting concrete

From experimental results it can be observed that flowability of SCC increased with the increase in size and quantity of coarse aggregate. For non-fibrous self compacting concrete, the slump test value ranged lowest slump diameter of 685mm for C40F60-12.5P and highest for C50F50-20P with 750mm. Based on EFANRC specifications the slump class falls under SF2 class as the slump values ranges from 660-750mm for non-fibrous SCC.

As per EFNARC specifications T_{50cm} i.e., flow time taken for concrete to reach 50cm diameter ranges from 2-5sec. All the mixes of non-fibrous self compacting concrete with three coarse aggregate sizes and quantities are in the range of 2-4sec. It was observed that increase in aggregate size and increase in fine aggregate quantity increased the T_{50cm} flow time. The flow time >2 represents VS2/VF2 class.

V-funnel test results indicate that for aggregate size 12.5mm has attained higher time limit than higher coarse aggregate size. The flow was in the range of 6-11.5sec. As per EFNARC specifications all the mixes for non-fibrous self compacting concrete indicated were within the range of 6-15sec. With the increase in fine aggregate content made the concrete viscous in nature.

The filling and passing ability of non-fibrous SCC were tested using L-box, it was observed that the values of h_2/h_1 are in the range of 0.88-0.94. From the blocking ratio values reveals that all the mixes were within the range of EFNARC specifications and offered good resistance against segregation.

J-ring apparatus tests the passing ability of the fresh concrete through the gaps of the reinforced bars. It was observed that the passing ability was reduced for higher coarse aggregate size mixes compared to other coarse aggregate sizes. All the J-ring values were within the range of EFNARC specifications.

Table 4.7 Fresh Properties of Non Fibrous Self Compacting Concrete

	Slump flow (mm)	**T_{50cm} (sec)**	**V funnel (sec)**	**T_{5min} (sec)**	**L box (h_2/h_1)**	**J ring (mm)**
EFNARC	**550-900**	**2-5**	**6-12**	**6-15**	**0.8-1.0**	**0-10**
C50F50-20P	750	2.13	6.00	8.00	0.94	6
C50F50-16P	730	2.50	8.25	11.00	0.91	7
C50F50-12.5P	720	3.00	9.00	13.00	0.90	7
C45F55-20P	735	3.00	7.36	9.56	0.93	7
C45F55-16P	710	3.00	9.00	12.34	0.91	8
C45F55-12.5P	707	3.56	11.00	14.00	0.89	8
C40F60-20P	705	3.50	9.00	11.00	0.92	8

C40F60-16P	700	3.50	10.00	13.58	0.90	9
C40F60-12.5P	685	4.00	11.50	15.00	0.88	8

4.9.1. (b) Fresh properties of fibrous self compacting concrete

From the values represented in table 4.8 for fresh properties of fibrous self compacting concrete, It was observed that the fibers obstructed the flow and passing characteristics of the fibrous self compacting concrete compared to non-fibrous self compacting concrete. The increase in flow characteristics with the increase in size and fine aggregate quantity was due to the decrease in specific surface area of aggregates.

The flow diameter from slump flow test for all the mixes ranged from 610-675 for steel fiber reinforced SCC. The mixes C50F50-20F' and C50F50-16F' falls under SF1 class as the flow diameter was 675mm and remaining mixes for all CA sizes with CA-FA quantity of 45-55 and 40-60 and the mix C50F50-12.5F' falls under SF2 class as per EFNARC specifications.

The flow time, T_{50cm} for all mixes was ranging in between 2.84 - 4.44sec. Therefore, as per EFNARC specifications the mixes fall under VS2/VF2 class as the flow time was >2.

The flow time as per V funnel test was ranging from 7.47-10.51sec for all mixes. As the size of the coarse aggregate decreased and fine aggregate quantity increased the mixes were viscous in nature reducing the flow characteristics.

The blocking ratio (h_2/h_1) from L-box test results were in the range of 0.8-0.92. The EFNARC specifications indicates that the mixes were having good passing ability and resistance to segregations.

The J-ring values for fibrous self compacting concrete indicate that the passing ability for high fines has obstructed the flow of the concrete through the reinforcing bars. The J-ring values ranged from 4-8 for all mixes of fibrous self compacting concrete.

From both non-fibrous and fibrous self compacting concrete, the results are indicative of improvement in flowability of self compacting concrete with increase in quantity and size of coarse aggregate. The increase in flow is due to decrease in specific surface area of aggregates. Further, increase in the fine aggregate content makes the concrete viscous. It was also observed that the mix with higher fine aggregate content and least coarse aggregate size obtained minimum flow for

same amount of super plasticizer. From L box and J Ring test values, it can be noticed that the passing ability of concrete decreased with increase in quantity and size of coarse aggregate. The higher content and larger size of coarse aggregates obstructed the passing ability of concrete compared to other mixes. However, all the results are within the range of EFNARC guidelines and satisfied the essential fresh properties of SCC.

Table 4.8 Fresh Properties of Fibrous Self Compacting Concrete

	Slump flow (mm)	**T_{50cm} (sec)**	**V funnel (sec)**	**T_{5min} (sec)**	**L box (h_2/h_1)**	**J ring (mm)**
EFNARC	**550-900**	**2-5**	**6-12**	**6-15**	**0.8-1.0**	**0-10**
C50F50-20F’	675	2.84	7.47	8.35	0.80	8
C50F50-16F’	675	2.96	8.12	9.43	0.83	8
C50F50-12.5F’	655	3.12	8.48	9.99	0.84	7
C45F55-20F’	655	3.17	8.18	10.24	0.85	7
C45F55-16F’	650	3.56	8.54	11.12	0.87	6
C45F55-12.5F’	640	3.84	8.75	11.22	0.88	6
C40F60-20F’	640	3.77	9.82	11.58	0.88	5
C40F60-16F’	635	3.98	10.12	12.34	0.91	5
C40F60-12.5F’	610	4.44	10.51	13.02	0.92	4

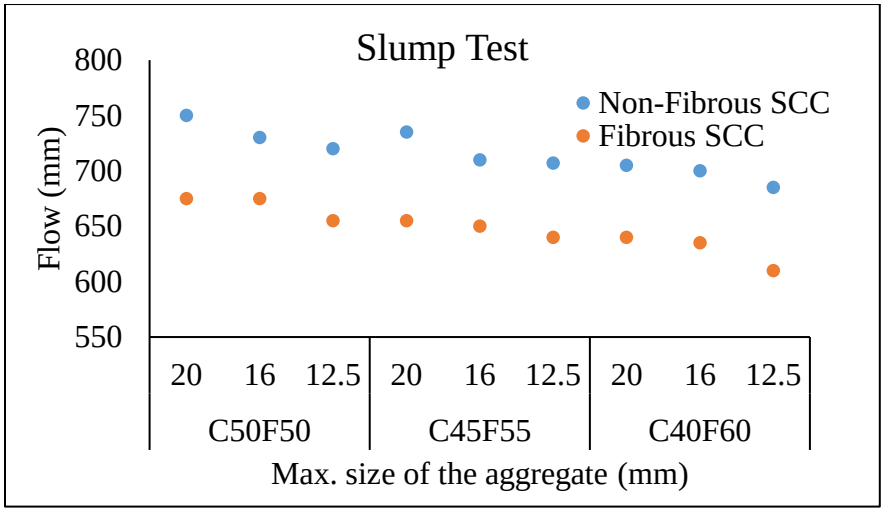

Figure 4.13. Fresh properties of SCC based on Slump test

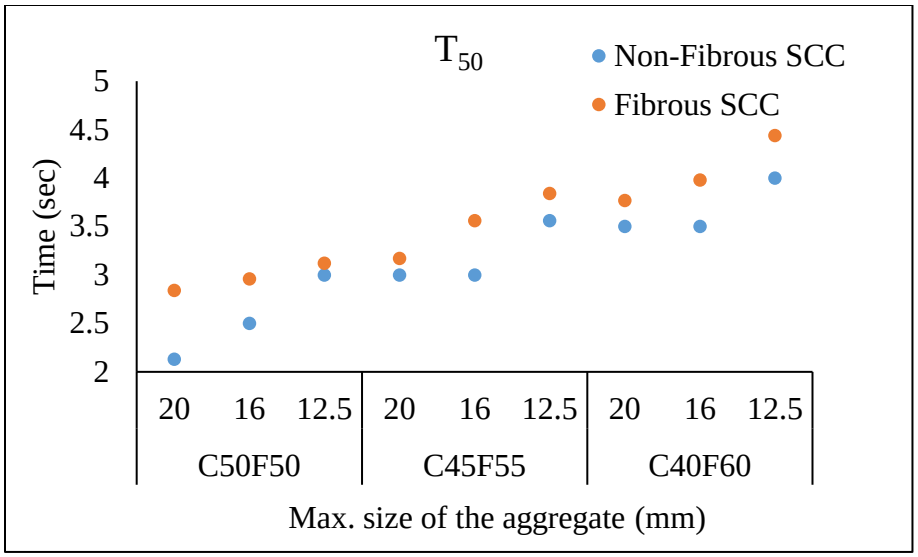

Figure 4.14. Fresh properties of SCC based on T_{50} Test

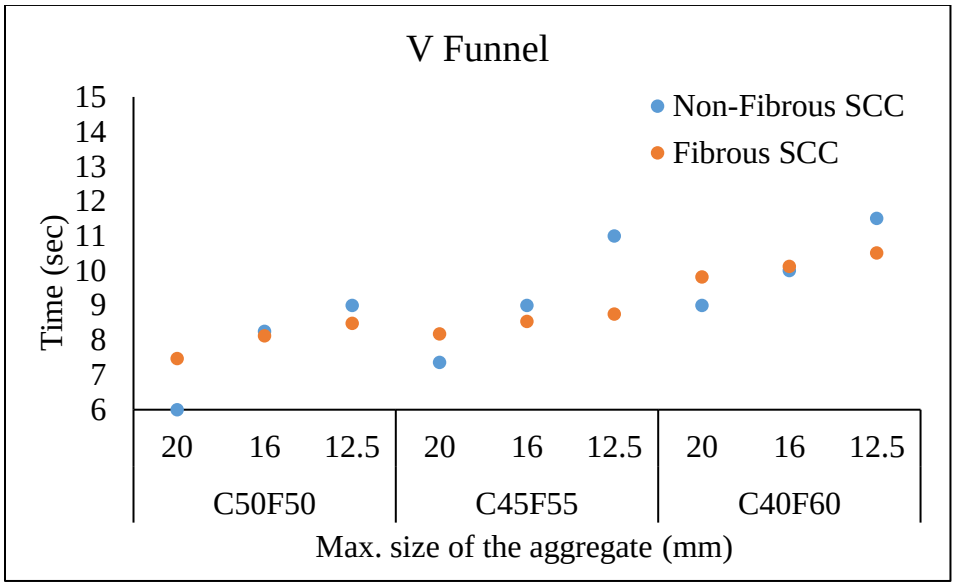

Figure 4.15. Fresh properties based on V funnel test

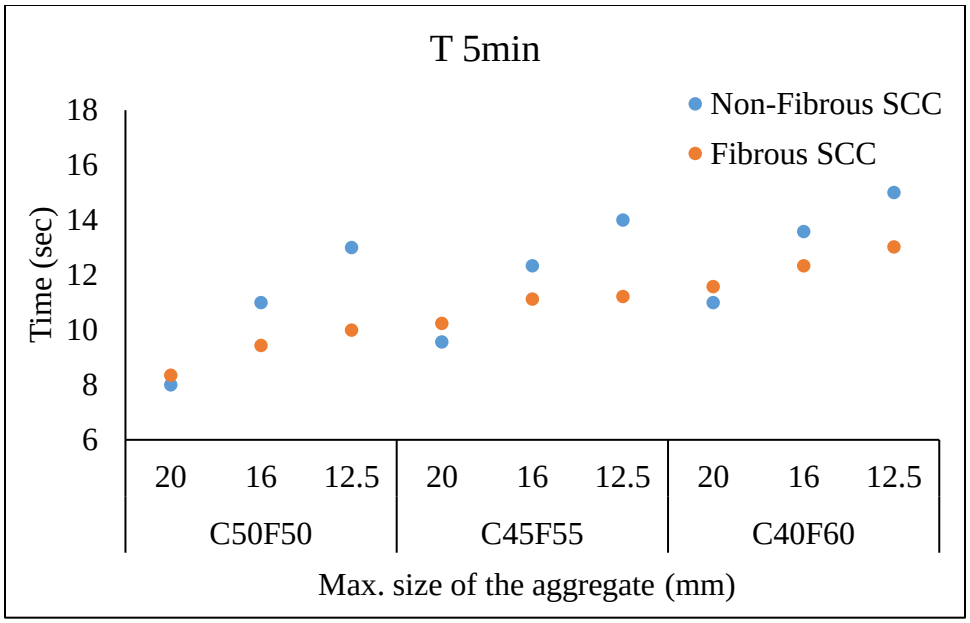

Figure 4.16. Fresh properties based on T 5min

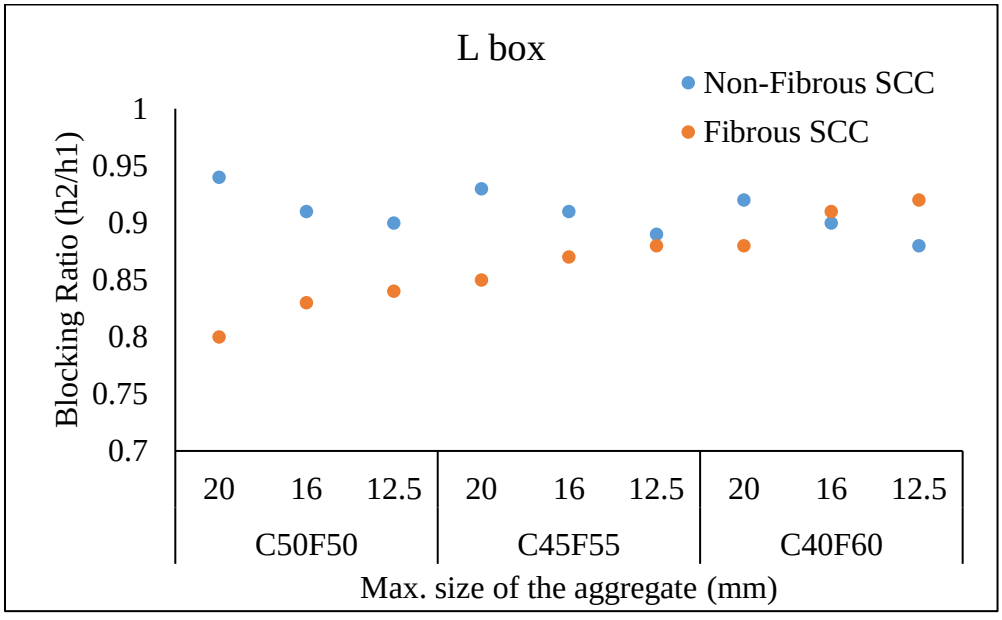

Figure 4.17. Fresh properties based on L Box test

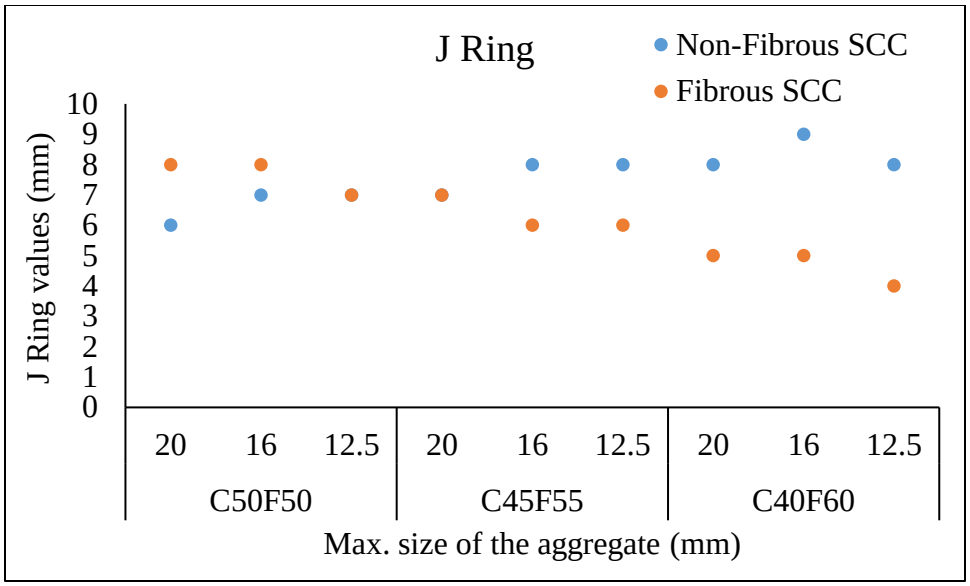

Figure 4.18 Fresh properties based on J Ring test

4.9.3. Hardened Properties

The compressive strength test was conducted for non-fibrous and fibrous SCC specimens at the end of 28days of curing as per IS 516 (2013) on standard cubes of 150mm × 150mm × 150mm and the average value of three cubes are presented in Tables 5 and 6. The results indicate a noteworthy impact of quantity and size of coarse aggregate and fibers' presence on compressive strength of self compacting concrete. The increase in volume of coarse aggregate increased the compressive strength of concrete and it is noticed for all sizes of aggregate. The increase in CA-FA content from 40-60 to 50-50 enhanced the compressive strength by 7.0%, 6.2% and 5.2% for non-fibrous SCC specimens, while, the strength improvement in fibrous SCC specimens is 5.9%, 5.1% and 6.1% for specimens with aggregate sizes 20mm, 16mm and 12.5mm respectively. It was also observed that for a particular volume proportion of aggregate, the smaller size coarse aggregate specimens attained high values of compressive strength compared to larger size coarse aggregate based specimens.

The splitting tensile strength results were obtained as per IS 5816 (BIS, 1999) using standard cylinder of 150mm diameter and 300mm height and the values of non fribrous and fibrous SCC specimens are shown in Tables 4.9 and 4.10 respectively. With the decrease in size of coarse aggregate from 20mm nominal size to 16mm, the increase in tensile strengths of fiber reinforced SCC was 1.7%, 1.7%, and 2.4%, whereas from 16mm to 12.5mm this was 4.4%, 2.2% and 3.5%

for aggregate proportions 50-50, 45-55 and 40-60 respectively. In case of non-fibrous SCC specimens, the increase in tensile strengths for decrease in size of aggregate from 20mm nominal size to 12.5mm was 4.3%, 4.4% and 3.2% for aggregate proportions 50-50, 45-55 and 40-60 respectively. The smaller size aggregate specimens attained high tensile strength compared to large size coarse aggregate based specimens. With the decrease in coarse aggregate size the surface area of the aggregate increases, proportionally there is an increase in number of aggregate particles and transition zone than the larger size aggregate. Therefore, in SCC as the relative strength of ITZ is much stronger than the aggregate strength, the crack path is through the aggregate. With an increase in coarse aggregate volume content the strength also increases because the coarse aggregate acts as a bridging particle for the crack to propagate. It also increases due to the increased transition zones around the aggregate particles.

Table 4.9. Mechanical properties of non fibrous self compacting concrete

Mix Designation	f_c' (N/mm^2)	f_t (N/mm^2)	E (GPa)
C50F50-20P	76.4	8.05	40.93
C50F50-16P	77.2	8.25	41.85
C50F50-12.5P	78.5	8.40	42.35
C45F55-20P	72.1	7.95	40.25
C45F55-16P	73.7	8.00	40.85
C45F55-12.5P	76.0	8.20	41.72
C40F60-20P	71.4	7.70	40.12
C40F60-16P	72.7	7.80	40.23
C40F60-12.5P	74.6	7.95	40.83

Table 4.10. Mechanical properties of fibrous self compacting concrete

Mix Designation	f_c' (N/mm^2)	f_t (N/mm^2)	E (GPa)
C50F50-20F'	82.4	9.05	45.39
C50F50-16F'	83.1	9.20	45.58
C50F50-12.5F'	85.5	9.45	46.23
C45F55-20F'	80.4	8.80	44.83
C45F55-16F'	81.3	8.95	45.08
C45F55-12.5F'	82.7	9.00	45.47
C40F60-20F'	77.8	8.50	44.10
C40F60-16F'	79.1	8.70	44.47
C40F60-12.5F'	80.6	8.80	44.89

4.9.4. Three point bend test

The fracture properties of non-fibrous and fibrous self compacting concrete were determined using three point bend test. As per RILEM TC 89, the evaluation of the fracture properties were done using size effect method. The testing was done on a closed loop servo controlled dynamic testing machine having a capacity of 1000kN. A constant rate of loading was adopted such that the maximum peak load was reached within ten minutes. From experimentation, peak load was recorded and this peak load was considered for the evaluation of fracture properties. The weight of the specimen was taken into consideration to the experimental load using the equation no. (4.2). The corrected peak loads for non-fibrous and fibrous self compacting concrete were tabulated in table 4.11. and 4.13.

4.9.4. (a) Fracture properties of non-fibrous self compacting concrete from size effect method

The fracture properties of non-fibrous self compacting concrete from size effect method were tabulated in Table 4.12. Linear regression was carried out for geometrically similar specimens and equation (4.3). Slope and intercept from the linear regression for the mix C50F50-20P were shown in the figure 4.19. The obtained slope values from linear regression for all the mixes were tabuled in table 4.12 under column A. The results reveal that, maximum size of coarse aggregate i.e.,

20mm achieved maximum peak load from the experimental data and the corresponding fracture energy was lowest among the 20mm, 16mm and 12.5mm coarse aggregate size. The fracture energy was highest for the mixes having coarse to fine aggregate quantity 50-50 and lowest for the quantity 40-60. The higher quantity of aggregate has more number of aggregate particles bridging the crack proliferation path which requires more energy to fracture. Whereas for aggregate particles according to size, the peak load was highest for lowest aggregate size that reflected in the fracture energy as size effect method considers only peak load which is a direct proportional to the fracture energy.

For coarse to fine aggregate quantity of 50-50, the variation in fracture energy for 20mm and 16mm with respect to 12.5mm was observed to be decreased by 32% and 13% respectively. Similarly for 45-55 quantity it was observed as 17% and 9% and for 40-60 it was observed as 26% and 13%. For constant coarse aggregate size of 12.5mm the change in coarse to fine aggregate quantity from 50-50 to 45-55, the reduction in fracture energy was observed to be 32%, while the comparison with 40-60 was to be 48%. Similarly, for 16mm coarse aggregate size it was about 29% and 52% for 50-50 to 45-55 and 50-50 to 40-60 respectively. On the other hand, for 20mm size the decrease was about 17% for 50-50 to 45-55 and 48% for 50-50 to 40-60.

Similar to fracture energy, fracture toughness K_{IC} also increased with the increase in coarse to fine aggregate quantity and decreased with the increase in coarse aggregate size. From K_{IC} values tabulated in table 4.12, for 20mm sized coarse aggregate increase in coarse to fine aggregate quantity from 45-55 to 50-50, K_{IC} increased by 9.55% and from 40-60 to 50-50 it was about 29.29%. Similarly for 16mm sized coarse aggregate the increase was about 16.33% and 31.68% for an increase of aggregate quantity from 45-55 to 50-50 and 40-60 to 50-50 respectively. And for 12.5mm it was about 18.34% and 32%.

4.9.4. (b) Brittleness number and size effect law for non-fibrous self compacting concrete.

Brittleness number (β) is the important parameter for predicting the fracture mode. As per RILEM specifications the fracture mode was predicted based on the value ranging from 0 to 10. If $\beta < 0.1$ the behavior is ductile and follows strength criterion and $\beta > 10$ the nature is brittle and structure follows linear elastic fracture mechanics, while ranging from $0.1 \leq \beta \leq 10$, the behavior is nonlinear elastic fracture mechanics. Figure 4.20. shows the variation of β with respect to specimen depth for three aggregate size and quantity variations. For all the mixes of non-fibrous self compacting

concrete, β was ranging in between 0.1 to 10 therefore, the behaviour was nonlinear elastic fracture mechanics.

Figure 4.21. shows the experimental load vs predicted loads obtained from equation (1) of size effect method for non-fibrous self compacting concrete. It can be observed that the fracture parameters for each mix can be used to predict the failure loads of the SCC structures. The size effect law predicted for non-fibrous self compacting concrete with varying coarse aggregate size and quantities were plotted in figure 4.22. The plot depicts that all the mixes were following strength criterion, which reflects that the higher quantity of coarse aggregate content is more ductile compared to lower quantities. The graph depicts that the experimental and predicted results were quite well.

Table 4.11 Corrected maximum loads from size effect method of non-fibrous self compacting concrete

Mix Designation	Depth (mm)	corrected maximum load		
		Beam 1 (kN)	Beam 2 (kN)	Beam 3 (kN)
C50F50-20	400	46.22	46.14	46.57
	200	25.53	25.60	25.60
	100	14.84	14.88	14.40
C50F50-16	400	48.24	48.84	48.03
	200	26.32	27.64	28.29
	100	15.13	15.79	14.48
C50F50-12.5	400	51.56	50.73	52.41
	200	28.12	29.40	28.76
	100	15.98	15.34	15.98
C45F55-20	400	42.11	42.19	42.63
	200	22.67	22.81	22.94
	100	12.50	13.07	13.00
C45F55-16	400	43.43	43.58	43.72
	200	23.11	24.27	24.35
	100	14.23	14.11	13.92
C45F55-12.5	400	45.40	45.48	45.55
	200	25.00	25.37	25.31
	100	14.55	14.48	14.48
C40F60-20	400	34.87	34.51	36.03
	200	19.74	20.33	20.77
	100	12.00	11.55	12.50
C40F60-16	400	40.22	40.80	39.48
	200	23.96	24.35	23.60

	100	13.73	14.40	13.82
C40F60-12.5	400	42.77	42.11	42.70
	200	26.89	26.98	26.98
	100	13.82	14.48	14.19

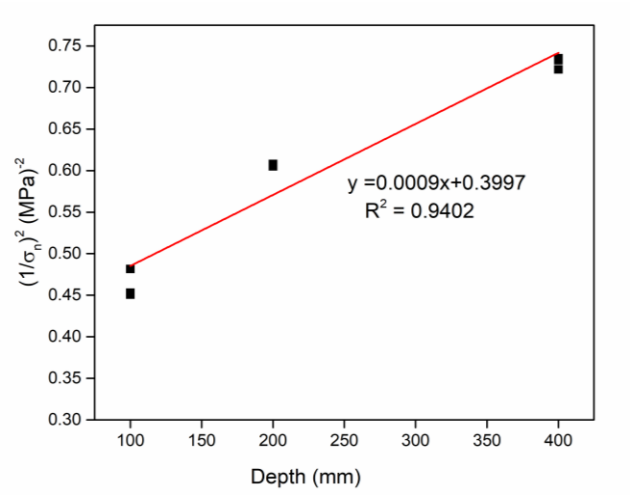

4.19 Linear regression for the mix C50F50-20P

Table 4.12 Fracture parameters of non-fibrous self compacting concrete from size effect method

Mix Designation	A	α	F(α)	g(α)	Bf_t	G_F (N/m)	C_f (mm)	K_{IC}	δ (mm)
C50F50-20	0.0009	0.15	0.9102	5.78	1.58	141.55	74.72	80.16	0.049
C50F50-16	0.0007	0.15	0.9102	5.78	1.65	181.50	89.26	90.89	0.060
C50F50-12.5	0.0006	0.15	0.9102	5.78	1.70	208.47	97.27	98.17	0.067
C45F55-20	0.0008	0.15	0.9102	5.78	1.43	117.26	74.42	72.50	0.045
C45F55-16	0.001	0.15	0.9102	5.78	1.51	128.27	73.79	76.04	0.046
C45F55-12.5	0.0009	0.15	0.9102	5.78	1.57	141.30	76.21	80.16	0.049
C40F60-20	0.0018	0.15	0.9102	5.78	1.36	72.85	50.87	56.68	0.029
C40F60-16	0.0015	0.15	0.9102	5.78	1.64	86.69	41.74	62.09	0.029
C40F60-12.5	0.0013	0.15	0.9102	5.78	1.72	99.09	43.91	66.69	0.031

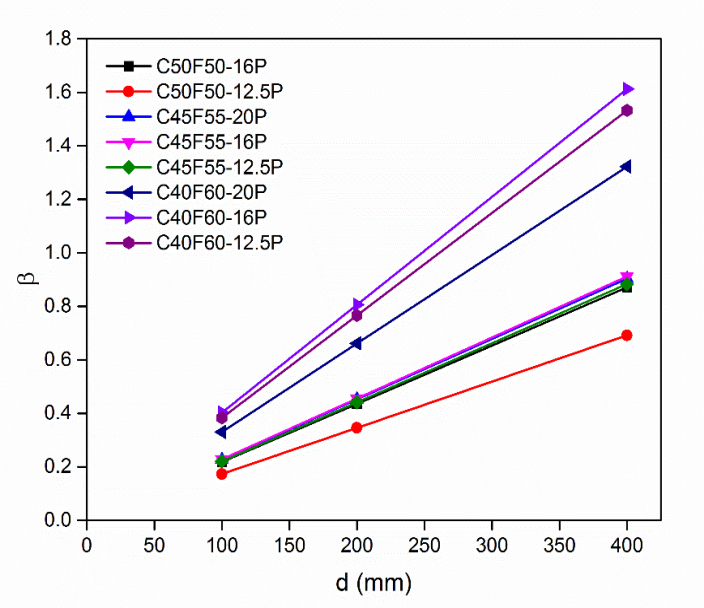

Figure 4.20 Variation of brittleness number with depth for non-fibrous self compacting concrete

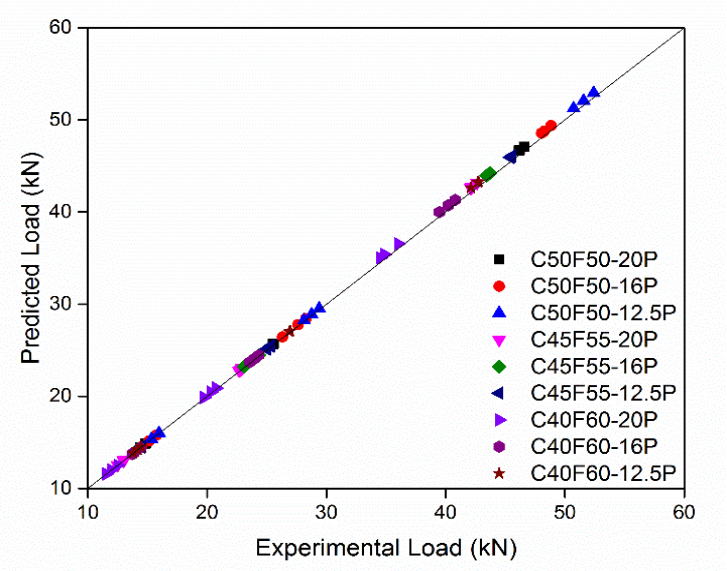

Figure. 4.21 Predicted load vs Experimental Load for non-fibrous self compacting concrete

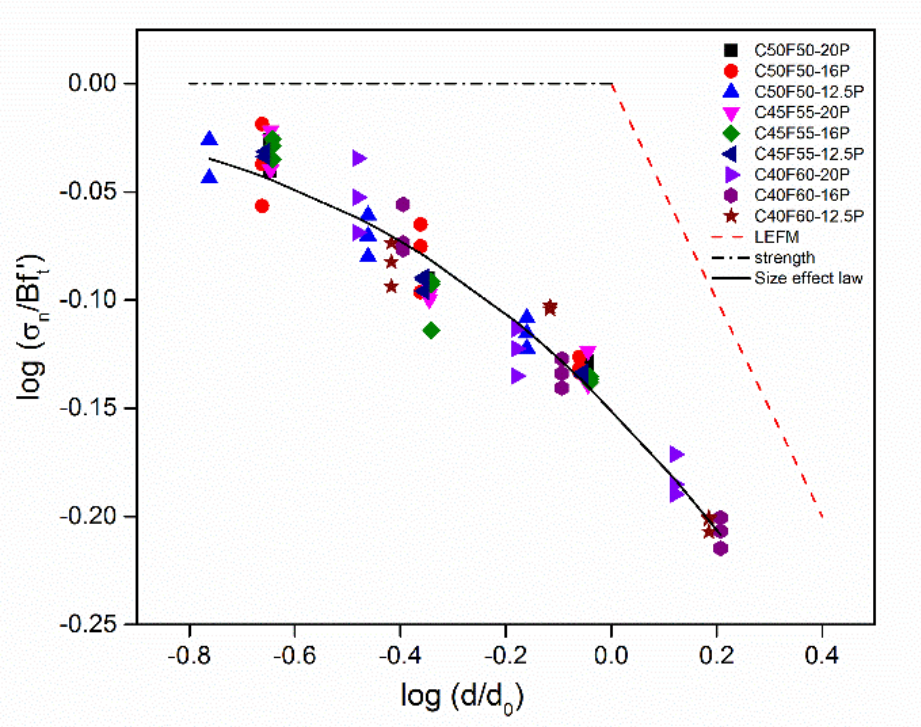

Figure 4.22. Size effect law plot for non-fibrous self compacting concrete

4.9.4. (c) Fracture properties of fibrous self compacting concrete using size effect method

The corrected peak load for fibrous self compacting concrete are tabulated in Table 4.13. The fracture properties evaluated are tabulated in Table 4.14 which were obtained based on the corrected peak load from testing the varying depth specimens under three point bend test. Based on the equation (4.2) for geometrically similar specimens, linear regression was carried out. Slope and intercept from the linear regression for the mix C50F50-20F' were shown in the figure 4.23. The fracture properties varied with the change in coarse aggregate size and quantity. The higher quantity of coarse aggregate showed higher fracture properties and for coarse aggregate sizes, the least aggregate size obtained higher fracture properties similar to non-fibrous self compacting concrete. The difference in fracture energy with the change in aggregate size from 12.5mm to 20mm was observed to be 31% decrease for 50-50, 18.8% decrease for 45-55 and 30% decrease for 40-60. Similarly, the change in aggregate size from 12.5 mm to 16mm the decrease was observed to be 8.7%, 10.34% and 14.58% for 50-50, 45-55 and 40-60 quantities respectively. And for the same coarse aggregate size of 20mm the decrease in quantity of coarse aggregate from 50-50 to 45-55, the fracture energy was decreased by 17.16% and 48.53% with the decrease from 50-50 to 40-60. Similarly, for 16mm it was about 29% and 52% for decrease in quantity by 50-50 to

45-55 and 50-50 to 40-60, respectively. The coarse aggregate size of 12.5mm showed about 32% for 50-50 to 45-55 decrease and 52% for 50-50 to 40-60 decrease. The experimental and predicted loads obtained from size effect method for fibrous self compacting concrete were plotted in figure 4.11.

Fracture toughness K_{IC} values for steel fiber self compacting concrete were tabulated in table 4.14. Similar to non-fibrous self compacting concrete, fibrous self compacting concrete also increased its K_{IC} with the increase in coarse to fine aggregate quantity. For 20mm sized coarse aggregate, increase in coarse to fine aggregate quantity from 45-55 to 50-50, K_{IC} increased by 10.56% and from 40-60 to 50-50 it was about 29.2%. Similarly for 16mm sized coarse aggregate the increase was about 18.34% and 32.06% for an increase of aggregate quantity from 45-55 to 50-50 and 40-60 to 50-50 respectively. And for 12.5mm it was about 17.84% and 29.94%.

4.9.4. (d) Brittleness number and size effect law for fibrous self compacting concrete.

As per RILEM the brittleness number (β) was plotted for varying depths in figure 4.24 for three aggregate size and quantity variations of fibrous self compacting concrete. The predicted fracture mode was nonlinear elastic fracture mechanics, as β was ranging in between 0.1 to 10.

The experimental load vs predicted load obtained from size effect method using equation (1) for fibrous self compacting concrete was shown in figure 4.25. Similar to non-fibrous self compacting concrete all the mixes of fibrous self compacting concrete were following strength criterion according to the size effect law plot in figure 4.26. It was observed that the experimental and predicted results from size effect conforms pretty well.

Table 4.13 Corrected maximum loads from size effect method of fibrous self compacting concrete

Mix Designation	Depth (mm)	corrected maximum load		
		Beam 1 (kN)	Beam 2 (kN)	Beam 3 (kN)
C50F50-20	400	49.69	49.61	50.07
	200	27.29	27.36	27.36
	100	15.83	15.87	15.35
C50F50-16	400	53.08	52.49	51.63
	200	28.13	29.53	30.23
	100	16.13	16.83	15.43
C50F50-12.5	400	55.39	54.49	56.29

	200	30.05	31.41	30.73
	100	17.03	16.35	17.03
C45F55-20	400	45.33	45.41	45.88
	200	24.25	24.40	24.54
	100	13.33	13.94	13.86
C45F55-16	400	46.73	46.89	47.04
	200	24.72	25.96	26.04
	100	15.17	15.05	14.84
C45F55-12.5	400	48.83	48.91	48.99
	200	26.73	27.13	27.06
	100	15.52	15.43	15.43
C40F60-20	400	37.63	37.24	38.86
	200	21.13	21.76	22.23
	100	12.79	12.33	13.33
C40F60-16	400	43.31	43.93	42.53
	200	25.63	26.03	25.24
	100	14.64	15.36	14.74
C40F60-12.5	400	46.03	45.33	45.95
	200	28.74	28.83	28.84
	100	14.73	15.43	15.13

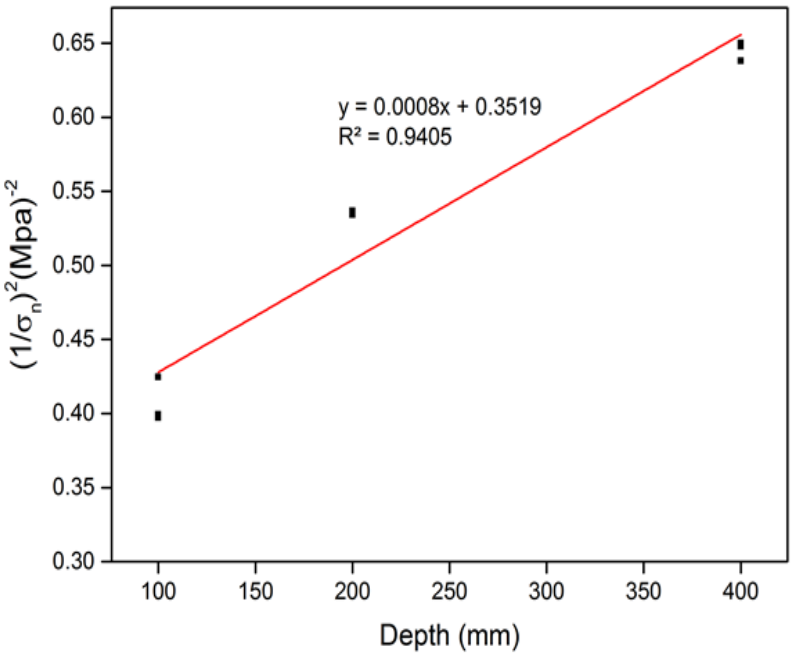

4.23. Linear Regression for the mix C50F50-20F’

Table 4.14. Fracture parameters of fibrous self compacting concrete from size effect method

Mix Designation	A	α	F(α)	g(α)	Bf_t	G_F (N/m)	C_f (mm)	K_{IC} ($N/mm^{3/2}$)	δ (mm)
C50F50-20F'	0.0008	0.15	0.9102	5.49	1.69	151.18	70.26	82.84	0.049
C50F50-16F'	0.0006	0.15	0.9102	5.49	1.75	200.74	87.24	95.65	0.063
C50F50-12.5F'	0.00054	0.15	0.9102	5.49	1.81	219.90	90.33	100.83	0.066
C45F55-20F'	0.001	0.15	0.9102	5.49	1.57	122.46	65.02	74.09	0.043
C45F55-16F'	0.0009	0.15	0.9102	5.49	1.63	135.31	67.03	78.10	0.045
C45F55-12.5F'	0.0008	0.15	0.9102	5.49	1.67	150.92	71.64	82.84	0.049
C40F60-20F'	0.0016	0.15	0.9102	5.49	1.45	77.80	47.76	58.58	0.029
C40F60-16F'	0.0013	0.15	0.9102	5.49	1.75	94.96	40.19	64.98	0.030
C40F60-12.5F'	0.0011	0.15	0.9102	5.49	1.83	111.18	43.31	70.64	0.033

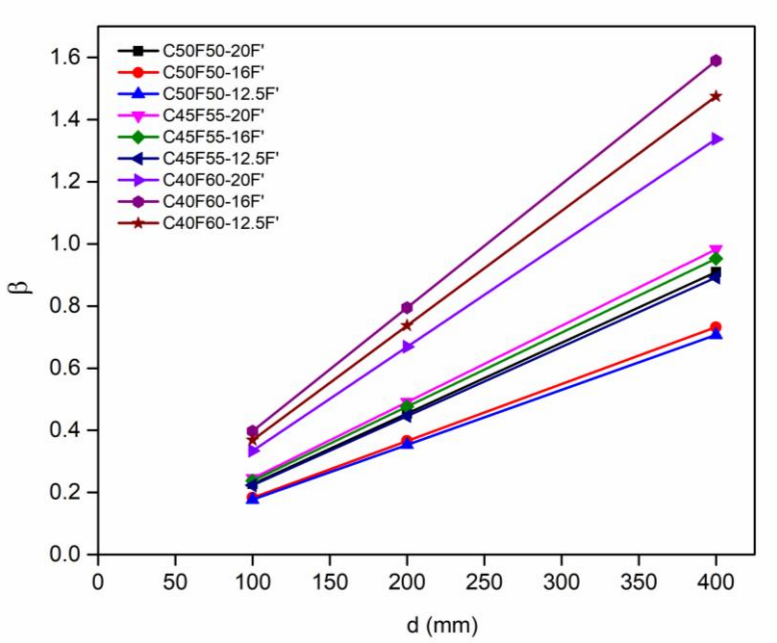

Figure 4.24. Variation of brittleness number with depth for fibrous self compacting concrete

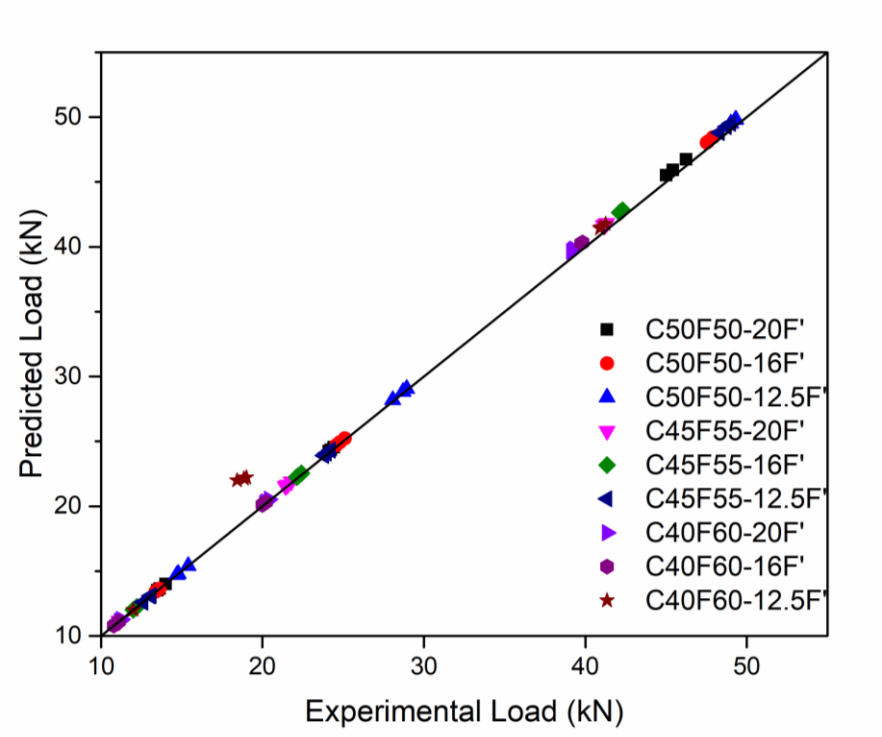

Figure. 4.25. Predicted load vs Experimental Load for fibrous self compacting concrete

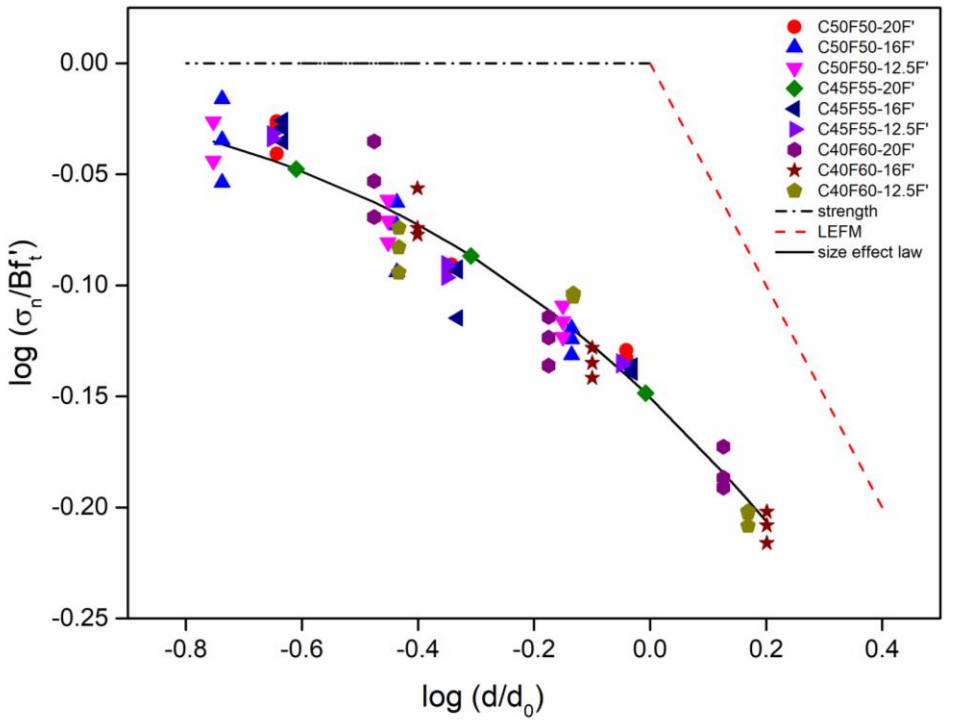

Figure 4.26. Size effect law plot for fibrous self compacting concrete

4.10. Comparison of fracture energies for non-fibrous and fibrous self compacting concrete

In figure 4.27 fracture energies were plotted for non-fibrous and fibrous self compacting concrete for three point bend test using size effect method for varying aggregate size and quantity. The fracture energy for fibrous self compacting concrete was higher than the non-fibrous self compacting concrete. The increase in fracture energy was about 10% compared to non-fibrous self compacting concrete. This increase in fracture energy was observed due to the higher peak load obtained for fibrous self compacting concrete compared to non-fibrous self compacting concrete which resulted in an increase in fracture energy.

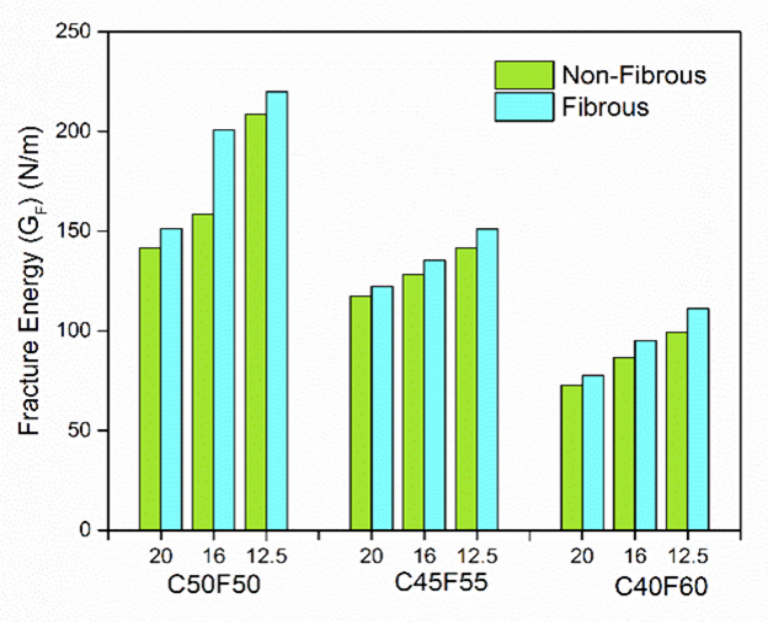

Figure 4.27 Fracture energy for non-fibrous and fibrous self compacting concrete

4.11. Wedge splitting test

The fracture properties for a wedge splitting test method are analysed using load vs crack mouth opening displacement (CMOD) plots obtained from the experimentation. The area under the load vs CMOD curves and the available ligament area for the crack to proliferate are the parameters considered for calculating the fracture properties for both non-fibrous and fibrous self compacting concrete. Load-CMOD curves for without and with guided notch were plotted for non-fibrous and fibrous self compacting concrete. The fracture properties are evaluated using the equations (4.13) - (4.15)

4.11.1 Non fibrous self compacting concrete

Figure 4.28 – 4.30 shows the load vs CMOD curves for specimens without guide notch for all the three coarse to fine aggregate quantities. Maximum splitting force and evaluated fracture properties for non-fibrous self compacting concrete with three coarse aggregate sizes and quantities were tabulated in table 4.13. Among all the three sizes of coarse aggregate, the least size i.e., 12.5mm coarse aggregate showed maximum splitting force and least fracture energy whereas 20mm coarse aggregate size showed higher fracture and least splitting force. After peak load there was abrupt drop in the load-CMOD curve due to the sudden failure of the specimen for least size of coarse aggregate i.e., for 12.5mm. This failure mechanism is due to the aggregate rupture for smaller size aggregate specimens and aggregate pull out for larger size aggregate. The coarse aggregate size 20mm achieved highest fracture energy and least splitting force. Crack proliferation path for a 20mm size coarse aggregate occurs by pulling out of the aggregate from matrix which requires higher energy. The fracture energy (G_F) for C50F50 coarse aggregate quantity, the higher coarse aggregate size 20mm has attained highest energy consumption having G_F value of 64.43N/m followed by 16mm with 54.17N/m then 12.5mm with 38.26N/m. The increase in fracture energy was about 29.37% with an increase in aggregate size from 12.5mm to 16mm and with an increase of aggregate size from 16mm to 20mm fracture energy enhanced by 15.92%. Similarly for C45F55 fracture energy enhanced by 17.63% with an increase of aggregate size from 16mm to 12.5mm and for aggregate size increment from 12.5mm to 16mm increased fracture energy by 32.8%. And for C40F60 quantity fracture energy enriched by 36.25% and 28.82% for an increase of aggregate size from 12.5mm to 16mm and 16mm to 20mm respectively.

Among all the sizes of coarse aggregate the higher coarse to fine aggregate content has attained higher fracture energy. This is due to the fact that the higher content of aggregates provide large number of aggregate particles providing large surface area, thereby resulting bridging and toughening of the particles which requires higher energy for the crack to proliferate. For 20mm size coarse aggregate the fracture energy G_F was increased by 8.98% and 19.81% with increase from coarse aggregate quantity from C45F55 to C50F50 and from C40F60 to C50F50 respectively. Similarly for 16mm the fracture energy was enhanced by 10.83% and 32.12% with increase from coarse aggregate quantity from C45F55 to C50F50 and from C40F60 to C50F50 respectively. The

fracture energy was enriched by 15.21% and 38.73% for 12.5mm sized coarse aggregate for coarse aggregate quantity increase from C45F55 to C50F50 and from C40F60 to C50F50 respectively.

Figure 4.31– 4.33 shows the load CMOD curves for non-fibrous self compacting concrete for specimens with guide notch. Specimens with guide notch creates a well-defined vertical path and reduces the ligament area. Therefore, the energy consumption is less compared to specimens without guide notch. The splitting force and fracture energy for a guided notch specimen were less compared to the without guided notch specimens. A similar trend was observed in with guided notch specimens also with respect to the splitting force and fracture energy. Despite having lesser defined area, for lower size aggregates (12.5mm), the crack follows weaker path through the aggregate leading to a sudden drop in the post peak behaviour. In contrast, specimens with large size aggregates attain gradual decrease in the loading curve after post peak due to the bridging of aggregates. The fracture energy enhanced with the increase in aggregate size and quantity. For C50F50 quantity increase in coarse aggregate from 12.5mm to 16mm and 20mm increased fracture energy by 26.61% and 36.4%. Similarly, for C45F55 and C40F60 quantities it was 34.12%, 42.65% and 34.38%, 53.29% respectively.

For 20mm size coarse aggregate the increase in aggregate quantity from C45F55 to C50F50 and from C40F60 to C50F50 increased in fracture energy was about 11.09% and 19.35% respectively. Whereas for 16mm size coarse aggregate the increase in fracture energy was 10.68% and 33.76% for increase in aggregate quantity from C45F55 to C50F50 and from C40F60 to C50F50 respectively. While for 12.5mm coarse aggregate it was about 19.82% and 40.77%.

Table 4.15. Fracture properties of non fibrous self compacting concrete using wedge splitting test

Mix Designation	Without Guide Notch				With Guide Notch			
	F_{sp} (kN)	G_F (N/m)	K_{IC} (N/mm$^{3/2}$)	l_{ch} (mm)	F_{sp} (kN)	G_F (N/m)	K_{IC} (N/mm$^{3/2}$)	l_{ch} (mm)
C50F50-20P	6.50	64.43	51.4	40.7	4.7	57.35	48.5	36.2
C50F50-16P	6.70	54.17	47.6	33.3	4.78	49.70	45.6	30.6
C50F50-12.5P	6.90	38.26	40.3	23.0	4.8	36.47	39.3	21.9
C45F55-20P	6.34	58.64	48.6	37.3	4.66	50.99	45.3	32.5
C45F55-16P	6.50	48.30	44.4	30.8	4.7	44.39	42.6	28.3
C45F55-12.5P	6.82	32.44	36.8	20.1	4.8	29.24	34.9	18.1
C40F60-20P	5.39	51.66	45.5	35.0	3.86	46.25	43.1	31.3
C40F60-16P	5.50	36.77	38.5	24.3	4.07	32.92	36.4	21.8
C40F60-12.5P	5.79	23.44	30.9	15.1	4.11	21.60	29.7	14.0

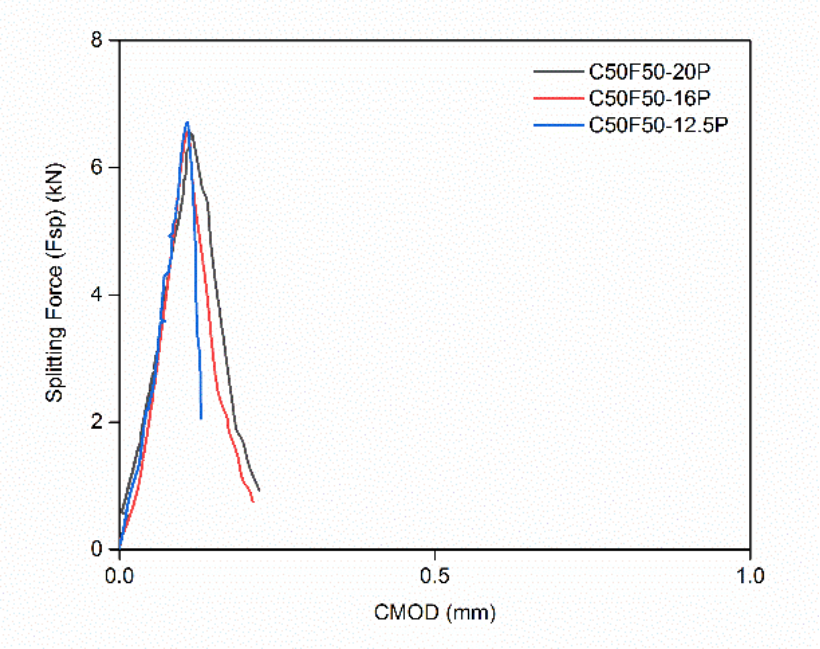

Figure 4.28. Load-CMOD curve of without guide notch specimen for C50F50 non-fibrous self compacting concrete

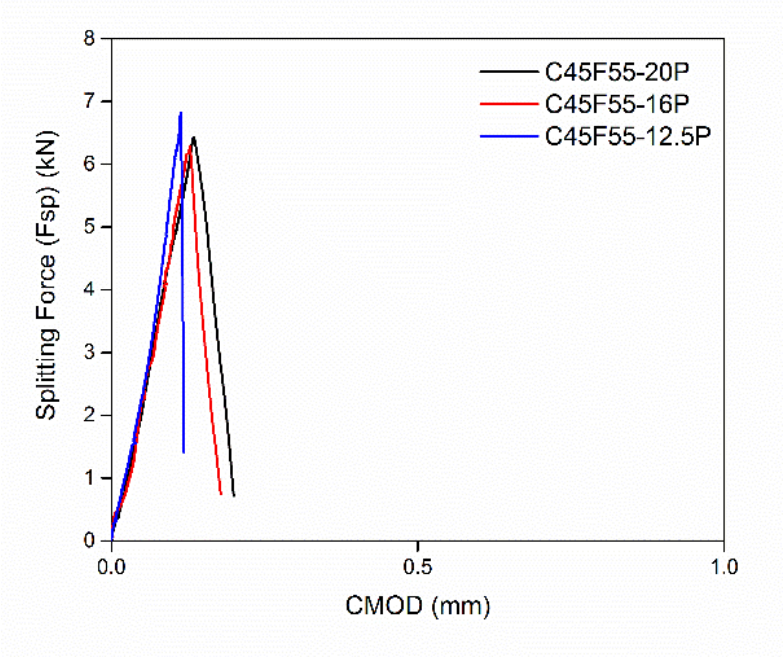

Figure 4.29. Load-CMOD curve of without guide notch specimen for C45F55 non-fibrous self compacting concrete

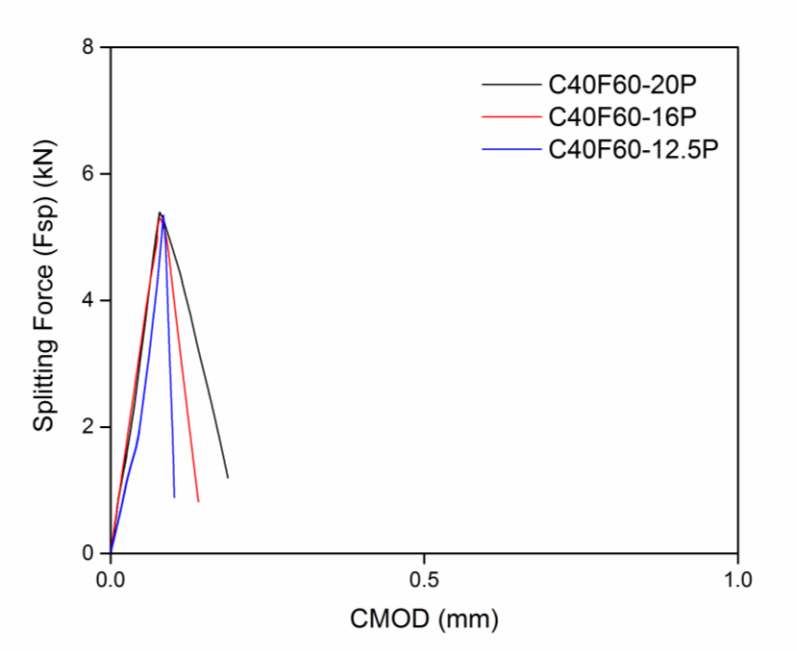

Figure 4.30. Load-CMOD curve of without guide notch specimen for C40F60 non-fibrous self compacting concrete

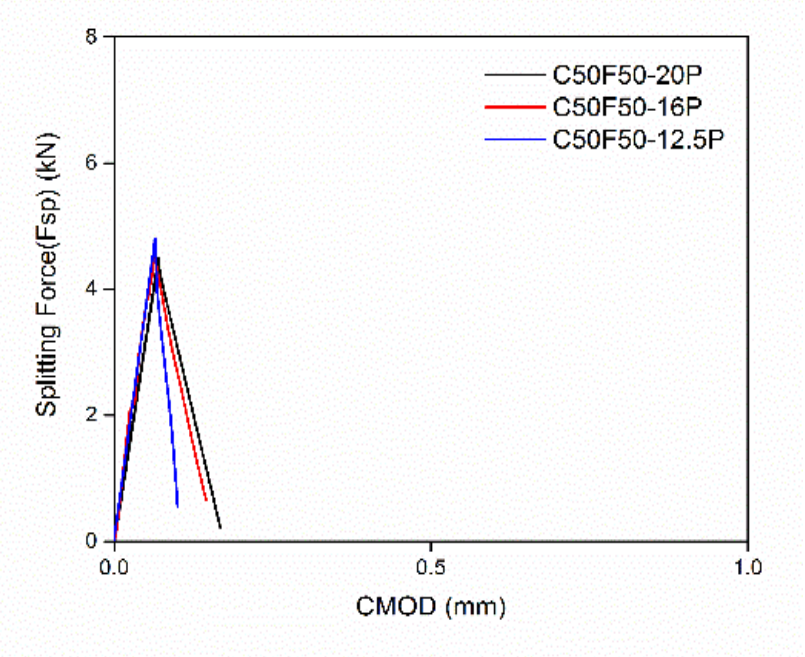

Figure 4.31. Load-CMOD curve of with guide notch specimen for C50F50 non-fibrous self compacting concrete

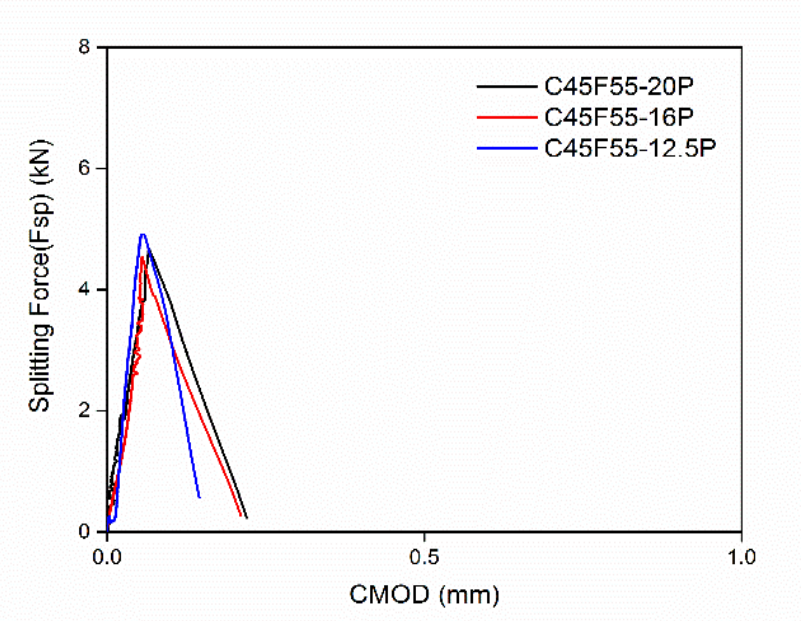

Figure 4.32. Load-CMOD curve of with guide notch specimen for C45F55 non-fibrous self compacting concrete

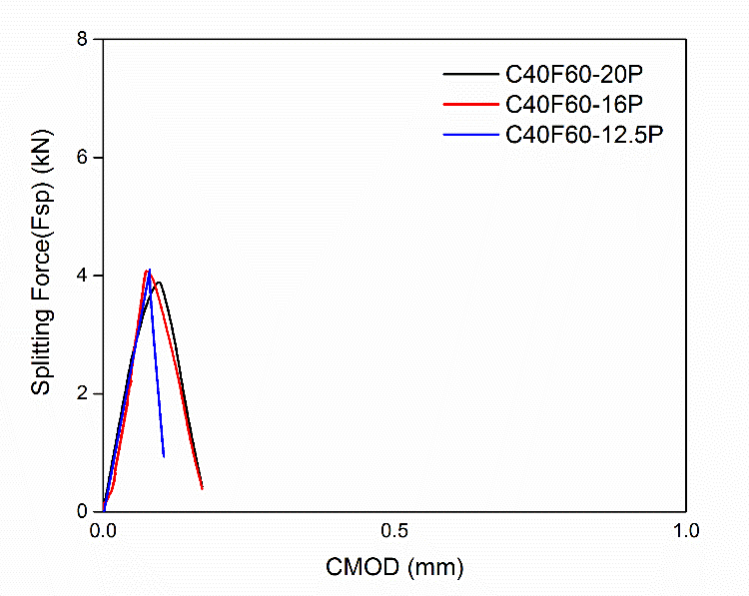

Figure 4.33. Load-CMOD curve of with guide notch specimen for C40F60 non-fibrous self compacting concrete

4.11.2. Fibrous self compacting concrete

Figures 4.34 – 4.36 shows the graphs of splitting force vs. CMOD for different quantities and sizes of coarse aggregate of without guide notch specimens of fibrous self compacting concrete. The maximum splitting force for each of the mixes were presented in Table 4.14. In each quantities of coarse aggregate, it was observed that the splitting force obtained was maximum for 12.5mm aggregates compared to 20mm and 16mm coarse aggregate based specimens. The post peak behaviour has significantly improved with large size aggregate based specimens i.e., 20mm. This is because of occurrence of crack proliferation around the coarse aggregate i.e., at interfacial transition zone and the load drop after post peak was gradual. In case of 12.5mm size, the path of the failure was through the aggregate and lead to a sudden drop in the loading curve after reaching the maximum splitting force. However, the steel fibers resists the crack propagation and thus modifies the nature of failure from brittle to ductile.

The energy required per unit area of the crack surface to open, defined as fracture energy (G_F) was calculated for mixes with three different quantities and sizes of coarse aggregate. The G_F values for without guide notch specimens were presented in Table 4.14. For Mix C50F50-20F, the fracture energy was enhanced from 2113.3 N/m to 3615.2 N/m compared to C50F50-12.5F, while

for C50F50-16F, it was 2717.5 N/m. The similar increase in fracture energy with increase in size of coarse aggregate was observed for the other quantities of aggregates (C45F55 and C40F60). The increase in G_F with increase in size of aggregate is due to the improved area of splitting force.

The splitting force vs. CMOD plots for with guide notch specimens were represented in figure 4.37 - 4.39 for three coarse aggregate size and quantities. For Mix with aggregate quantity C50F50, the fracture energy values obtained are 3155.0N/m, 2314.1 and 2059.2N/m for sizes 20, 16 and 12.5mm respectively. With the decrease in the maximum size of aggregate from 20mm to 16mm, the decrease in G_F was 26.7% while, with reduction from 16mm to 12.5mm aggregates, the drop was 34.7%. It was also noticed that the decrease in quantity of coarse aggregate by 10% (50% to 40%) reduced the fracture energy by 20.8%, 39.6% and 40.9% with sizes 20mm, 16mm and 12.5mm. Similar observation was made in other quantities and sizes of coarse aggregates.

Figure 4.40 shows the failure pattern of specimens without guide notch under wedge split test. It can be noticed that the crack propagation doesn't follow a well-defined path during splitting and the crack tends towards horizontal for a without guided notch specimens. Figure 4.41 shows the failure pattern of specimens with guide notch under wedge split test.

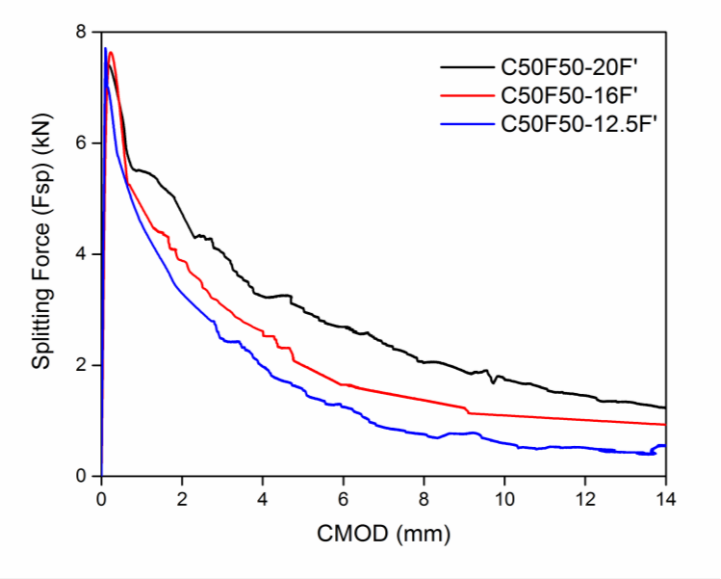

Figure 4.34. Load-CMOD curve of without guide notch specimen for C50F50 fibrous self compacting concrete

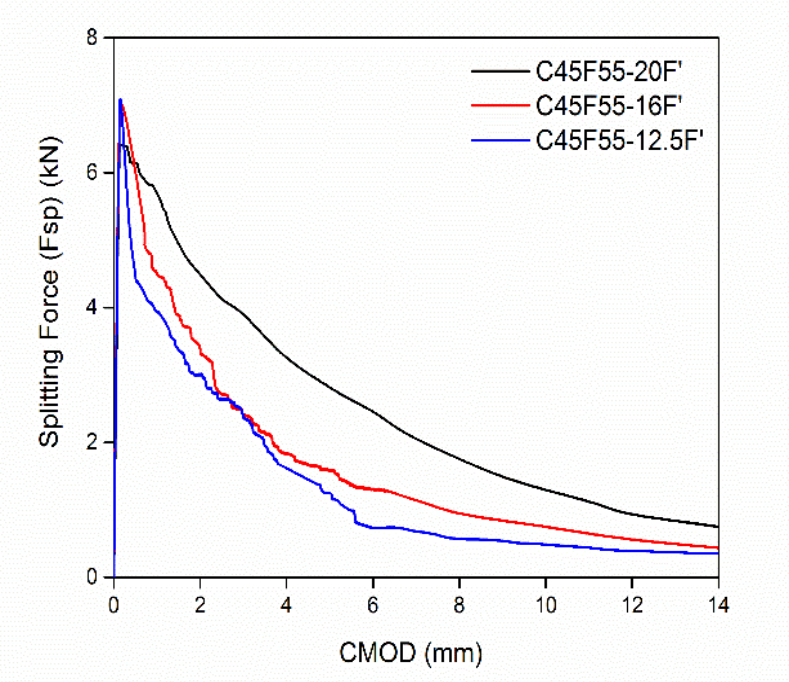

Figure 4.35. Load-CMOD curve of without guide notch specimen for C45F55 fibrous self compacting concrete

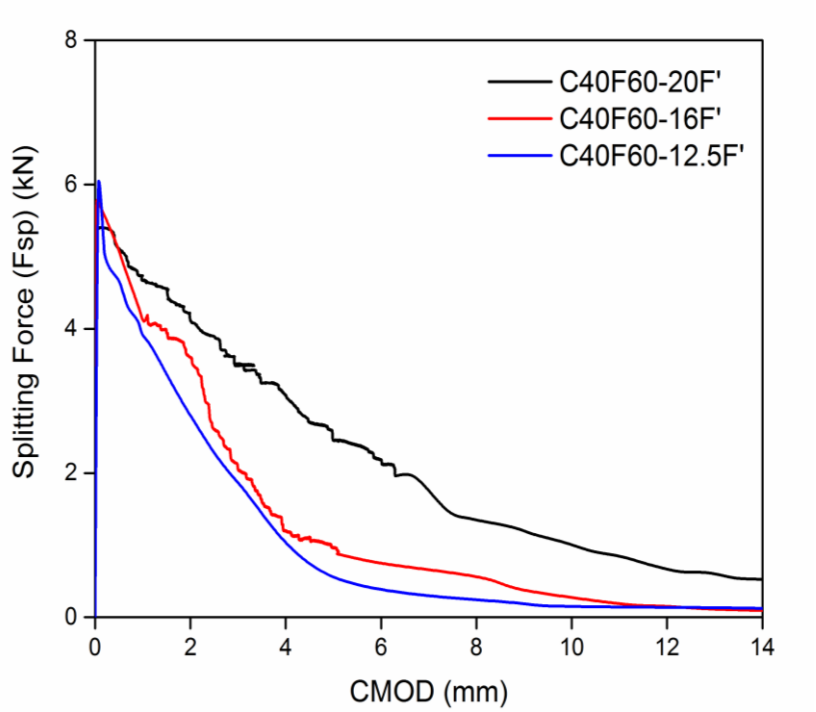

Figure 4.36. Load-CMOD curve of without guide notch specimen for C40F60 fibrous self compacting concrete

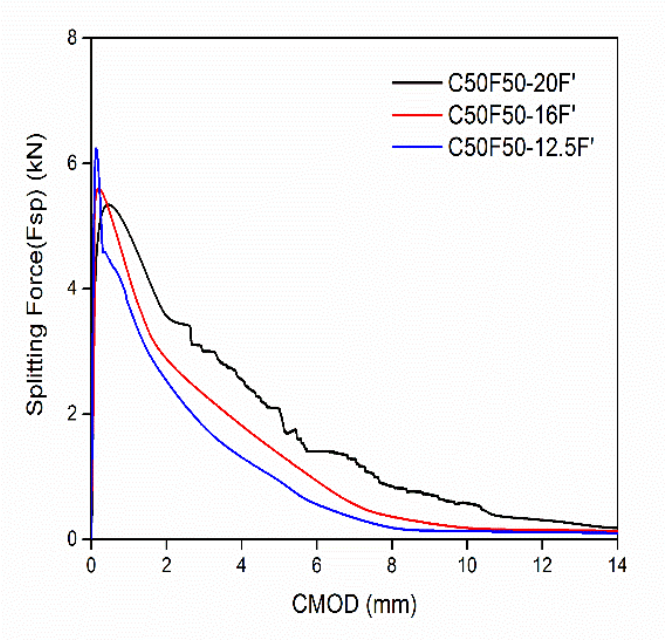

Figure 4.37. Load-CMOD curve of with guide notch specimen for C50F50 fibrous self compacting concrete

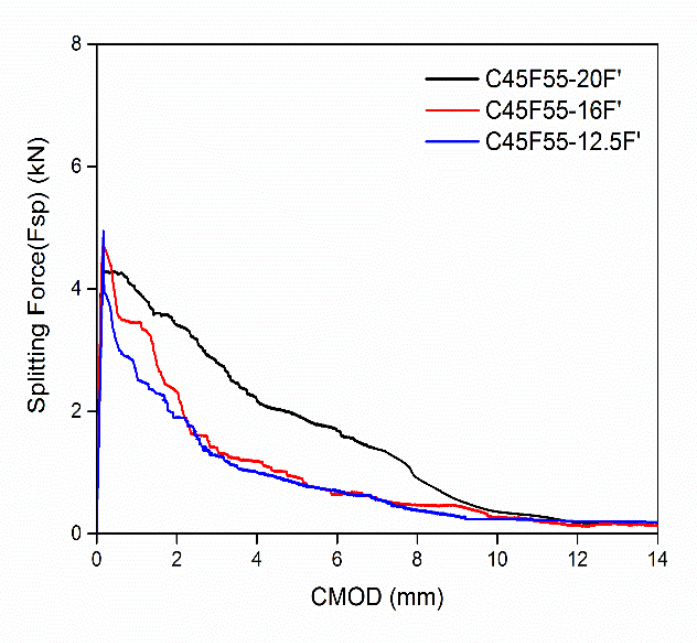

Figure 4.38. Load-CMOD curve of with guide notch specimen for C45F55 fibrous self compacting concrete

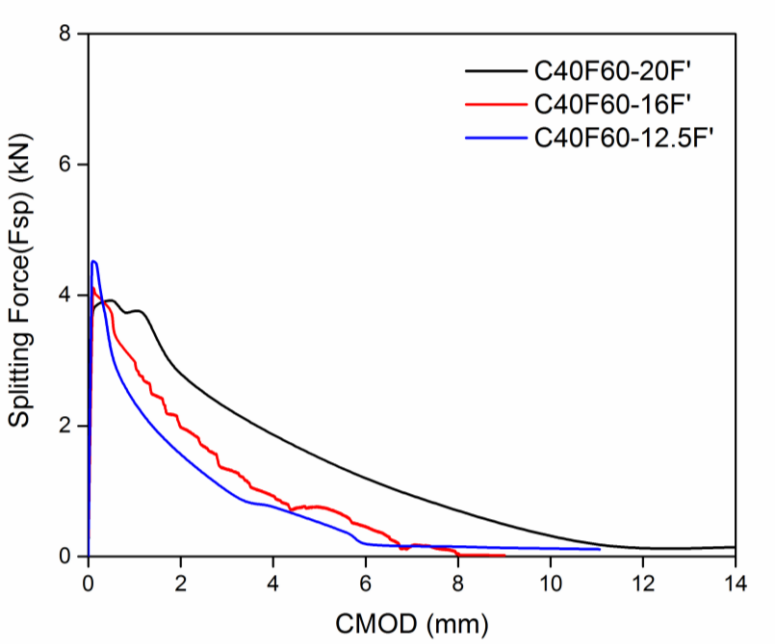

Figure 4.39. Load-CMOD curve of with guide notch specimen for C40F60 fibrous self compacting concrete

Table 4.16. Fracture properties of fibrous self compacting concrete using wedge splitting test

Mix Designation	Without Guide Notch				With Guide Notch			
	F_{sp} (kN)	G_F (N/m)	K_{IC} (N/mm$^{3/2}$)	l_{ch} (mm)	F_{sp} (kN)	G_F (N/m)	K_{IC} (N/mm$^{3/2}$)	l_{ch} (mm)
C50F50-20F	7.32	3615.2	405.1	2003.5	5.22	3155.0	378.4	1748.5
C50F50-16F	7.46	2717.5	351.9	1463.4	5.40	2314.1	324.8	1246.2
C50F50-12.5F	7.65	2113.3	312.6	1219.7	5.60	2059.2	308.5	1188.4
C45F55-20F	5.75	3192.9	378.3	1848.4	4.35	2931.8	362.5	1697.2
C45F55-16F	5.78	2126.4	309.6	1196.7	4.67	1886.8	291.6	1061.9
C45F55-12.5F	5.97	1736.1	281.0	974.6	4.94	1655.6	274.4	929.4
C40F60-20F	5.75	2747.9	348.1	1677.3	3.92	2497.7	331.9	1524.5
C40F60-16F	5.78	1602.3	266.9	941.4	4.11	1397.5	249.3	821.1
C40F60-12.5F	5.97	1330.6	244.4	771.3	4.52	1216.9	233.7	705.4

Figure 4.40. Failure pattern of specimens without guide notch

Figure 4.41. Failure pattern of specimens with guide notch

4.12. Comparison of the size effect method and wedge splitting test

The fracture energies evaluated from the three point bend test and wedge splitting test differed a lot. Though the size effect method is size independency method, the discrepancy in the method is that it uses only the peak load from the experimental data for the analysis. Figure 4.42 represents the fracture energy evaluation from size effect method and wedge splitting test. The drawback for size effect method is that for a fibrous concrete the effect of the fiber is not considered i.e., post peak, as it considers only peak load for evaluating fracture properties. Due to this the difference in the two method varied much i.e., wedge splitting test method obtained higher fracture energy compared to three point bend test using size effect method. And also, for an aggregate variation the increase in aggregate size for size effect method showed less fracture energy whereas for wedge splitting test increase in aggregate size had an increase in fracture energy. This shows that size effect method gets effected with respect to aggregate properties also. The size effect method does not consider the aggregate property for evaluating the fracture parameters. Wedge splitting test

indicated better result as maximum aggregate size i.e., 20mm has higher fracture energy as it makes the crack proliferation path tortuous due to pull-out of the aggregate from the matrix. The maximum load in both the test results revealed that 12.5mm coarse aggregate size attained higher peak load and 20mm achieved lesser peak load. The trend for other parameters i.e., stress intensity factor and brittleness number showed similar result for both size effect method and wedge splitting test.

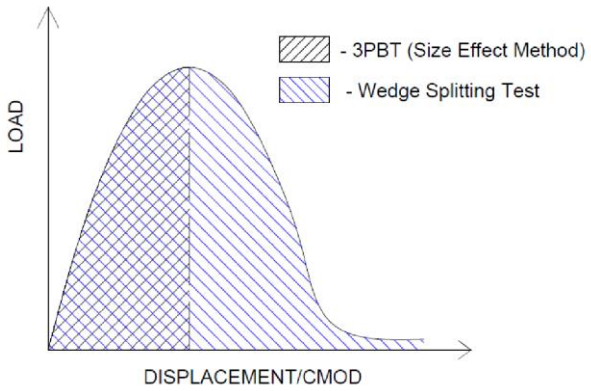

Figure 4.42. Fracture energy representation for size effect method and wedge splitting test from experimental data

4.13. Conclusions

A detailed investigation on fracture parameters of non fibrous and fibrous SCC by size effect method and wedge splitting test concluded the following salient points.

- Size Effect Method analysis for three point bend test underestimated fracture properties of fibrous SCC in comparison to non-fibrous SCC.
- The fracture energy for non-fibrous and fibrous self compacting concrete from size effect method reveals that the higher quantity of coarse aggregates (50-50) has higher fracture energy, while maximum coarse aggregate sized specimen (20mm) achieved lesser fracture energy.
- The non-fibrous and fibrous self compacting concrete with higher coarse to fine aggregate quantities and least coarse aggregate size approached strength criterion from size effect law.

- The brittleness number indicated a non-linear fracture mechanics for both non-fibrous and fibrous self compacting concrete.
- In case of size effect method, the influence of aggregate properties was under estimated in evaluating the fracture properties, as the method uses only peak load for analysis.
- The splitting force was maximum for both non fibrous and fibrous SCC specimens with aggregate size 12.5mm and 50-50 aggregate quantity.
- The fracture energy was higher for fibrous SCC and the post peak was enhanced by the inclusion of steel fibers whereas for non-fibrous SCC, the post peak had a sudden drop leading to catastrophic failure.
- Fracture energy was maximum for 20mm size of coarse aggregate based specimens for all the CA-FA quantities.
- Mixes with higher coarse aggregate content i.e., 50-50 has higher fracture energy then followed by 45-55 and 40-60 volume of CA-FA.
- The specimens without guide notch attained maximum splitting force compared to specimens with guide notch. This is same for all sizes and all quantities of C.A.
- The maximum splitting force in specimens without guide notch can be attributed to indefinite failure path and more ligament area which assisted in attaining better fracture energy.

The studies on fracture properties of non fibrous and fibrous self compacting concrete using three point bend test and wedge splitting test are influenced by the aggregate properties. Therefore, internal behaviour is needed to be examined. In chapter 5, the internal failure behaviour was examined using digital image processing technique.

CHAPTER 5

INTERNAL FAILURE BEHAVIOUR OF SCC BASED ON IMAGE ANALYSIS

CHAPTER 5
INTERNAL FAILURE BEHAVIOUR OF SCC BASED ON IMAGE ANALYSIS

5.0 General

Based on the experimental evaluation of fracture properties using wedge splitting test reveals that coarse aggregate size and quantity effects the crack proliferation path. The crack proliferation path was predicted as transgranular for smaller size aggregate and intergranular failure for larger size aggregates. In order to predict this internal failure behaviour, Digital Image Processing technique was chosen. Digital Image processing technique, an image based technique that is performed on an image in order to extract some useful data. For the present study computed tomography was chosen to study the internal failure behaviour of the self compacting concrete. Often other image based analysis like digital image correlation (DIC), optical microscopy and scanning electron microscopy have their own limitations like limited specimen size, repeatability and 2D surface studies. All these limitations can be overcome by the Computed Tomography i.e., CT scan.

5.1. Introduction

The internal failure behaviour was studied for wedge splitting test specimen for non-fibrous and fibrous self compacting concrete. As the fracture properties vary with the properties of the bridging materials, the present study was focused on the quantification of the failure causing ingredients. The internal failure was quantified using images obtained from the computed tomography of wedge splitting test specimen. For the study aggregate size and aggregate quantity was varied to evaluate the fracture properties for both non-fibrous and fibrous self compacting concrete, so that the aggregate size and quantity were quantified. The detailed analysis procedure is discussed in the subsequent sections.

5.2. Experimental Procedure for Computed Tomography

Scanning studies were done on wedge splitting test specimens at RADAR diagnostic centre, Warangal, India, on a TOSHIBA®, Alexion (Model). The properties of the scanning equipment and the reconstructed specimen dimension were shown in Table.6.1. A total of 270 images (± 15) were obtained from scanning each of the specimen, which were in DICOM (Digital imaging and

communication in medicine) format. DICOM images obtained for each data set were further analysed by image analysis3.

Table 5.1. Computed Tomography specification for 3D image analysis

X-ray source		Exposure time	Voxel size (l x b x d)			Reconstructed Specimens Volume (L x B x D)		
Voltage (KV)	Current (mA)	(ms)	(mm)	(mm)	(mm)	(mm)	(mm)	(mm)
135	200	750	0.56	0.56	0.56	150	150	150

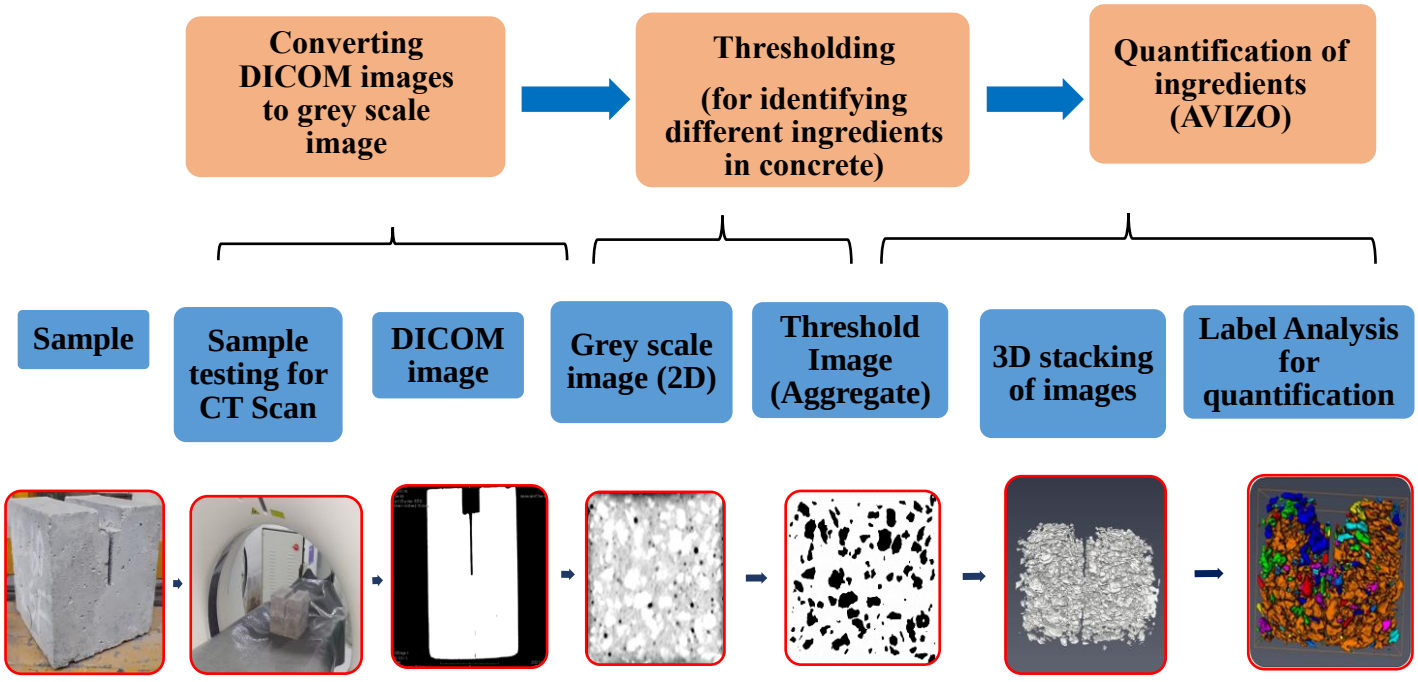

Figure 5.1 Flow chart for sequence of steps involved in image analysis using computed tomography

Figure 5.1. shows the sequence of steps involved in image analysis using Computed Tomography (CT scan). DICOM images obtained from the CT scan are raw images which cannot be used for analysis for desired properties. Therefore, these DICOM images are converted to readable form i.e., grey scale images using HOROS® software. To capture the exact scale of the specimen for the DICOM image, the scale is set to actual. The grey scale images obtained from HOROS® software

are in the form of .tiff. The obtained .tiff images from HOROS® software were imported into an open source software Fiji® using the image sequence option and the voxel properties were assigned to the data set. The data set of .tiff files were further analysed to separate the parameters such as Coarse aggregate, Fibers, Matrix, pores and fractures in the specimen. Identification of each of the ingredients of the concrete was done by thresholding in Fiji® software. A region of interest (ROI) was chosen, and parameters of interest were separated using Otsu's method of threshold and stored as various data sets of coarse aggregate, fiber, matrix, pores and fractures present in the specimen. Otsu's method of thresholding was selected, as it can identify an optimal threshold values automatically and stably, not based on the differentiation (local property), but on the integration (global property) of the histogram. Each parameter of interest was stored as data set for further analysis using Fiji® and AVIZO®. Thresholding was done for each 2D slice and converted to .tiff images which are further analysed for 3D to quantify the aggregate and fibers. 3D analysis and quantification of coarse aggregate and fibers were done using AVIZO® software.

The separated datasets for coarse aggregate, fiber, matrix, pores and fractures present in the samples was quantified using AVIZO® software. Each individual data set was imported into AVIZO® and voxel parameters were assigned, in order to determine the exact size of the materials present in the non-fibrous and fibrous self compacting concrete. Figure 5.2. shows the sequence of steps involved for quantification of coarse aggregate and fiber in AVIZO® software. The major steps for analysis in AVIZO® software are interactive thresholding, label analysis, analysis filter and sieve analysis for quantification. Interactive thresholding was used to separate the objects like matrix, cracks, aggregate and fibers. Label analysis module was used to calculate the area, volume, equivalent diameter. The diameter of the particle was calculated using the equation 5.1. This helps in quantifying the aggregate particle distribution.

$$\text{Equivalent diameter} = \sqrt[3]{\frac{6*Volume\ 3D}{\pi}} \qquad \text{Eq. (5.1)}$$

Analysis filter, to visualize only particles which Volume3d belongs to a specified range. Sieve analysis was used to define a set of value ranges that can then be used for displaying a histogram using this distribution. Apart from these major quantification modules there are few basic modules which are to be performed like bounding box, ortho slice and volume rendering. Bounding box is assigned to the data set, ortho slice is to view each of the 2D slice in all three directions i.e. x, y

and z for a 3D stacked image. Volume rendering option is for visualizing the 3D stacked images for each of the data sets presenting thresholded ingredients.

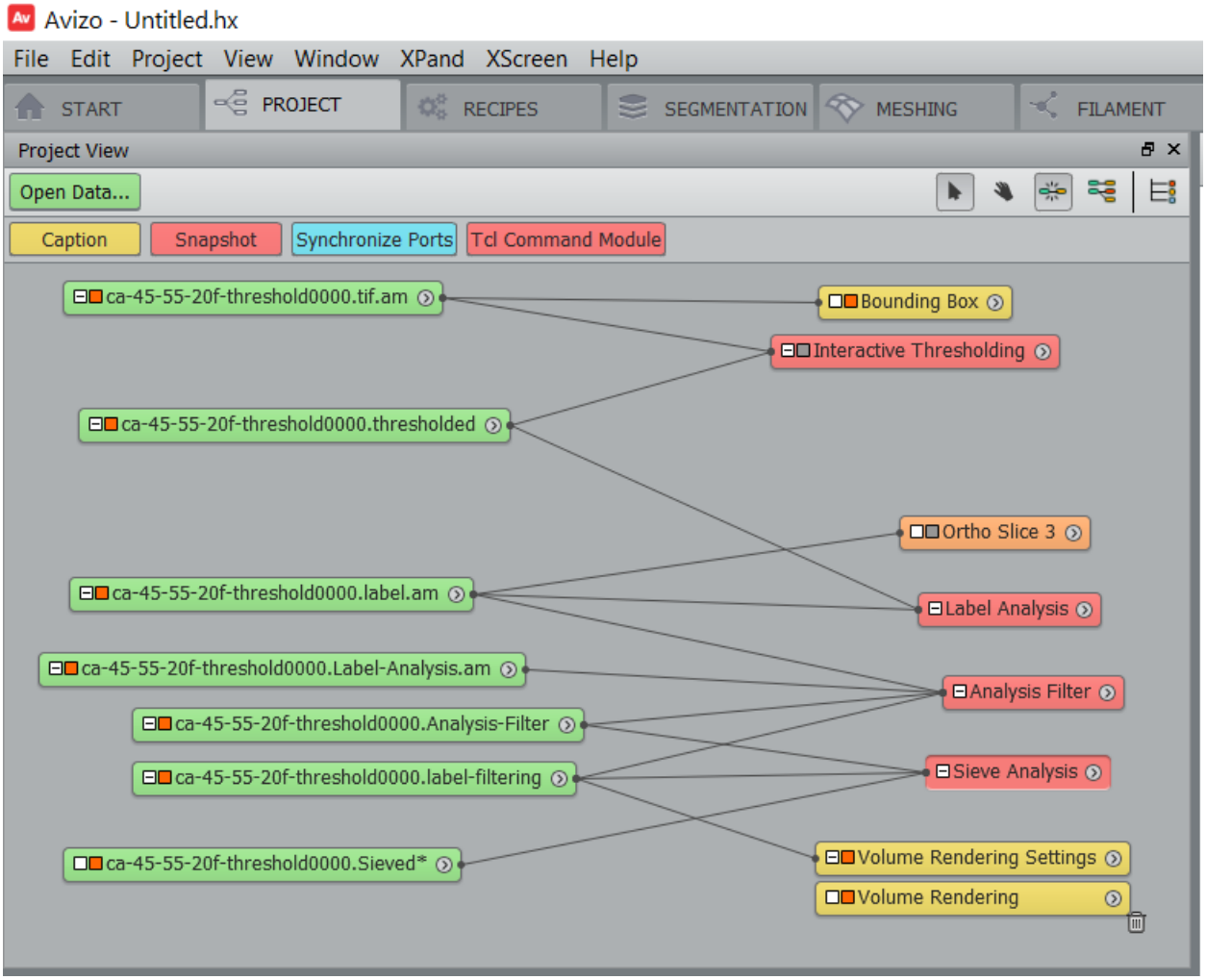

Figure 5.2. AVIZO software showing the sequence of steps for analysis

5.3. Specimen details for CT scan

For CT scan study, wedge splitting test specimens with mixes having coarse aggregate size of 20mm and 12.5mm with aggregate quantities of 45-55 and 40-60 were chosen to quantify the aggregates causing failure behaviour. Along with non-fibrous specimens, the specimens with above specified mixes for fibrous self compacting concrete were considered for the study to quantify the fibers causing failure. As shown in figure 5.3(a) the region of interest (ROI) for non–fibrous self compacting concrete was selected from the tip of the notch to the bottom of the specimen viz., in between the two red lines. And for fibrous self compacting concrete the region

of the interest chosen was middle region from the tip of the notch to the bottom of the specimen as represented in figure 5.3(b). Hence an ROI 75 x 150 x 150 mm for non-fibrous self compacting concrete and 75 x 30 x 150 mm was considered and further analysed to quantify aggregates and fibers

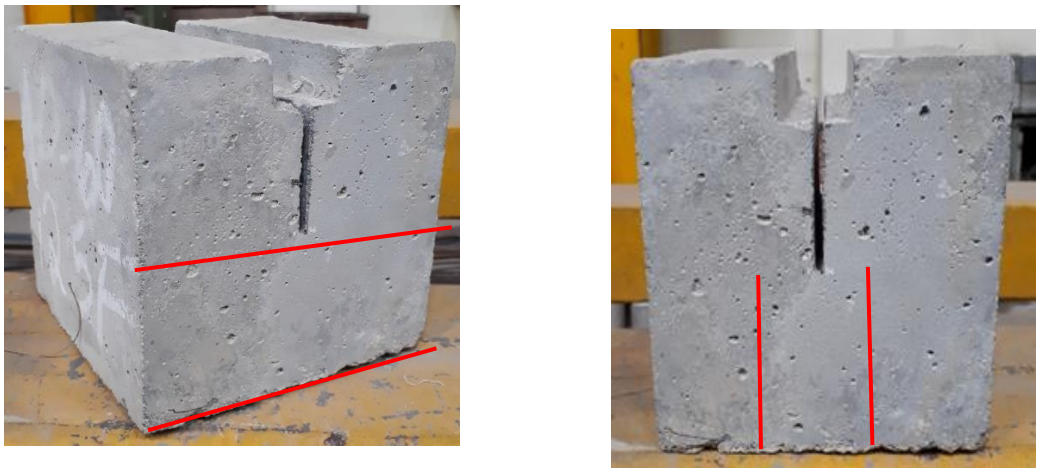

(a) Non-fibrous self compacting concrete (b) Fibrous self compacting concrete

Figure 5.3 Representation of region of interest (ROI)

5.4. Analysis and interpretation of results

5.4.1. 2D Image Analysis

Two datasets of image for each of the mix are obtained from high resolution computed tomography for before and after wedge splitting test of non-fibrous and fibrous SCC. Images obtained from CT scan are a stack of 2D slices taken one after the other, across the depth of the specimen. These 2D images are placed one over the other, for 3D visualization which represents the entire specimen. DICOM 2D images converted to grey scale, which are in .tiff format are analysed by thresholding each of the data sets. Each of the 2D slices represent the constituents present in SCC specimens i.e., coarse aggregate, pores (air voids), Matrix (PC+fine aggregate), steel fiber, distributed randomly in the hardened SCC specimen. Each 2D slices are analysed individually, in order to obtain the crucial information of coarse aggregate and steel fiber that participated in absorbing the fracture energy in wedge splitting test. These thresholding values depend on the ingredients present in the concrete. The grey scale image, an 8-bit image has a pixel ranging from 0-255 and it is dependent on the density of the material. For non-fibrous and fibrous self compacting concrete the histograms showing the range of the thresholding values was represented in the figure 5.4.

A probe line was drawn on 2D slice image for both the non-fibrous and fibrous self compacting concrete as shown in figure 5.4 (a) and (c). The grey scale value was represented on y- axis and probe length on x-axis. Higher grey scale values represented on the y-axis are an indication that the material is highly dense, while the lower grey scale values on y-axis is an indication that the material is highly porous. The variation of grey scale value depends on the density of the ingredient in which probe line is passing through. The range for pore, matrix, coarse aggregate and fiber was in between 0-255. The X-rays pass through the pore at a lower grey scale value while highest was observed for coarse aggregate and fiber. The registered grey scale value for pores is '0' and '255' for coarse aggregate and steel fibers from the figure 5.4 (b) and (d) histograms of non-fibrous and fibrous self compacting concrete. Figure 5.5 shows the 2D image slice of the non-fibrous self compacting concrete showing grey scale image in figure 5.5. (a) and in figure 5.5. (b) shows aggregates in thresholded image. The data sets obtained before and after testing consists of various materials like coarse aggregate, pores, matrix and steel fiber. Care has to be taken to identify the coarse aggregate and steel fiber present in fibrous specimens, as it is difficult to separate these two values based on the threshold values. Separation of the steel fiber and coarse aggregate is done manually after Otsu's methods of filtering is applied for the images. As grouping of steel fibers take place, differentiation between a steel fiber and CA is hard to make by artificial thresholding.

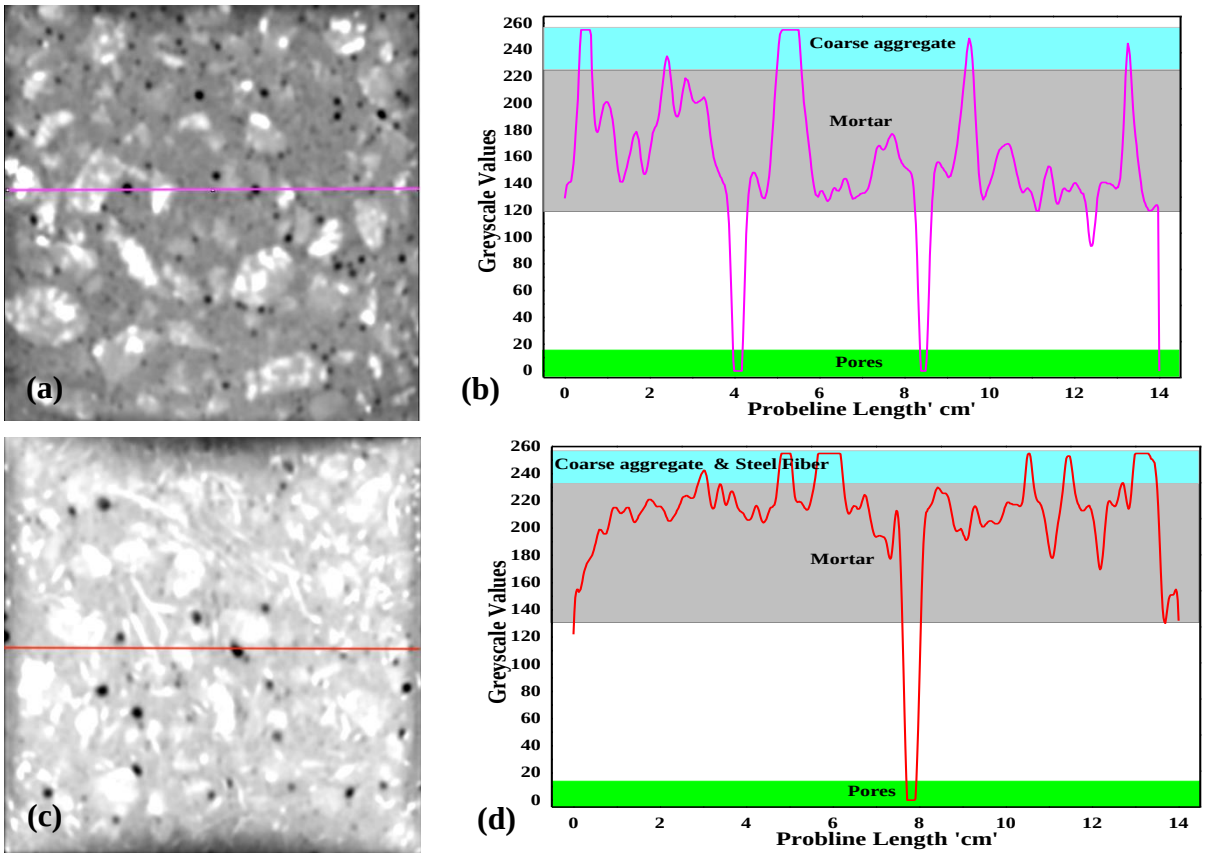

Figure 5.4 (a) 2D image of non-fibrous SCC (b) Histogram of the non-fibrous SCC (c) 2D image of fibrous SCC (d) Histogram of the fibrous SCC.

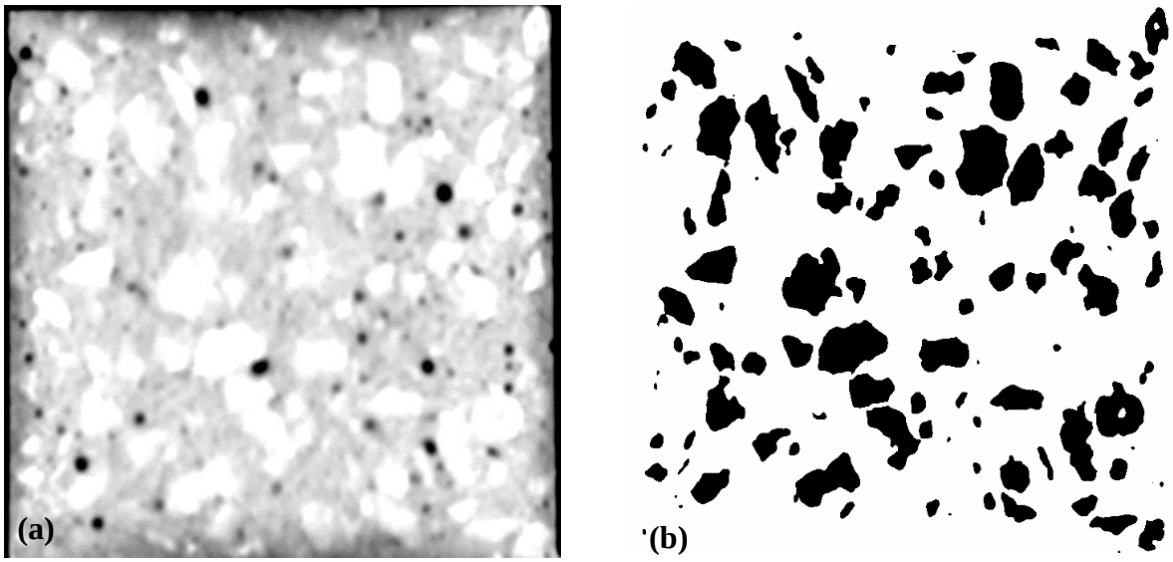

Figure 5.5. 2D slice image of Non-fibrous self compacting concrete showing (a) Grey Scale Image (b) Threshold image of aggregate

The failure was visualized on the surface of non fibrous self compacting concrete with increasing load under wedge splitting test. At the peak load, the specimen was split in to two halves without any warning, to understand the participation of coarse aggregate in observing the fracture energy, due to external loads CT scan tests are conducted. Before testing images captured from CT scan of non fibrous self compacting concrete specimens, showed proper distribution of coarse aggregate across the specimen depth. From after testing images, it was observed that the failure plane path propagated was greater in mortar, with respect to coarse aggregate. With the increasing loads, at a depth of 75-85mm i.e., near the crack tip, breakage of coarse aggregate was not observed even in their presence. The failure of the matrix region surrounding the CA was captured at a depth of 75 - 85 mm Figure 5.6(a). As concrete consists of many cracks at various length scales prior to loading, when load is increasing gradually under wedge splitting test these cracks proliferate through weaker phases i.e., mortar. With the increase in loading these cracks start to nucleate, mortar sections record weakness due to the coalescence of the cracks at multiple length scales, leading to crack growth across the specimen depth. Since the matrix region fails to resist increasing loads, load is to be taken by coarse aggregate present in the specimens. Hence, participation of CA in the failure plane increased across the depth of the specimen, Figure 5.6(b). Depending on the strength of coarse aggregate and Interfacial Transition Zone (ITZ) the failure path is proliferated. One can infer from Figure 5.6(b), the crack has propagated through the weaker plane present in coarse aggregate, in which the coarse aggregate was split in to two. Failure plane of the non fibrous self compacting concrete specimen before and after the wedge splitting test was captured at an approximate depth of 100 mm, figure 5.7. The resistance offered by coarse aggregate is sufficient enough to cause a shift in failure plane. Specimen depth of 100 mm, is arrived based on the number of slices i.e. 200 slice (200 x 0.50 = 100 mm), before and after the scan. Although, same specimen was placed under the CT scan facility, variations in the distribution of coarse aggregate was observed in the images, due to the position from which the initial scan has been initiated. Due to which the visual dissimilarity in the shape of coarse aggregate, shown in figure 5.7(a) & (b). The 2D slice representing the distribution of pores, matrix and coarse aggregate across the specimen, as show in figure 5.7(a), while the failure plane after the wedge splitting test in figure 5.7(b). It is evident from figure 5.7(b) that the fracture energy produced from wedge splitting test, sufficient enough to propagate the crack through the coarse aggregate. Such phenomenon across the depth of the entire specimen leads to the breaking of coarse aggregate, causing the non fibrous self

compacting concrete specimens to disintegrate. The formation of the failure plane is not a perfect line, as coarse aggregate has higher resistance to fracture loads, compared to the mortar surrounding coarse aggregate. It is also evident, that the coarse aggregate plays a crucial role in resting the growth of fracture plane, there by governing the specimens strength. As observed from figure 5.6(b) and 5.7(b) splitting of coarse aggregate is evident, and energy dissipated by fracture load is sufficient enough to break the coarse aggregate and propagate across the depth of the specimen. From the figure 5.8(a) and 5.8(b), it is also evident that the crack proliferation in aggregates occurs either in transgranular or intergranular form.

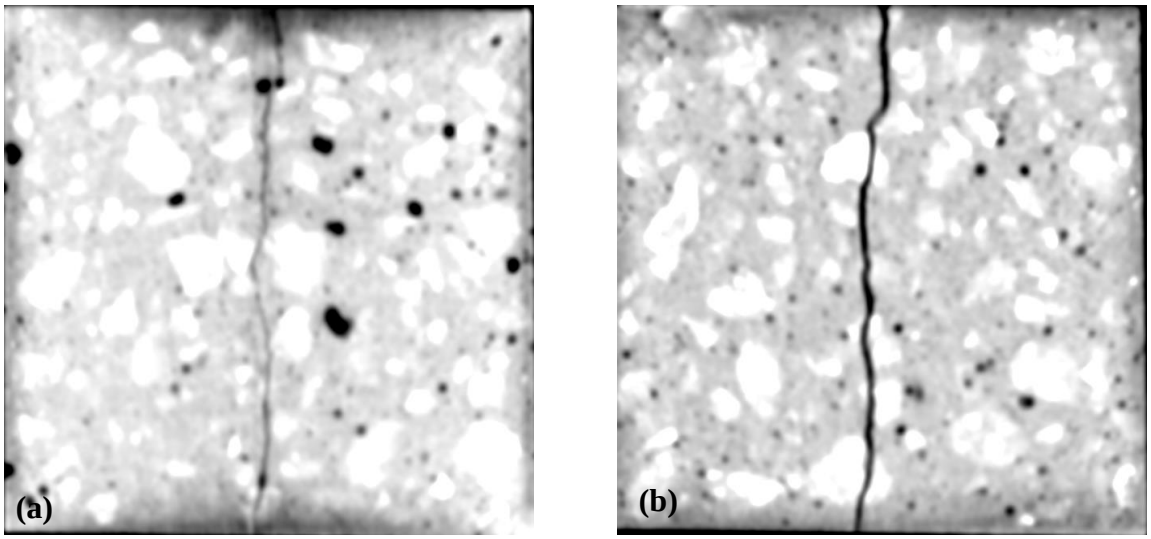

Figure 5.6. Crack propagating through the (a) matrix & (b) coarse aggregate in non fibrous SCC specimens.

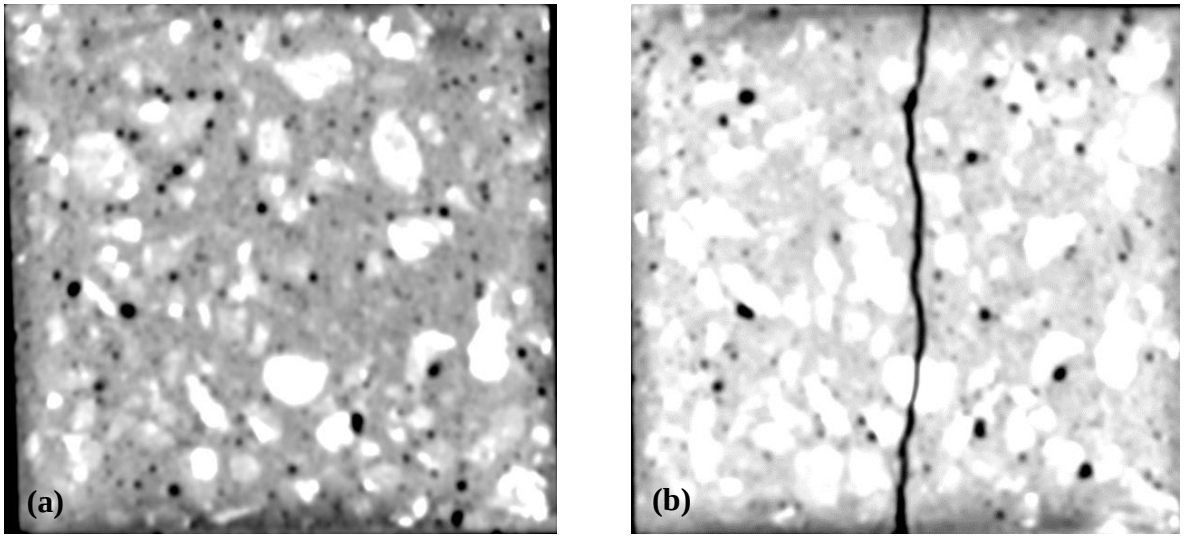

Figure 5.7. 2D image of plain SCC at depth of 100mm (a) before and (b) after testing.

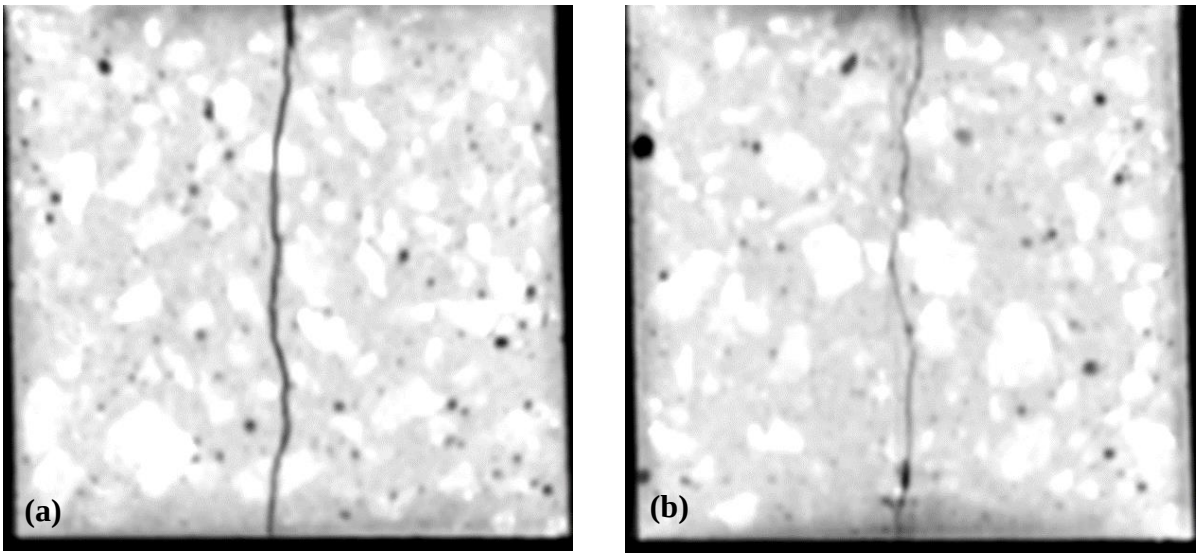

Figure 5.8. 2D image of non-fibrous SCC at depth of 100mm (a) Failure through the aggregate (b) Failure around the aggregate

The inclusion of steel fiber in self compacting concrete specimens showed completely different behaviour with respect to non fibrous self compacting concrete specimens. The steel fiber distribution across the specimens of fibrous SCC is not as uniform *i.e.* higher concentrations of steel fiber were observed across depth of the specimen. Grouping of steel fiber was also observed across the depth of the fibrous self compacting concrete specimens, captured using CT scan, Figure 5.9(a) & (b). From the images, higher distribution of steel fibers was observed with respect to

coarse aggregate, across the depth of the notch before failure. The participation of steel fiber in resisting the crack propagation, before and after the wedge splitting test is shown in Figure 5.10. The 2D slice at an approximate depth of 100 mm before and after the wedge splitting test is shown in Figure 5.10(a) and (b). The failure of fibrous self compacting concrete specimens was not sudden, as specimens are still intact, due to higher anchorage offered steel fibers relative to coarse aggregate. The anchorage provided by the steel fiber due to the effect of bridging, is shown in the 2D images captured by CT scan, Figure 5.10(b).

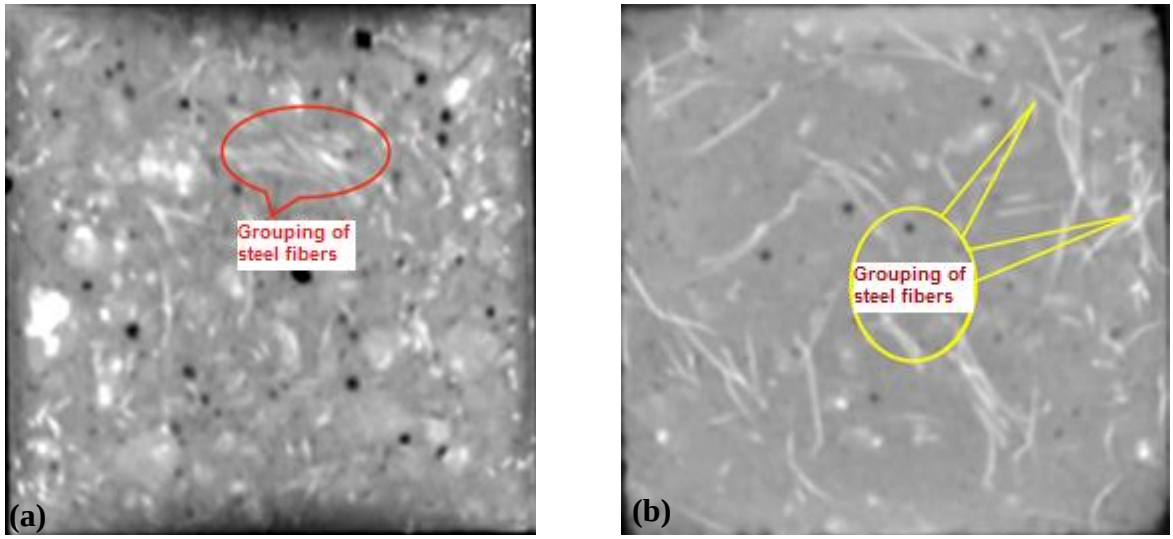

Figure 5.9. 2D images showing the grouping of fibers in fibrous SCC specimen at a depth of (a) 80 mm & (b) 140 mm.

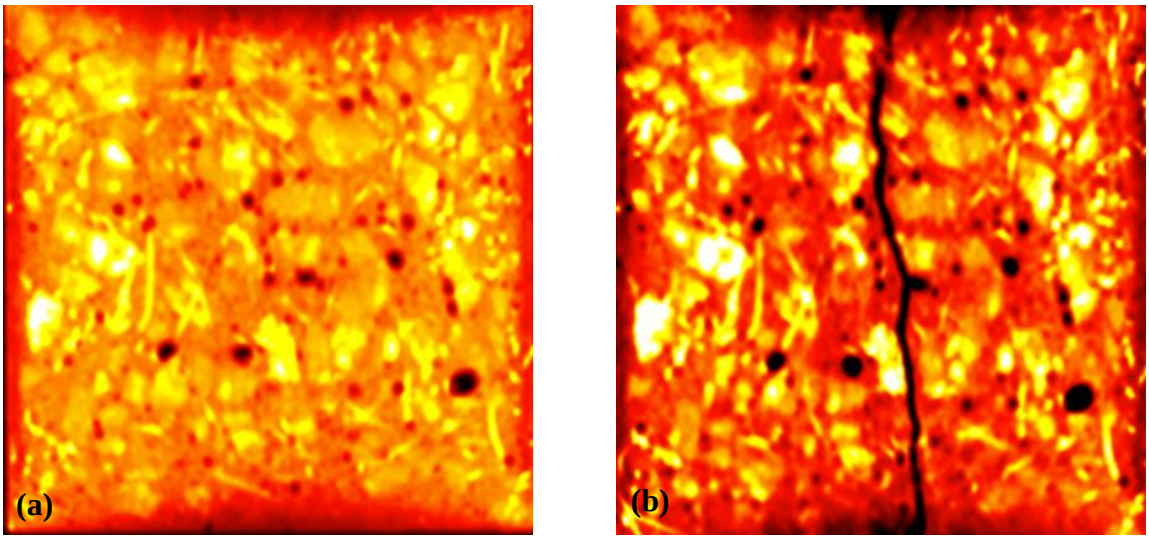

Figure 5.10. 2D image of fiber SCC at a depth of 100mm (a) before and (b) after testing

In case of fibrous self compacting concrete specimens, participation of coarse aggregate in resisting the crack propagation is relatively low. Steel fibers spread across the fracture plane, absorb the fracture energy, because of their higher anchorage length. A single 2D slice at an approximate depth of 100 mm, before and after the wedge splitting test is shown in Figure 5.10. The 2D slice before the wedge splitting test is shown in figure 5.10(a), from the image one can observe the random distribution of CA and steel fiber across the area of the specimen. The same 2D slice after wedge splitting test, captured the failure plane, breakage and elongation of steel fiber in figure 5.10(b). The fracture plane is not a straight line, due to the resistance offered by the steel fibers in preventing the crack propagation. The steel fiber participation in the bridging action, fracture and pull out in the fibrous self compacting specimens, captured in Figure 5.11. Image captured by CT scan for fibrous self compacting concrete shown the breaking, elongation, pull-out of steel fibers, along with splitting of some coarse aggregate present in the specimen. The effect of steel fiber distribution inside the specimen controls the direction of crack propagation.

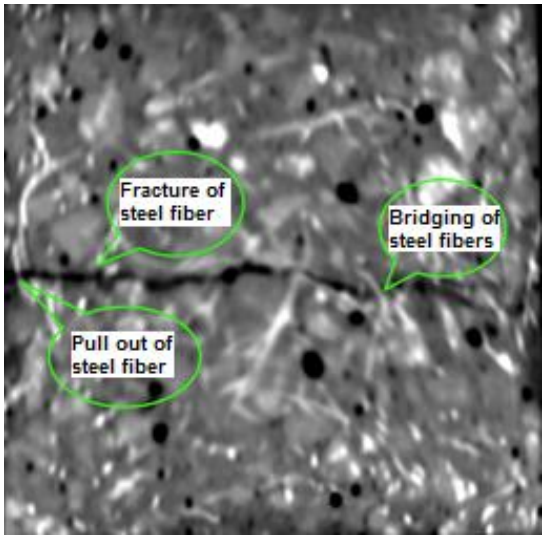

Figure 5.11. 2D image showing the bridging, facture and pull-out of steel fiber.

From 2D scanning images of both non-fibrous and fibrous self compacting concrete specimen of before and after testing, shows that internal failure can be visualized with the image processing technique across the depth using computed tomography technique.

5.4.2. 3D Image Analysis

5.4.2(a) Non-Fibrous Self compacting concrete

Coarse aggregate participation from each of the slice obtained from 2D image analysis of non-fibrous self compacting concrete specimens was captured using Fiji®. 2D images of the specimen used for image analysis were used for 3D reconstruction of the specimens. The 3D reconstructed matrix image of non-fibrous self compacting concrete specimen before and after testing were represented in the figure 5.12 (a) and (b). The figure 5.12 (c) and (d) shows the left and right parts of the fractured surface of the non-fibrous self compacting concrete which was split in to two after testing. The separate datasets of 2D images of pores and crack profile were stacked across the depth to form 3D image. The figure 5.13. represents the 3D stack image of crack profile and pores for one of the non-fibrous self compacting concrete specimen. Similarly for coarse aggregate, 3D reconstructed image was shown in the figure 5.14 obtained from AVIZO software. Quantification of coarse aggregate before and after testing of non-fibrous self compacting concrete was done on AVIZO software using thresholded 2D images of aggregates. Here for non-fibrous self compacting concrete specimens region of interest (ROI) was selected from the tip of the notch to the bottom of the specimen. The ROI showing aggregates before and after testing for one of the specimen in the figure 5.15 (a) and (b).

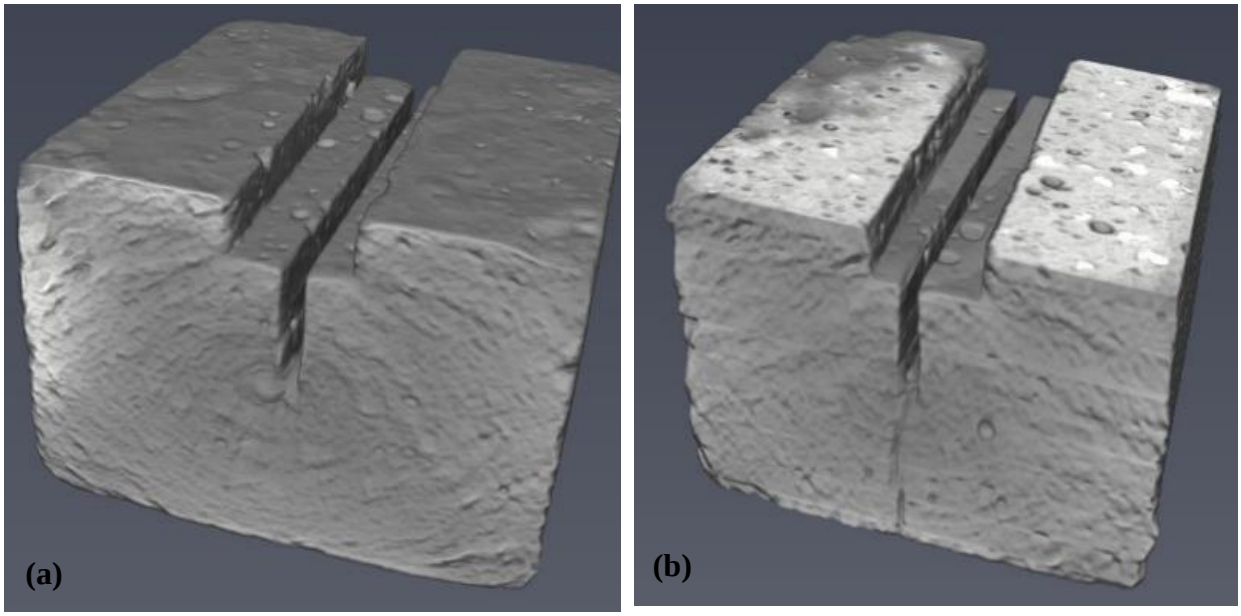

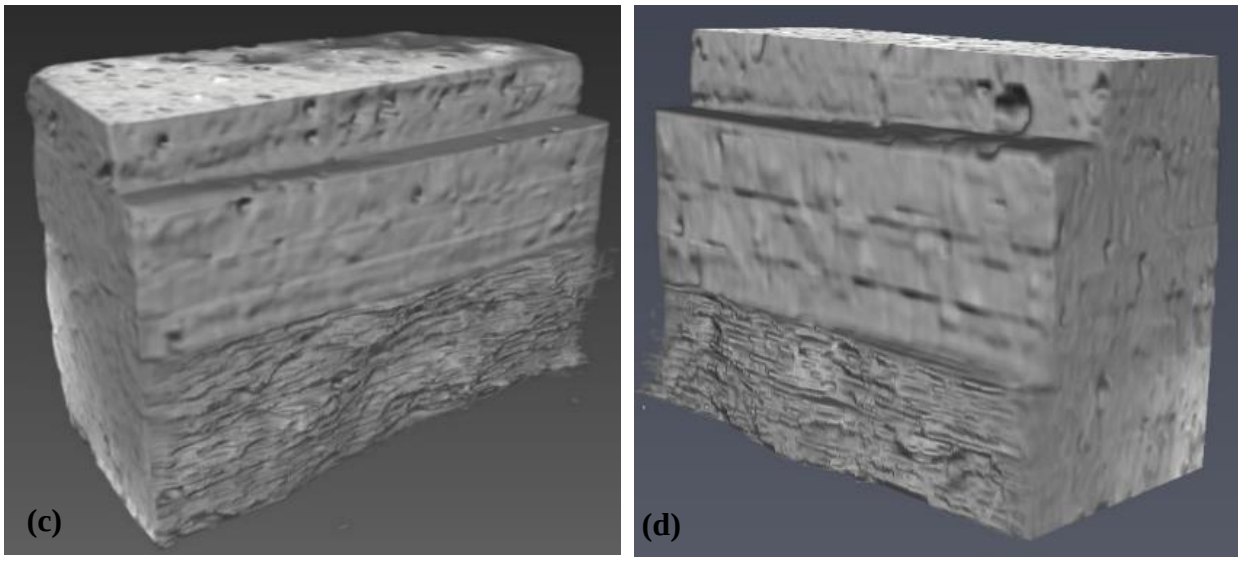

Figure 5.12. 3D image of the matrix (a) before testing (b) after testing (c) Left part of the fractured surface (d) Right part of the fractured surface

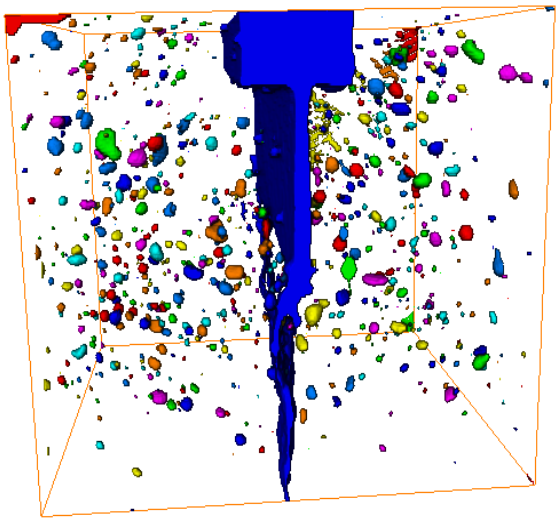

Figure 5.13. 3D Image of crack profile with pores for non-fibrous self compacting concrete

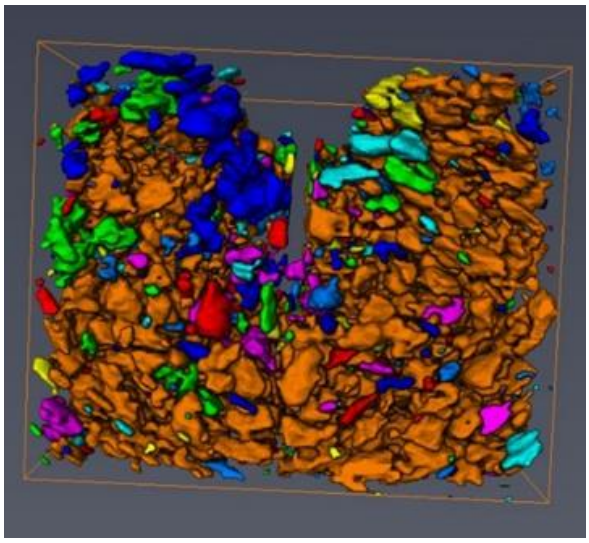

Figure 5.14. 3D Image of crack profile with pores for non-fibrous self compacting concrete

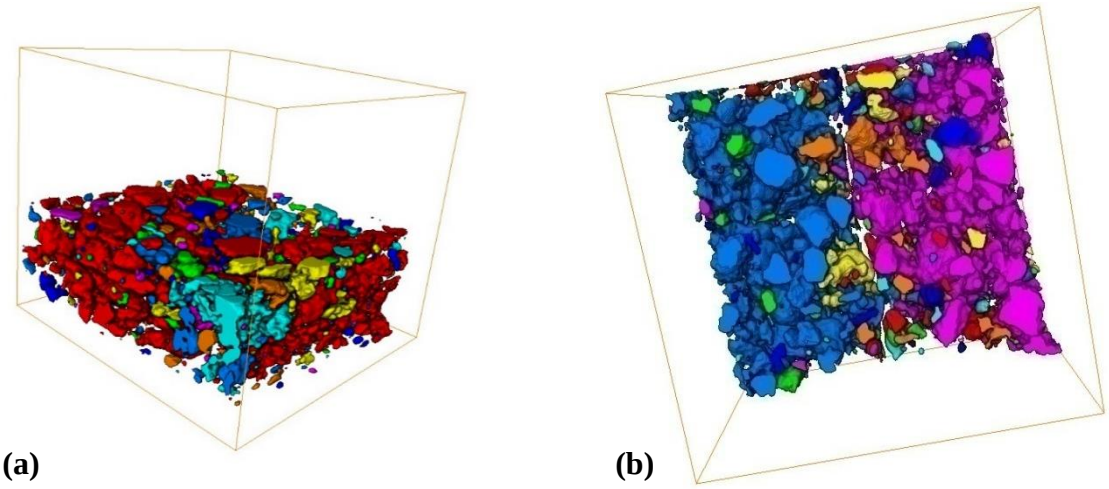

(a) **(b)**

Figure 5.15. Aggregates in ROI (a) Before testing (b) After testing (top view)

The image based analysis for quantifying the aggregate particles was carried out using sieve analysis in AVIZO software. Table 5.2 represents the quantification of aggregate based on the particle size ranges for both before and after testing of C40F60-20P and C40F60-12.5P mixes. Figure 5.16. shows the graphical representation of aggregate quantification for mix C45F55-20P. From table 5.2., for same quantities of coarse aggregate and varying coarse aggregate size i.e., 20mm and 12.5mm, the rupture of aggregates were maximum in the range of 4.75-10mm and 10-12.5mm range. From the table 5.2, it can be observed from before and after particles for C40F60-20P mix that, the ruptured aggregates were maximum in the size range of 0-4.75mm. A similar observation was drawn for C40F60-12.5F mix also. This reveals that the breaking of the smaller aggregates were the cause for crack proliferation. The transgranular failure of the smaller sized aggregate is evident through this image processing study. The results report that for both the mixes the breakage of aggregates were maximum in the range (mm) of 4.75-10 and 10-12.5 and marginal number of breakages were observed in 12.5-16 range.

Table 5.2 Coarse aggregate quantification for mix C40F60

Range of particle size (mm)	C40F60-20P		C40F60-12.5P	
	Before	After	Before	After
	No. of aggregates	No. of aggregates	No. of aggregates	No. of aggregates
0-4.75	556	604	574	702
4.75-10	160	156	165	128
10-12.5	43	29	45	30
12.5-16	30	28	44	35
16-20	30	28	4	3
20-35	7	6	-	-

The aggregate quantification for mixes C45F55-20P and C40F60-20P are tabulated in the table 5.3. The table 5.3. represents the mixes with same coarse aggregate size i.e., 20mm with varying coarse to fine aggregate quantities i.e., 45-55 and 40-60. Figure 5.17 shows the graphical representation of aggregate quantification for mix C40F60-20P and figure 5.18. shows the graphical representation of aggregate quantification for mix C40F60-12.5P. The availability of aggregate particles was higher in the 45-55 compared to 40-60 mix. Despite the higher aggregate particles, the crack proliferation was following the weaker path. The failure of coarse aggregate particles ranging 4.75-10mm and 10-12.5mm was observed to be higher and this failed aggregate particles resulted in the more aggregate particles ranging from 0-4.75mm.

Table 5.3 Coarse aggregate quantification for mixes C45F55 and C40F60

Range of particle size (mm)	C45F55-20P		C40F60-20P	
	Before	After	Before	After
	No. of aggregates	No. of aggregates	No. of aggregates	No. of aggregates
0-4.75	623	707	556	604
4.75-10	197	160	160	156
10-12.5	60	27	43	29
12.5-16	28	21	30	28
16-20	40	36	30	28
20-35	13	10	7	6

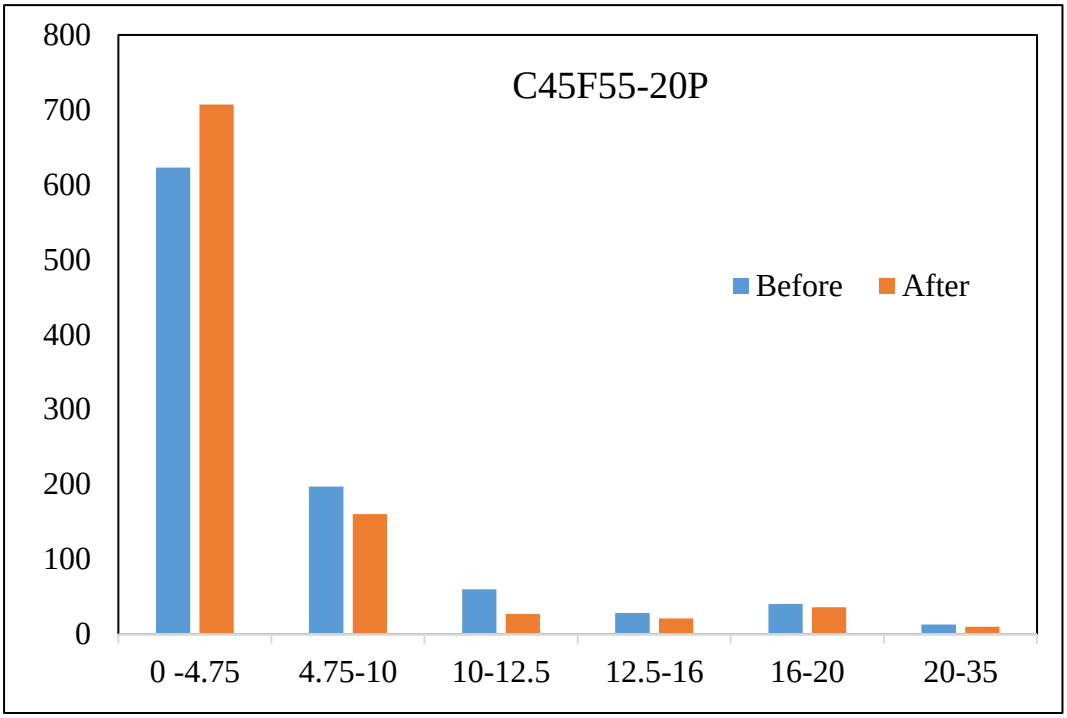

Figure 5.16 Graphical representation of aggregate quantification for mix C45F55-20P

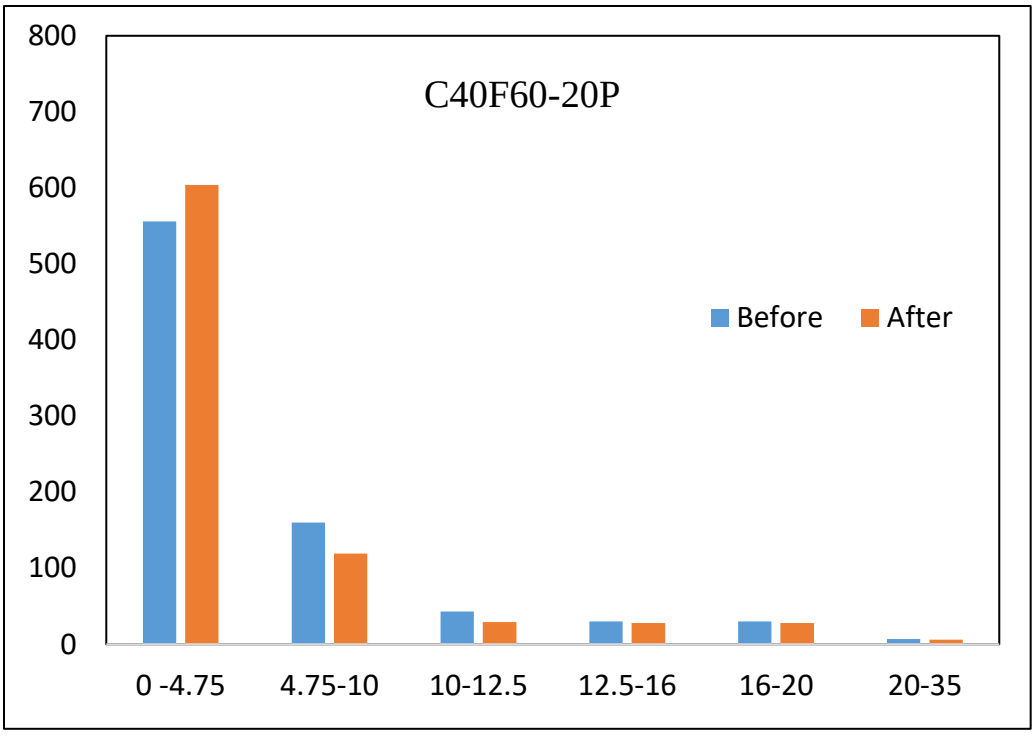

Figure 5.17 Graphical representation of aggregate quantification for mix C40F60-20P

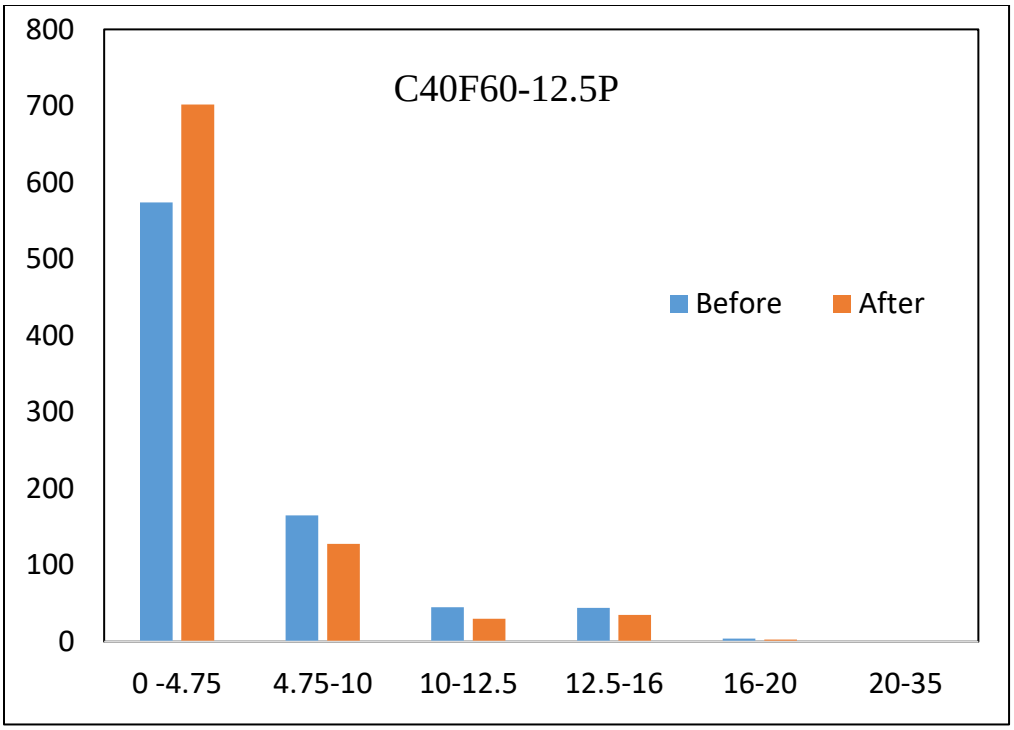

Figure 5.18 Graphical representation of aggregate quantification for mix C40F60-12.5P

5.4.2. (b) Fibrous self compacting concrete

2D images from scanning of fibrous self compacting concrete reveals that the failure occurred by absorbing the energy dissipated during the testing of wedge splitting test specimen. Phase quantification of the coarse aggregate and steel fibers causing failure were analysed using stacking of 2D images to form 3D reconstruction image. Along with the quantification, visualization of the respective phases absorbing the fracture energy, across the depth of the specimen can be reconstructed. 3D image of matrix for fibrous self compacting concrete is shown in figure 5.19. From 3D image of matrix it is evident that the after testing the specimen is intact without splitting due to the presence of fibers. All the tensile force is taken by the fibers by bridging the crack. Figure 5.20 shows that the crack profile and pores were indentified at lower threshold values. Figure 5.21 shows the combined 3D image of the aggregate and fibers in fibrous self compacting concrete.

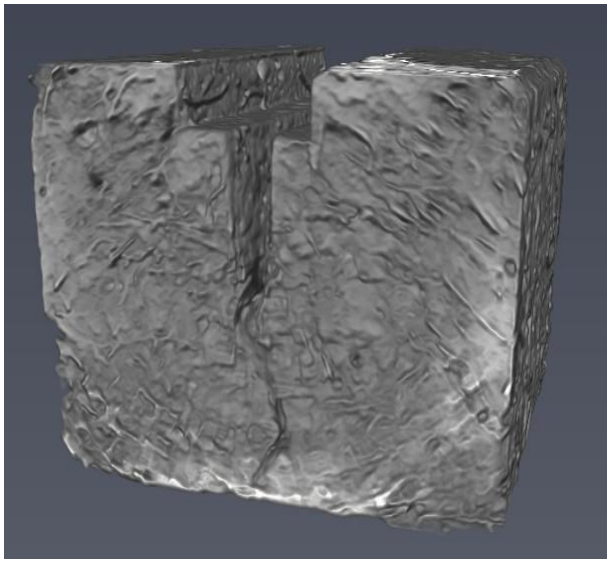

Figure 5.19. 3D Image of matrix for fibrous self compacting concrete

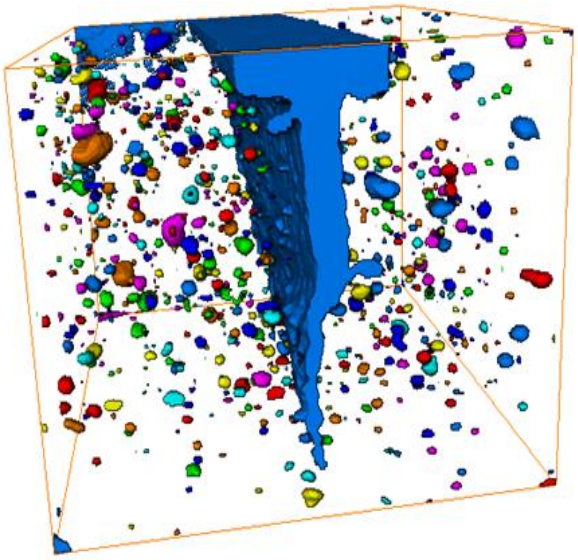

Figure 5.20. 3D Image of crack profile with pores for fibrous self compacting concrete

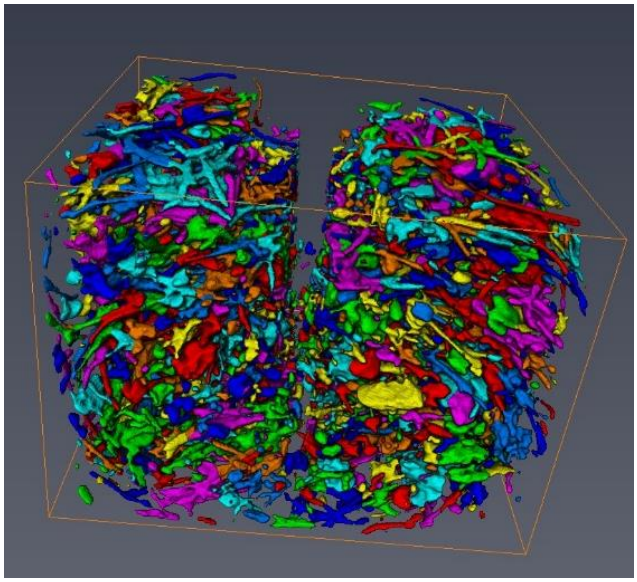

Figure 5.21. 3D image of fibrous self compacting concrete showing aggregates and fibers

For fibrous self compacting concrete the ROI was considered as 75 x 30 x 150 mm from tip of the notch to the bottom of specimen i.e., central region of the specimen.

Under the ROI, for the mix C40F60-20F, the aggregates that were fractured in the failure region were 4 in number as shown in figure 5.22(a) and fibers were 64. The actual steel fiber present in

non-fibrous self compacting concrete might be slightly higher, due to the grouping of steel fibers. As the steel fibers are in contact with one another, the software treats them as a single fiber. The fiber distribution acted like layers of steel across the specimen depth, captured in Figure 5.22(b), thereby increasing the ductility of non-fibrous SCC specimen. The advantage of incorporating hooked steel fiber in to the SCC, is the wider distribution of steel across the failure plane relative to coarse aggregate. And for the mix C40F60-12.5F, aggregates that participated in failure were 11 and fiber were 46. For the same coarse to fine aggregate quantity 40-60 and varying aggregate size of 20 and 12.5mm, aggregate failure was on higher side for 12.5mm. The availability of smaller size aggregate particles in failure plane created the weakest link for the aggregates to fail in trangranular. The energy dissipation in 12.5mm size coarse aggregate was taken by both coarse aggregate and fibers. Whereas in 20mm sized coarse aggregate, the stress is taken care by the fibers as it is evident from the figure 5.19 that lesser number of aggregate failure was observed compared to 12.5mm.

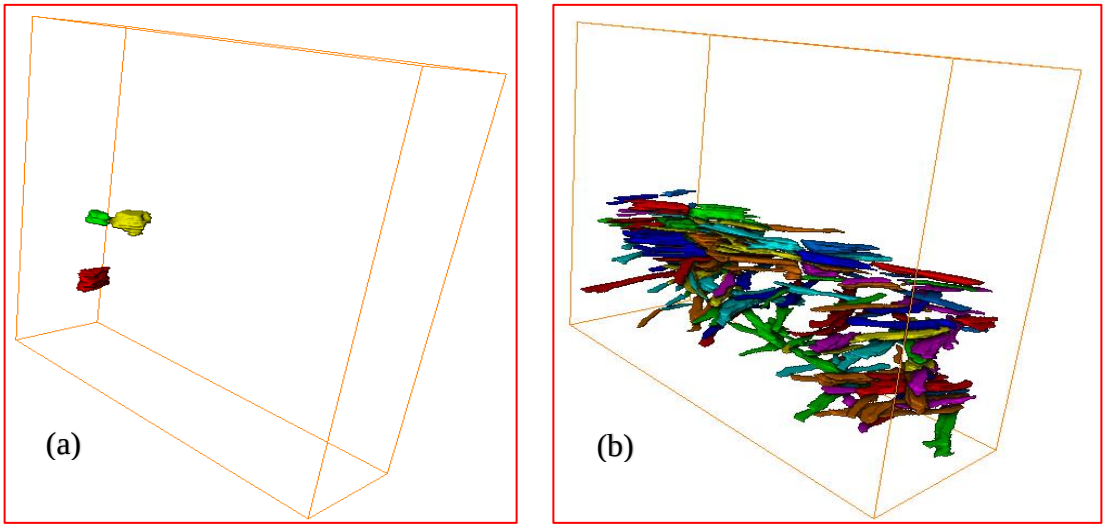

Figure 5.22. 3D image of ROI showing failure quantification of (a) coarse aggregate (b) steel fiber in mix C40F60-20F

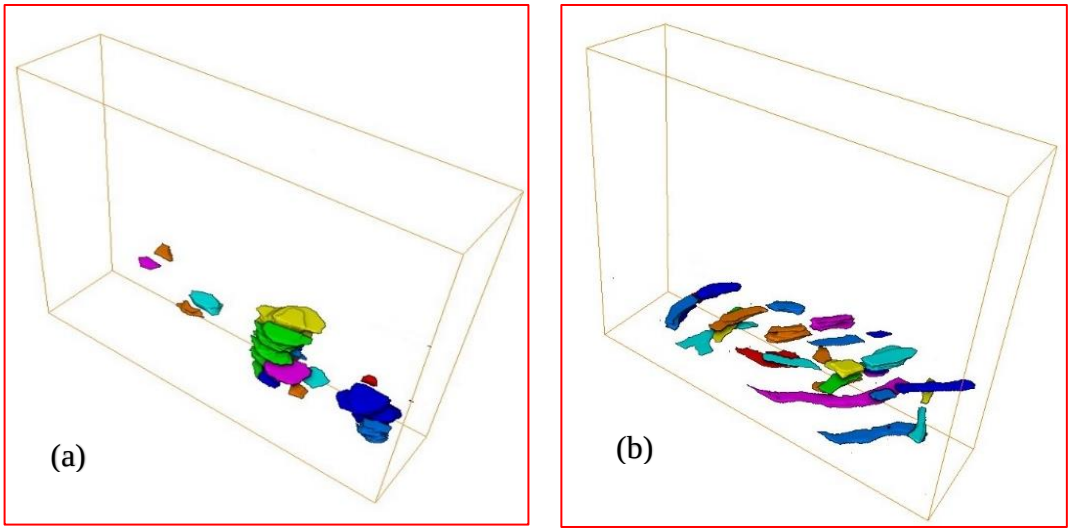

Figure 5.23. 3D image of ROI showing failure quantification of (a) coarse aggregate (b) steel fiber in mix C40F60-12.5F

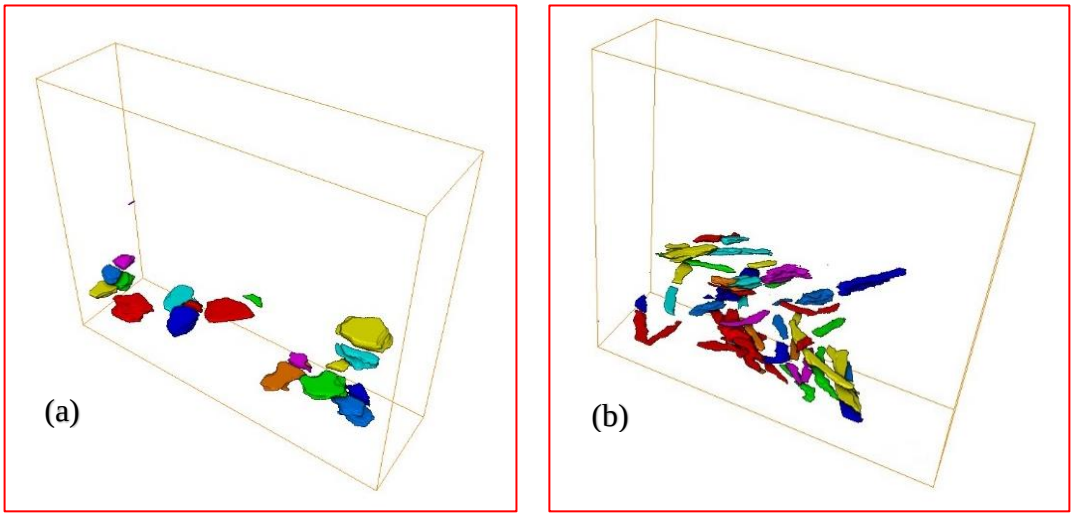

Figure 5.24. 3D image of ROI showing failure quantification of (a) coarse aggregate (b) steel fiber in mix C45F55-20F

Considering the mixes C45F55-20F and C40F60-20F i.e., for same aggregate size 20mm and varying coarse to fine aggregate quantity 45-55 and 40-60. The quantified aggregate that were failed in the specimen for C45F55-20F are 10 and that of fibers were 58. And that for specimen C40F60-20F are 4 in number for aggregates and 64 fibers. Figure 5.19 shows the ROI for the mix C40F60-20F, figure 5.23(a) is the quantification of coarse aggregate and figure 5.23(b) is for steel fibers. Figure 5.24(a) shows the quantification of coarse aggregate that were failure after testing in the specimen with the mix C45F55-20F and figure 5.24(b) is for steel fibers in the mix C45F55-

20F. The mix C45F55-20F has encountered more number of aggregate particle failure than C40F60-20F. This is because the availability of more number of aggregate particles in higher coarse to fine aggregate quantity. For the mix C40F60-20F, failure path occurred through the matrix as less number of aggregate particles were available for bridging the crack. And all the stress is taken by the fibers. The fiber participation in the mix C40F60-20F were slightly higher compared to mix C45F55-20F. For the mix C45F55-20F, the stress is taken by the both coarse aggregate and fibers that were passing through the crack proliferation path.

5.5. Conclusions

Conclusions drawn from the above study are as follows:

- From high resolution computed tomography scans, images obtained was useful in capturing the participation of steel fiber and coarse aggregate in the failure zones.
- Pores, matrix, coarse aggregate and steel fibers were visualized using the computed tomography technique. Each of the ingredients were identified and separated by thresholding the 2D images. Pores and matrix were identified at lower threshold values while coarse aggregate and steel fibers were identified at higher threshold values.
- From quantification of the coarse aggregates based on the particle size, concludes that the failure plane followed the weakest path. In crack proliferation path, if the bridging material is smaller sized coarse aggregate, failure occurs in transgranular i.e., aggregate splits in to two. Whereas for larger sized coarse aggregate, failure path was around the aggregate which is called as intergranular fracture. The transgranular and intergranular failure was clearly visualized through the computed tomography based image analysis.
- The concentration of steel fibers increased across the depth of the specimen, while most of the strain energy was absorbed by the steel fibers during the failure of non fibrous self compacting concrete.

CHAPTER 6

NUMERICAL MODELLING OF SCC UNDER WEDGE SPLITTING TEST METHOD

CHAPTER 6
NUMERICAL MODELLING OF SCC UNDER WEDGE SPLITTING TEST METHOD

6.0 General

Internal failure behaviour for non-fibrous and fibrous self compacting concrete using computed tomography for wedge splitting test specimen was studied in the previous chapter. The fracture behaviour gets effected with the change in aggregate size and quantities. Numerical modelling helps in reducing specimen casting procedure that are to be studied for various parameter considerations that influence the behaviour of concrete. For the present numerical study, the fracture behaviour with varying specimen depth and notch were studied. Numerical modelling for the present study was carried out using finite element method.

6.1. Numerical Modelling

One of the numerical simulation method is finite element method (FEM), which estimates a certain behaviour of the investigated component under a given load by computing relevant quantities of a structure (like stresses, strains, etc.,). Finite element method (FEM) analyse the problem based on discretization of elements and further integrating all the elements. There are many FEM based software's to analyse any structure or element. For the present study ABAQUS v6.14/CAE software was used to analyse the wedge splitting test specimen with varying parameters. In order to assess the fracture behaviour for a concrete, many parameters are to be considered in terms of specimen depth, type of specimen and notch depth. To reduce these many numbers of physical prototypes and experiments, numerical modelling comes in handy which can optimize components in their design phase and develop better products at faster rate. Numerical modelling further benefits to reduce issues related to inadequacy of lab resources. Numerical simulation mathematically represents a physical or any other behaviour, based on compatible hypotheses and simplifying assumptions.

6.2. Methodology For Developing Fracture Curve

The fracture properties are usually influenced by the specimen size and material properties. Usually, laboratory specimens tested are in the depths ranging less than 500mm. Influence of size variation on fracture properties may affect the structural behaviour. Therefore, fracture curve or safe design diagram developed should be independent of material and size of the specimen. Boundary effect model (BEM) was considered to study the fracture behaviour of self compacting concrete using wedge splitting test method. For the present numerical

modelling, varying specimen depth and notch depth for wedge splitting test was used to develop a fracture curve for self compacting concrete.

6.2.1 Procedure to calculate the fracture parameters using BEM

BEM consists of determination of nominal stress distribution in fictitious crack growth by characteristic crack and equivalent crack. The material parameters tensile strength (f_t) and fracture toughness (K_{IC}) are determined based on the modified boundary effect theory which considers the aggregate influence and size of the specimen (Hu, X et al 2017). Often, these two parameters affect the structural fracture of concrete. Fracture curve was developed based on the following procedure as per Guan J, et al., 2019. The fracture curve represented in figure 6.1 shows the material behavior and structural behavior based on the material parameters tensile strength and fracture toughness with three controlled fracture behavior i.e., f_t controlled, quasi brittle and K_{IC} controlled.

Figure 6.1. shows the material and structural behaviour from fracture curve as per boundary effect method (Guan J, et al., 2019). The solid yellow curve details its quasi-brittle fracture behaviour, which is controlled by the specimen dimension and the equivalent crack a_e, i.e. when $a_e \rightarrow 0$, no matter the specimen height W is big or small, the quasi brittle fracture is located at the left side and its failure is controlled by f_t. On another side, when the equivalent crack a_e is big enough (usually longer than 100 mm), brittle fracture happens instead of quasi-brittle fracture, as shown by the right side of the fracture curve. In this situation, the fracture failure is controlled by K_{IC}, which is given by LEFM. However, for most cases, quasi-brittle fracture develops for normal-size specimens, and the fracture failure is controlled by both f_t and K_{IC}. The intersection point of f_t and K_{IC} in the figure 6.1., is material inherent property, responds to the characteristic crack a_∞^*.

The effect of specimen geometry and size including loading condition are considered by the structural parameter a_e equivalent crack.

$$a_e = \left[\frac{\frac{2(1-\alpha)^2}{2+\alpha} \times Y(\alpha)}{1.12}\right]^2 ; \ \alpha = \frac{a_0}{W} \qquad \text{Eq (6.1)}$$

Where, a_0 - crack length; W - depth of specimen

Y (α) for wedge splitting specimen is given by

$$Y(\alpha) = \frac{(2+\alpha)\left(0.866+4.64\alpha-13.32\alpha^2+14.72\alpha^3-5.6\alpha^4\right)}{4\sqrt{\pi\alpha}\,(1-\alpha)^{3/2}} \qquad \text{Eq (6.2)}$$

For constant distribution, the nominal stress is evaluated using equation 3

$$\sigma_n(P_{max},\ \Delta a_{\text{fic}} = \beta\, \mathrm{d}_{\max}) = \frac{\frac{\mathrm{P}_{\max}(3\gamma_4+\gamma_2)}{6\mathrm{B}}}{\frac{\gamma_2{}^2}{6}+\frac{\Delta a_{\text{fic}}}{6}\gamma_2+\frac{\Delta a_{\text{fic}}}{3}+\left(\frac{\Delta a_{\text{fic}}}{2}+\frac{\gamma_2}{2}\right).\Delta a_{\text{fic}}} \qquad \text{Eq (6.3)}$$

Where B is the thickness of the specimen

$$\Delta \mathrm{a}_{\text{fic}} = \beta \mathrm{d}_{\max}$$

$$\gamma_1 = W - a_0\ ;\ \gamma_2 = \gamma_1 - \Delta \mathrm{a}_{\text{fic}}; \gamma_2 = \gamma_1 - \Delta \mathrm{a}_{\text{fic}};\ \gamma_2 = \gamma_1 - \Delta \mathrm{a}_{\text{fic}}$$

The material parameters tensile strength (f_t) and fracture toughness (K_{IC}) were determined using curve fitting equation (4)

$$\frac{1}{{\sigma_n}^2} = \frac{1}{{f^2}_t} + \frac{1}{{f^2}_t}\frac{a_e}{a^*_\infty} = \frac{1}{{f^2}_t} + \frac{4a_e}{{K_{IC}}^2} \qquad \text{Eq (6.4)}$$

$a_\infty{}^*$ Characteristic Crack is given by equation (5)

$$a_\infty{}^* = 0.25\ (K_{\text{IC}}/f_{\text{t}})^2 \qquad \text{Eq (6.5)}$$

Fracture curve is given by equation (6)

$$\sigma_n = \frac{f_t}{\sqrt{1+\frac{a_e}{a^*_\infty}}} \qquad \text{Eq (6.6)}$$

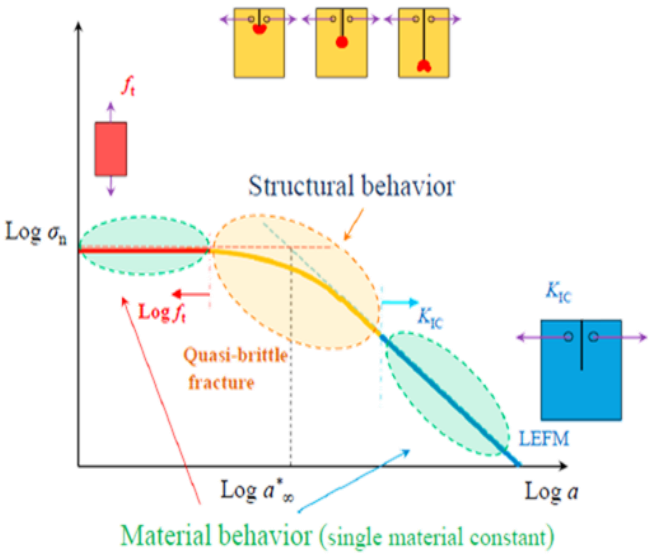

Figure 6.1. Material and structural behaviour from fracture curve (Junfeng Guan et al., 2019)

6.3. ABAQUS Simulation

The numerical modelling for wedge splitting test specimen was performed on three notch depth variation and two specimen depth variation. The parameters for modelling are tabulated in table. The ABAQUS simulation was performed based on the following modules:

Module 1: Part, Module 2: Property, Module 3: Assembly, Module 4: Step, Module 5: Interaction, Module 6: Load, Module 7: Mesh, Module 8: Job, Module 9: Visualization.

Each of the module was explained in detail for analysis to be carried out.

Table 6.1. Parameters for modelling of wedge splitting test specimen

S.No	Specimen Depth	Specimen Thickness	Notch Depth
1.	150mm	150mm	1/3 1/2 2/3
2.	200mm	150mm	1/3 1/2 2/3

Module 1: part – Creating the part

The wedge splitting test specimen of cubical in shape with dimension has mentioned in the table with a cast groove of 30mm wide and 22mm deep are modelled using this module. Apart from this, a 3D triangular wedge of angle 15 degrees was created has a discrete rigid element. The roller support one at the bottom of the specimen and two roller at the contact between the triangular wedge and the cast groove. Figure 6.2. shows the wedge splitting test specimen model.

Module 2: Property – assigning the materials

The material for each of the modelled part is defined and assigned in this module. For the present wedge splitting model, concrete properties were defined by density, elasticity and poissions ratio. The experimental data i.e., yield stress and plastic strain was given has input parameter. The input data was chosen from the experimental non-fibrous mix with 50-50 coarse aggregate quantity and 20mm size coarse aggregate. The material input parameters obtained

from experimental strain-strain curve of mix C50F50-20P are tabulated in table 6.2. and corresponding Plasticity data was represented in table 6.3.

Table 6.2. Material input parameters for ABAQUS

Mix	C50F50-20P
Density	2400 kg/m3
Elastic modulus	4093 MPa
Poisson's ratio	0.15

Table 6.3 Plasticity Input data for ABAQUS modelling

S.No	Yield Stress	Inelastic Strain
1.	28.812	0
2.	35.052	0.0004
3.	38.04	0.0008
4.	38.8296	0.0012
5.	38.1216	0.0016
6.	36.4548	0.002
7.	34.2084	0.0024
8.	26.2884	0.0036
9.	17.8764	0.005
10.	3.54	0.01

Module 3: Assembly – Assemble all the parts

All the individual parts modelled in part module were assembled in this module. When a part is created in the part module, each of the part was created in its own coordinate system, irrespective of other parts. Assembly module helps to create instances of the parts and assemble the instances in global coordinate system using the operations like rotate and translate. Figure 6.3 shows the assembled model.

Module 4: Step – analysis steps

Step module instructs in solving the analysis with predefined increments and steps. There are two step involved. One is initial and the other is analysis step, initial step is a model sequence created at the beginning of the model. Analysis steps helps in analysing the predefined variation

in stress, temp, heat etc., for the present model static general was chosen and no of increments were given.

Module 5: Interaction

All the assembled parts were given interaction so that the mechanical contact between instances is enforced. The proximity of the surfaces between the instances is given by the interaction module as assembly is not just enough. For present modelling general contact with frictional coefficient and hard contact was given as input.

Module 6: Loading – Defining and assigning the loads

Loads and boundary conditions acting were assigned in this module. The loading was given to the wedge splitting test setup in displacement control. The loading was assigned in boundary conditions. The bottom roller under the specimen was given fixed boundary conditions. The triangular wedge was restrained in all direction except in vertical direction. The connecting side rollers in between triangular wedge and specimen was restrained in all direction except in x-direction.

Module 7: Mesh – Meshing of the parts

Meshing module helps in discretizing the member in order to solve the finite element model. Meshing module helps in defining the mesh shape, size and element type. Meshing was done for individual part with C3D8R 8node element. Figure 6.4 shows the meshing of the assembled model.

Module 8: Job – Run Analysis

Once all the input data was given to the assembled model, the model is run for analysis in job module. Before starting of the analysis by the ABAQUS, it checks all the input parameters, assigned properties, meshing. If any missing data was observed, it shows an error.

Module 9: Visualization – To visualize and extract output

The modelled analysis was extracted for the output in this module. The required plots like load CMOD curves were generated using XY data in visualization. The output visualization with deformation in the members can be seen.

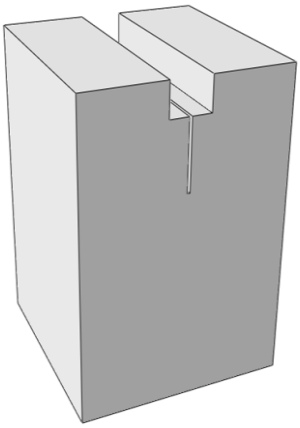

Figure 6.2. Modelling of Wedge splitting test specimen

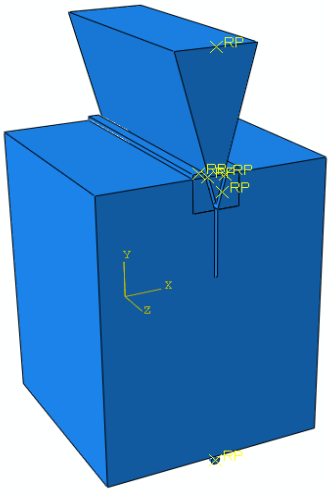

Figure 6.3. Assembly of the parts

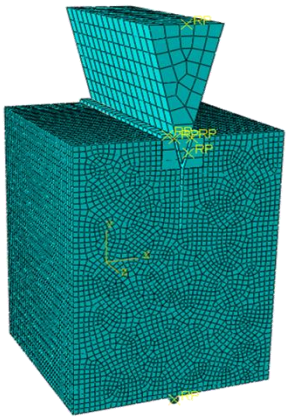

Figure 6.4. Meshing of the Wedge splitting test

6.4. Simulation Output

From the simulated output load, crack mouth opening displacement (CMOD), angle of rotation (Ɵ) and stress distribution in the ligament dimension were extracted. The plots for load vs CMOD and load vs angle of rotation were plotted. Angle of rotation was as represented in the figure 6.5.

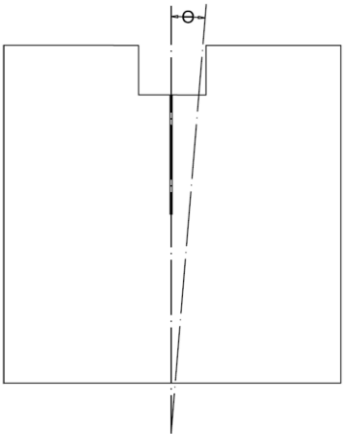

Figure 6.5 Representation of angle of rotation

6.5 Results and Discussions

The figure 6.6. represents the experimental load vs CMOD curve for 150mm specimen depth and notch depth of 1/2 times the specimen depth. The experimental load vs CMOD curve was taken from the figure 4.28 of chapter 4. The validation of numerical data with experimental

data was about 17% higher to experimental data. From this comparison, it can be concluded that the numerical modelling can be applied to the other specimen depths and notch variations for developing a fracture curve which is independent of the specimen size and notch variation using boundary effect method.

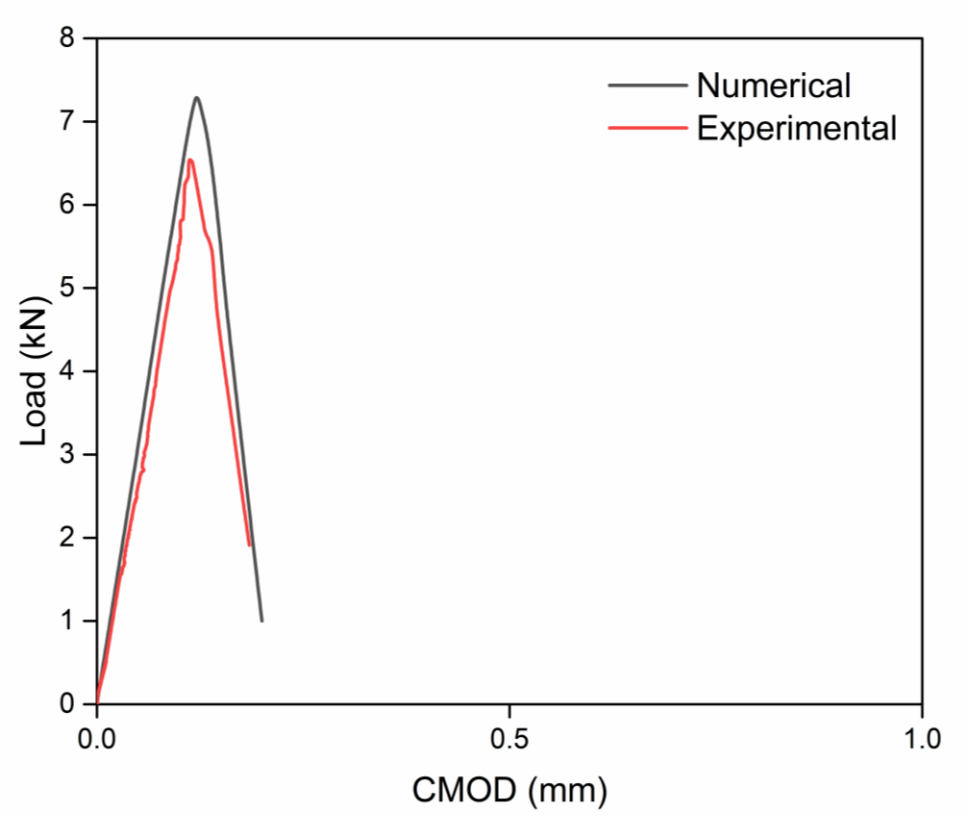

Figure 6.6. Load vs. CMOD curve from experimental and numerical modelling

Figure 6.7 – 6.9 shows the stress variation in the ligament area with the variation of the notch depth for 150mm specimen depth. The stress variation for all the three notches depict that the compression region is 0.5 times the overall ligament depth. And the initial stress was same for all the three notch depth variation. This shows that the irrespective of the notch length the compression and tension zones are same. Figure 6.10 - 6.12 reveals that the stress variation is 0.64 times the overall ligament depth for the specimen with 200mm depth. With the variation of the depth, the increase in depth increased the compression zone. This effects the load carrying capacity and eventually the fracture energy. It was also observed that the initial failure stress was about 40N/mm^2 for all the depth notch depths and specimen depths. The stress required for the crack to propagate is same for all specimens, irrespective of the size and notch depth variation. The tension and compression region was varying with specimen depth, for

greater specimen depth the compression and tension region increased, as available ligament depth offered resistance against applied loading.

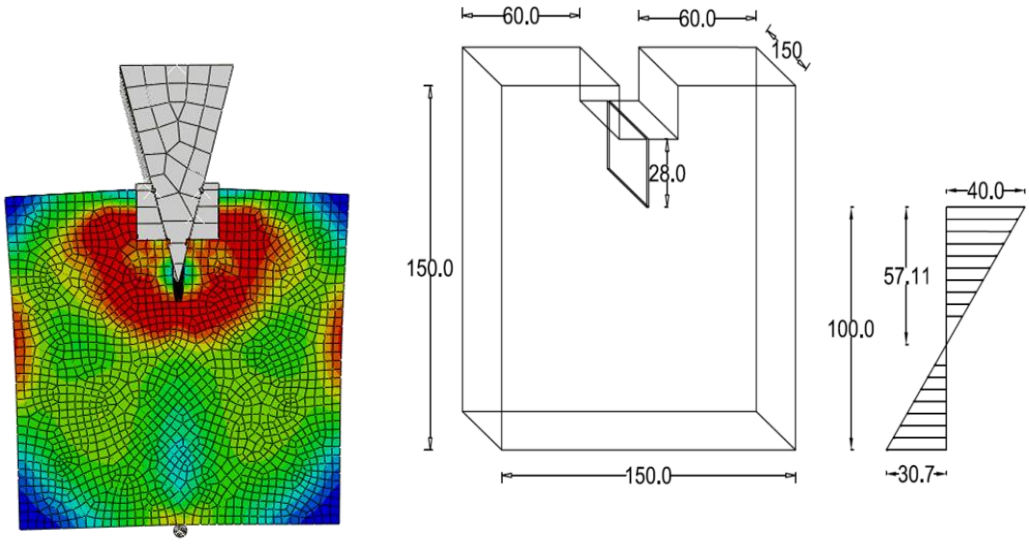

Figure 6.7. Stress variation in 150 mm depth specimen with 1/3 notch length

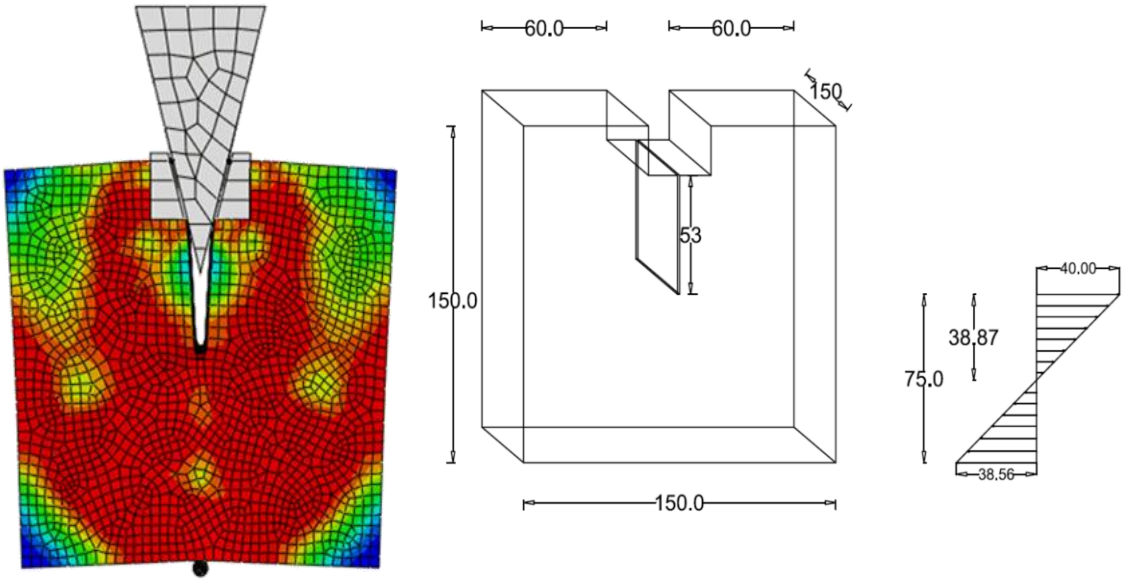

Figure 6.8. Stress variation in 150 mm depth specimen with 1/2 notch length

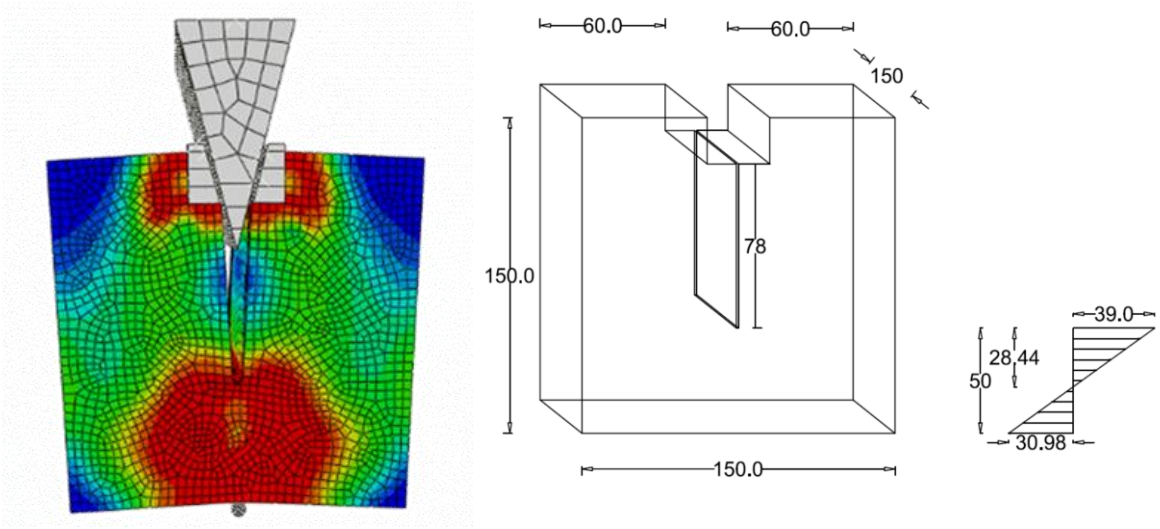

Figure 6.9. Stress variation in 150 mm depth specimen with 2/3 notch length

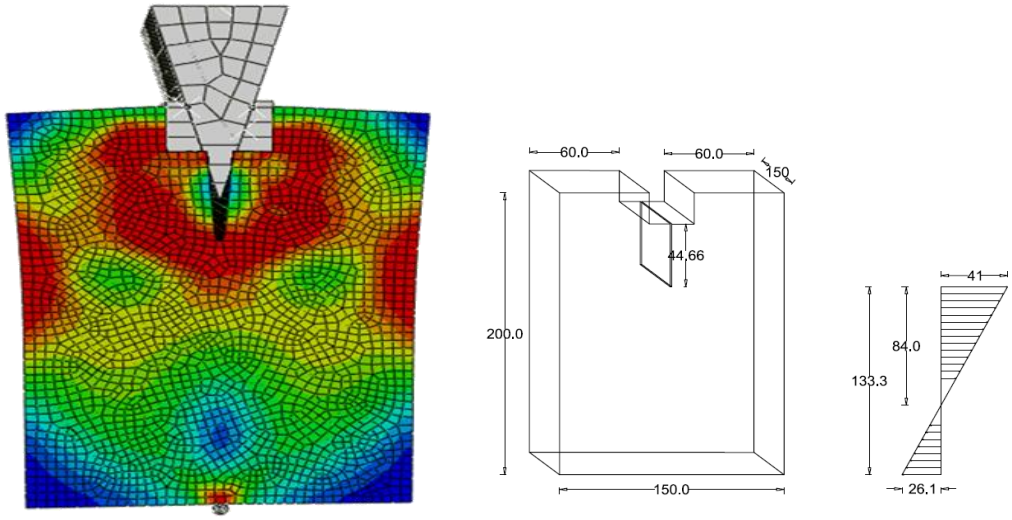

Figure 6.10. Stress variation in 200 mm depth specimen with 1/3 notch length

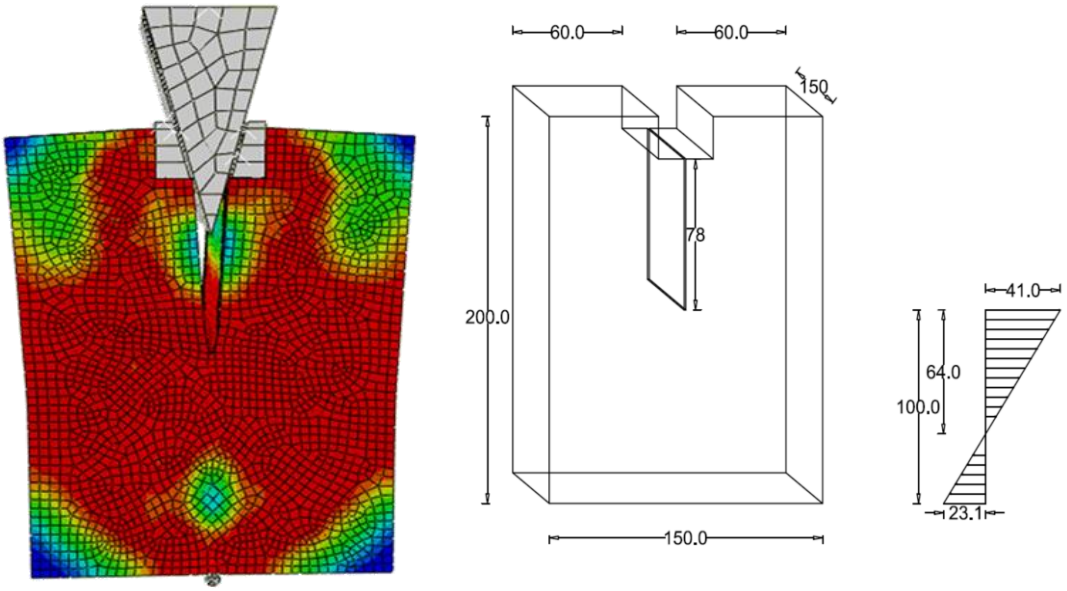

Figure 6.11. Stress variation in 200 mm depth specimen with 1/2 notch length

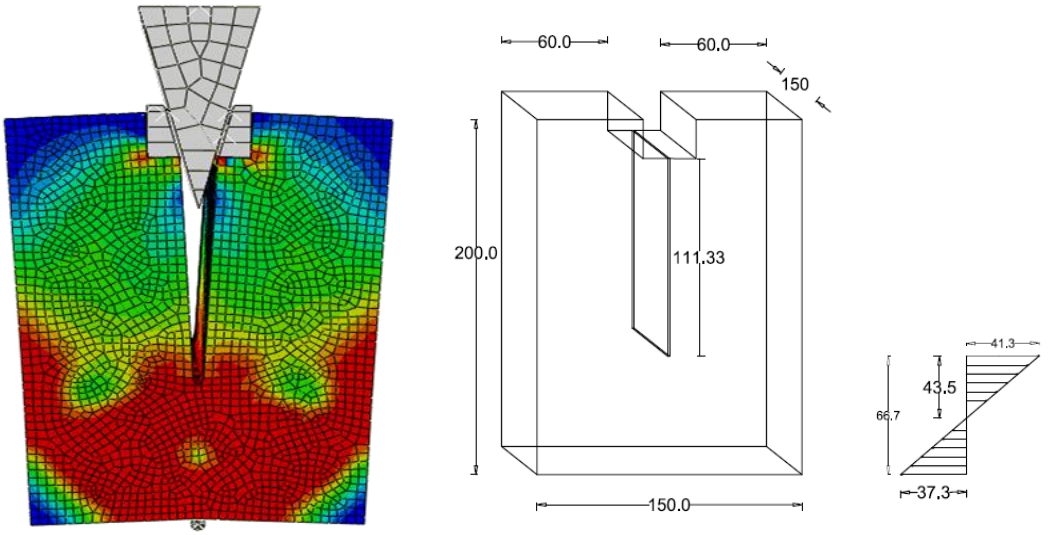

Figure 6.12. Stress variation in 200 mm depth specimen with 2/3 notch length

Figure 6.13 and 6.14 are the representation of the load vs. CMOD of three notch depth variation for 150mm and 200mm depth respectively. For both the depths, the notch variation of 1/3 of the depth had highest load carrying capacity followed by 1/2 and 2/3. Based on the load CMOD curves, fracture energy was calculated using area under the load vs CMOD curve and ligament depth. The fracture energy was higher for 1/3 notch depth for both 150mm and 200mm depth specimens. In comparison to specimen depth 200mm depth has higher fracture energy than 150mm specimen depth.

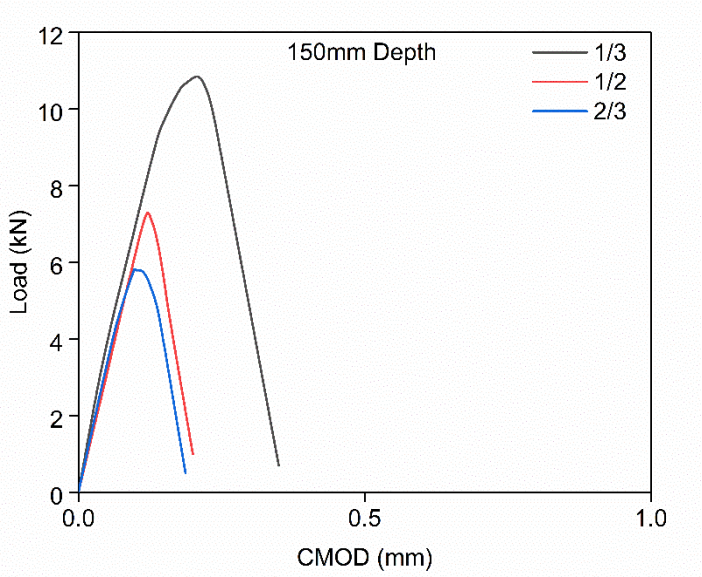

Figure 6.13. Load vs. CMOD curve for 150mm depth

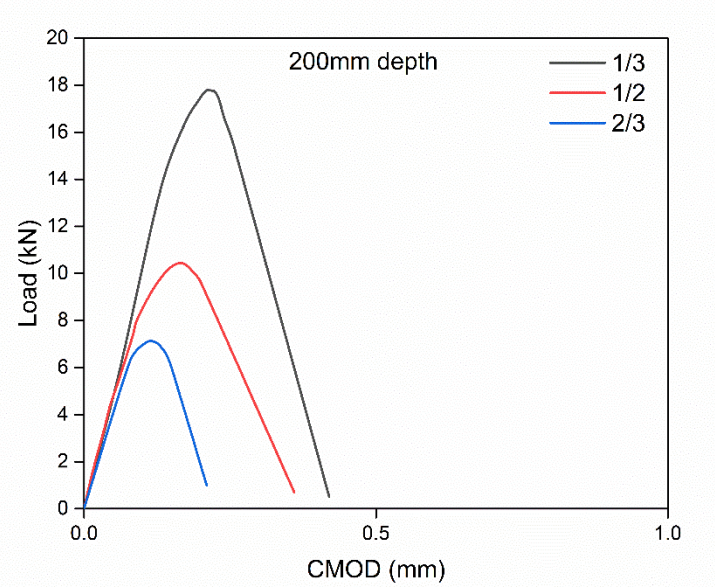

Figure 6.14. Load vs. CMOD curve for 200mm depth

Figure 6.15 and 6.16 represents the load vs angle of rotation of 150mm and 200mm depth of the specimen for three notch depth variations. It was observed that the 150mm specimen depth had higher angle of rotation than the 200mm specimen for all the notch depths. In particular for notch depth variation 1/3 notch depth has lower angle of rotation followed by 1/2 and 1/3.

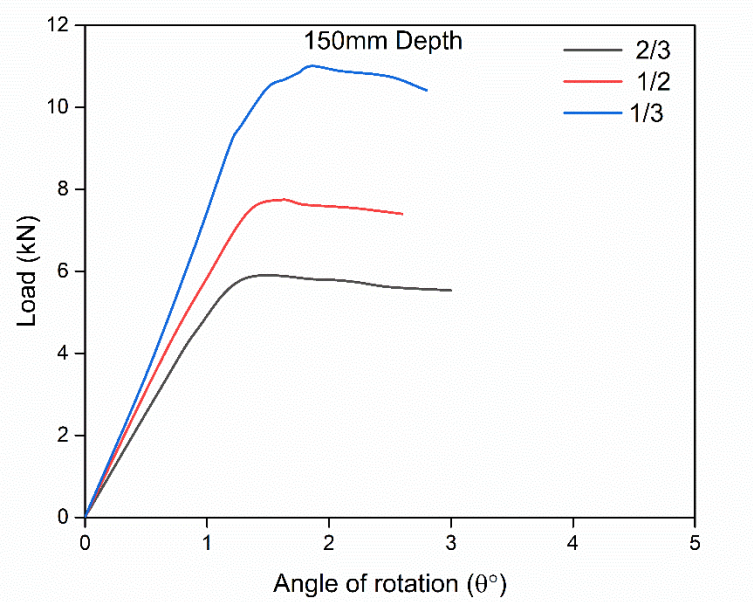

Figure 6.15. Load vs. deviation angle for 150mm depth

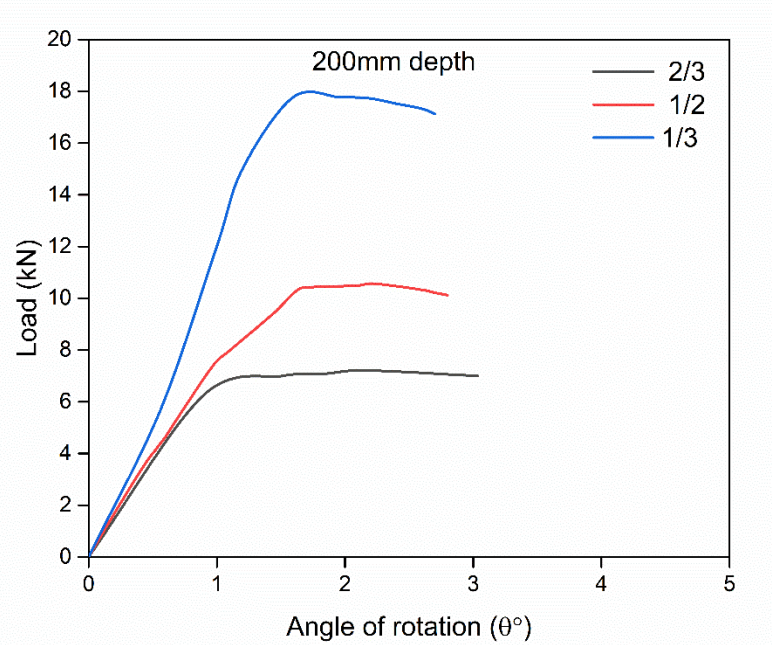

Figure 6.16. Load vs. deviation angle for 200mm depth

6.5.1. Evaluation of fracture parameters

Based on the above formulation of boundary effect method, from equation 6.1-6.6, fracture curve was developed for three notch depth variations and two specimen depth variations. Using peak load from numerical modelling, the fracture curve was developed. Table 6.2. Shows the fracture parameters obtained from numerical modelling evaluated using boundary effect method for wedge splitting test. Figure 6.17. Represents the curve fitting for determining f_t and

K_{IC}. Based on the f_t and K_{IC} obtained, fracture curve was developed by nominal stress and equivalent crack for all the specimen depths and notch variations and it is represented in figure 6.18. For both specimen depths and for all notch depths, fracture behavior was quasi brittle failure following nonlinear elastic fracture mechanics (NLEFM).

Table 6.4. Fracture parameters from numerical modelling

Depth (W) (mm)	Thickness (B) (mm)	Notch length (a_0) (mm)	α (a_0/W)	Max. Load (N)	Fracture Energy G_F(N/m)	a_e (mm)	Nominal stress (σ_n) (N/mm^2)	$1/\sigma_n^2$	log a_e	log σ_n
200	150	133.33	0.67	7209	93.71	7.089	7.437	0.018	0.851	0.871
200	150	100	0.50	10559	151.20	11.493	5.215	0.037	1.060	0.717
200	150	66.67	0.33	17777	210.61	16.785	4.983	0.040	1.225	0.697
150	150	100	0.67	5808	87.90	5.316	7.164	0.019	0.726	0.855
150	150	75	0.50	7739	71.479	8.620	4.704	0.045	0.936	0.672
150	150	50	0.33	11000	115.18	12.589	3.865	0.067	1.100	0.587

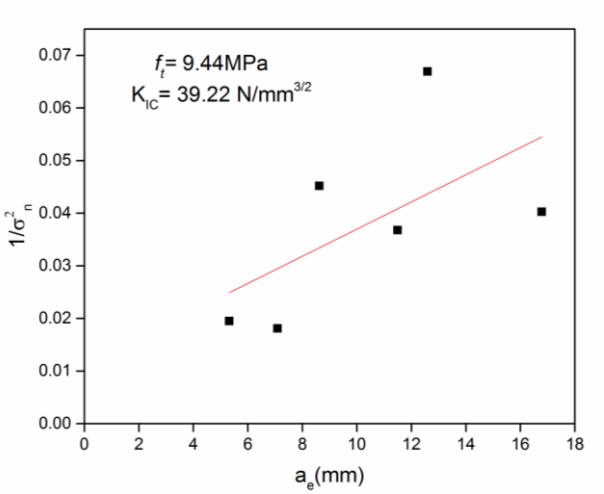

Figure 6.17. Curve fitting to determine f_t and K_{IC}

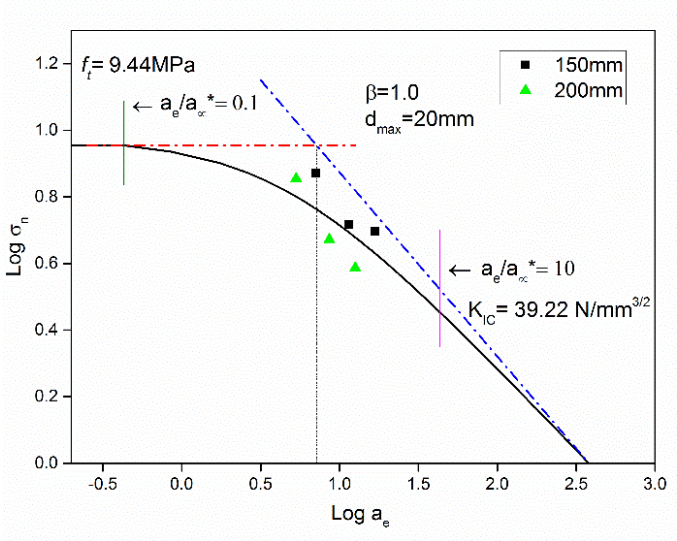

Figure 6.18. Fracture curve from numerical modelling

The fracture parameters from experimental and numerical study were tabled in table 6.5. The maximum load was observed to be 7.73kN for numerical study and 6.5kN from the experimental. The difference was 15.9% higher for numerical study than the experimental. The evaluated fracture energy G_F from numerical study was 71.47N/m and 64.43N/m from experimental study. The variation was observed to be 9.8%.

Table 6.5 Fracture parameters from experimental and numerical modelling

Mix Designation C50F50-20P	**Experimental**	**Numerical**
Maximum Load (F_{sp}) (kN)	6.50	7.73
Fracture Energy (G_F) (N/m)	64.43	71.47

6.6 Conclusions

The following conclusions are drawn from the experimental and numerical simulation of self compacting concrete using wedge splitting test.

- Through experimental and numerical validation, it is evident that wedge splitting test method can be analysed using numerical modelling approach. Furthermore, the analysis can be advanced with crack analysis.
- The load-CMOD plots revealed that the load-carrying capacity increases with increased specimen depth, on the other side decreases with increased notch depth.

- Specific fracture energy is found to be higher for specimens of greater depth with smaller notch depth. The available ligament dimensions available for the crack to propagate increased with increase in depth and decrease in notch depth. This resulted in an increase in energy dissipation requirement.
- The angle of rotation increased with the decrease in depth of specimen and increase in notch length. The increase in load carrying capacity of the specimen makes lesser deviation angle.
- The portion in the ligament area is subjected to both tensile and compressive stresses which are quantified and found to follow a straight line variation. The increase in compressive zone is observed in the specimen with higher specimen depth and least notch depth. In particular, for same specimen depth and varying notch, the variation of compressive zone is higher for specimen depth of 200mm.
- The fracture curve strongly revealed fracture behaviour with quasi brittle failure following non-linear elastic fracture mechanics (NLEFM).

CHAPTER 7

CONCLUSIONS AND SCOPE FOR FURTHER WORK

CHAPTER 7
CONCLUSIONS AND SCOPE FOR FUTURE WORK

7.0 Conclusions

From the detailed experimental, image study and numerical study on fracture behaviour of non-fibrous and fibrous self compacting concrete the following conclusions were drawn.

Evaluation of fracture properties of self Compacting Concrete using three point end test.

The study on physical, mechanical and fracture properties of non-fibrous and fibrous self compacting concrete using three point bend test were concluded as follows.

- The fresh properties of the non-fibrous and fibrous SCC were verified according to EFNARC specifications. Fibrous SCC based specimens attained less workability compared to non-fibrous SCC mixes. With the decrease in coarse aggregate size and quantity, the mix becomes viscous in nature.
- The fresh property values were moderately on lower side for the mixes (minimum aggregate size and lower aggregate volume) C40F60-12.5P and C40F60-12.5F due to the higher specific surface area of the particles.
- In case of mechanical properties, the specimens with minimum coarse aggregate size (12.5mm) and maximum coarse aggregate quantity i.e., 50-50 achieved better compressive strength and splitting tensile strength results.
- The increase in size and volume of coarse aggregate improved the compressive strength of fibrous SCC. The increase in coarse aggregate volume by 10% (i.e., 40-60 to 50-50) enhanced the compressive strength by 5.9%, 5.1% and 6.1% for specimen with coarse aggregate size 20mm, 16mm and 12.5mm respectively. For non-fibrous SCC it was observed to be 7%, 6.1% and 5.22% for aggregate size 20mm, 16mm and 12.5mm respectively.
- The addition of steel fibers in SCC enhanced the strength of concrete by 7 to 7.5% when compared to non-fibrous SCC specimens.
- The non-fibrous and fibrous self compacting concrete with higher coarse to fine aggregate quantities and least coarse aggregate size approached strength criterion from size effect law.
- The brittleness number indicated a non-linear fracture mechanics for both non-fibrous and fibrous self compacting concrete.

- The post peak effect was not depicted in the fibrous self compacting concrete as the fracture properties were underestimated in comparison to non-fibrous self compacting concrete.

Assessment of fracture properties of Self Compacting Concrete using wedge splitting test method.

The study on fracture properties of non-fibrous and fibrous self compacting concrete using wedge splitting test method for without and with guided notch. The following are the conclusions from the Phase – II.

- The splitting force was maximum for fibrous SCC than the non-fibrous SCC and enhanced post peak behaviour was noticed in fibrous SCC specimens due to the presence of steel fibers. In addition to this, the size and volume of aggregate affected the value of splitting force. The splitting force was maximum for both non-fibrous and fibrous SCC specimens with aggregate size of 12.5mm and 50-50 coarse to fine aggregate quantity.
- The specimens without guide notch attained maximum splitting force compared to specimens with guide notch. This observation was same for all sizes and quantities of coarse to fine aggregate. The maximum splitting force in specimens without guide notch can be attributed to indefinite failure path and more ligament area which assisted in attaining better fracture energy.
- The fracture energy was higher for fibrous SCC and the post peak was enhanced by the steel fibers whereas for non-fibrous SCC, the post peak had a sudden drop leading to a catastrophic failure for non-fibrous SCC. The smaller aggregate size i.e., 12.5mm had less fracture energy compared to 20mm and 16mm size coarse aggregate for both non-fibrous and fibrous SCC. Mixes with higher coarse aggregate content i.e., 50-50 has higher fracture energy then followed by 45-55 and 40-60 volume of CA-FA.
- Fracture energy was maximum for 20mm size of coarse aggregate based specimens for all the CA-FA ratios. This is because, the crack proliferates through the aggregate in the smaller size aggregate leading to transgranular failure and in case of large size aggregate crack proliferates around the aggregate leading to intergranular failure.
- The characteristic length l_{ch} and critical stress intensity factor K_{IC} indicate the brittleness of the material. Higher values of l_{ch} and K_{IC} indicate ductility of the material. The higher volume and size of aggregates i.e., Mixes C50F50-20P of non-fibrous SCC and C50F50-20F of fibrous SCC indicated ductile nature in comparison to all other mixes.

Internal behaviour of non fibrous and fibrous self compacting concrete using computed tomography

- A novel Digital Image Processing Technique namely X-Ray Computed Tomography was used to capture the internal failure pattern.
- Quantification of aggregates causing failure was determined using HRCT techniques. Bridging, breaking and pull-out of the steel fibers in fibrous SCC was visualized and quantified using HRCT.
- The post peak behaviour in fibrous SCC observed by WST is due to the presence of steel fiber, which is typically identified through HRCT studies.
- CT images has shown strong evident that smaller aggregates had transgranular failure and 20mm size aggregates showed intergranular failure.

Numerical Studies on Self Compacting Concrete Using Wedge Splitting Test

- The load-CMOD plots shows that the load carrying capacity increases with the specimen depth and decreases with the notch length.
- Specific fracture energy was higher for a specimen with greater depth and smaller notch depth.
- The angle of rotation increased with the increase I depth of specimen and notch.
- The portion in the ligament area is subjected to both tensile and compressive stresses which are quantified.
- The fracture curve reveals a structural behaviour with quasi brittle failure following nonlinear elastic fracture mechanics.

7.1 Significant Contribution from Research Work

- A detailed experimental investigation has been carried and studied the influence of aggregate size and its volume proportion on fracture process parameters of fibrous and non-fibrous Self Compacting Concrete.

- An Image based advanced technique namely Computed Tomography is used to capture the internal microstructure and failure behavior of fibrous and non-fibrous Self Compacting Concrete.

- A detailed numerical study has been conducted to validate the experimental results obtained using Wedge Splitting Test.

7.2 Scope for Future Work

- Evaluate the fracture properties of non-fibrous and fibrous SCC considering size effect of wedge splitting specimen and maximum aggregate size.
- Evaluate the fracture properties of SCC with the effect of temperature on wedge splitting specimens.
- Crack analysis for Wedge Splitting Test specimens in ABAQUS using Extended Finite Element Method (XFEM).
- Developing a model in ABAQUS from the CT scan image data.

BIBLIOGRAPHY

Abdalla, H.M. and Karihaloo, B.L., 2003. Determination of size-independent specific fracture energy of concrete from three-point bend and wedge splitting tests. Magazine of concrete research, 55(2), pp.133-141.

Afzali-Naniz, O., Mazloom, M. and Karamloo, M., 2021. Effect of nano and micro SiO2 on brittleness and fracture parameters of self-compacting lightweight concrete. Construction and Building Materials, 299, p.124354.

Aldeen Odaa, S., Hason, M.M. and Sharba, A.A.K., 2021. Self-compacting concrete beams reinforced with steel fiber under flexural loads: A ductility index evaluation. Materials Today: Proceedings.

Al-Hadithi, A.I. and Hilal, N.N., 2016. The possibility of enhancing some properties of self-compacting concrete by adding waste plastic fibers. Journal of Building Engineering, 8, pp.20-28.

Alyhya, W.S., Dhaheer, M.A., Al-Rubaye, M.M. and Karihaloo, B.L., 2016. Influence of mix composition and strength on the fracture properties of self-compacting concrete. Construction and Building Materials, 110, pp.312-322.

Al-Yousuf, A., Pokharel, T., Lee, J., Gad, E., Abdouka, K. and Sanjayan, J., 2021. Effect of fly ash and slag on properties of normal and high strength concrete including fracture energy by wedge splitting test: Experimental and numerical investigations. Construction and Building Materials, 271, p.121553.

Amparano, F.E., Xi, Y. and Roh, Y.S., 2000. Experimental study on the effect of aggregate content on fracture behavior of concrete. Engineering Fracture Mechanics, 67(1), pp.65-84.

Atewi, Y.R., Hasan, M.F. and Güneyisi, E., 2019. Fracture and permeability properties of glass fiber reinforced self-compacting concrete with and without nanosilica. Construction and Building Materials, 226, pp.993-1005.

Balázs, G.L., Czoboly, O., Lublóy, É., Kapitány, K. and Barsi, Á., 2017. Observation of steel fibres in concrete with Computed Tomography. Construction and Building Materials, 140, pp.534-541.

Bažant, Z.P. and Oh, B.H., 1983. Crack band theory for fracture of concrete. Matériaux et construction, 16(3), pp.155-177.

Bažant, Z.P., 1984. Size effect in blunt fracture: concrete, rock, metal. Journal of engineering mechanics, 110(4), pp.518-535.

Bažant, Z.P., Kim, J.K. and Pfeiffer, P.A., 1986. Determination of fracture properties from size effect tests. J. Struct. Eng. ASCE, 112(2), pp.289-307.

Beygi, M.H., Kazemi, M.T., Amiri, J.V., Nikbin, I.M., Rabbanifar, S. and Rahmani, E., 2014. Evaluation of the effect of maximum aggregate size on fracture behavior of self compacting concrete. Construction and Building Materials, 55, pp.202-211.

Bignozzi, M.C. and Sandrolini, F., 2006. Tyre rubber waste recycling in self-compacting concrete. Cement and concrete research, 36(4), pp.735-739.

Bordelon, A.C. and Roesler, J.R., 2014. Spatial distribution of synthetic fibers in concrete with X-ray computed tomography. Cement and Concrete Composites, 53, pp.35-43.

Bouzoubaâ, N. and Lachemi, M., 2001. Self-compacting concrete incorporating high volumes of class F fly ash: Preliminary results. Cement and concrete research, 31(3), pp.413-420.

Broberg, K.B., 1971. Crack-growth criteria and non-linear fracture mechanics. Journal of the Mechanics and Physics of Solids, 19(6), pp.407-418.

Du Plessis, A. and Boshoff, W.P., 2019. A review of X-ray computed tomography of concrete and asphalt construction materials. Construction and Building Materials, 199, pp.637-651.

Dugdale, D.S., 1960. Yielding of steel sheets containing slits. Journal of the Mechanics and Physics of Solids, 8(2), pp.100-104.

EFNARC (2005) The European Guidelines for Self-Compacting Concrete: Specification, Production and Use, The European Guidelines for Self Compacting Concrete.

Erdem, S., 2014. X-ray computed tomography and fractal analysis for the evaluation of segregation resistance, strength response and accelerated corrosion behaviour of self-compacting lightweight concrete. Construction and Building Materials, 61, pp.10-17.

Felekoğlu, B., Türkel, S. and Baradan, B., 2007. Effect of water/cement ratio on the fresh and hardened properties of self-compacting concrete. Building and Environment, 42(4), pp.1795-1802.

Ferrara, L., Park, Y.D. and Shah, S.P., 2007. A method for mix-design of fiber-reinforced self-compacting concrete. Cement and Concrete Research, 37(6), pp.957-971.

Ghasemi, M., Ghasemi, M.R. and Mousavi, S.R., 2018. Investigating the effects of maximum aggregate size on self-compacting steel fiber reinforced concrete fracture parameters. Construction and Building Materials, 162, pp.674-682.

Ghasemi, M., Ghasemi, M.R. and Mousavi, S.R., 2019. Studying the fracture parameters and size effect of steel fiber-reinforced self-compacting concrete. Construction and Building Materials, 201, pp.447-460.

Giaccio, G. and Zerbino, R., 1998. Failure mechanism of concrete: combined effects of coarse aggregates and strength level. Advanced Cement Based Materials, 7(2), pp.41-48.

González, D.C., Mínguez, J., Vicente, M.A., Cambronero, F. and Aragón, G., 2018. Study of the effect of the fibers' orientation on the post-cracking behavior of steel fiber reinforced concrete from wedge-splitting tests and computed tomography scanning. Construction and Building Materials, 192, pp.110-122.

Grdic, Z.J., Toplicic-Curcic, G.A., Despotovic, I.M. and Ristic, N.S., 2010. Properties of self-compacting concrete prepared with coarse recycled concrete aggregate. Construction and Building Materials, 24(7), pp.1129-1133.

Guan, J., Li, C., Wang, J., Qing, L., Song, Z. and Liu, Z., 2019. Determination of fracture parameter and prediction of structural fracture using various concrete specimen types. Theoretical and Applied Fracture Mechanics, 100, pp.114-127.

Gültekin, A., Beycioğlu, A., Arslan, M.E., Serdar, A.H., Dobiszewska, M. and Ramyar, K., 2022. Fresh Properties and Fracture Energy of Basalt and Glass Fiber–Reinforced Self-Compacting Concrete. Journal of Materials in Civil Engineering, 34(1), p.04021406.

Haach, V.G. and Ramirez, F.C., 2016. Qualitative assessment of concrete by ultrasound tomography. Construction and Building Materials, 119, pp.61-70.

Hu, X., Guan, J., Wang, Y., Keating, A. and Yang, S., 2017. Comparison of boundary and size effect models based on new developments. Engineering Fracture Mechanics, 175, pp.146-167.

Hu, X.Z. and Wittmann, F.H., 1992. Fracture energy and fracture process zone. Materials and Structures, 25(6), pp.319-326.

Huang, Y., Yang, Z., Ren, W., Liu, G. and Zhang, C., 2015. 3D meso-scale fracture modelling and validation of concrete based on in-situ X-ray Computed Tomography images using damage plasticity model. International Journal of Solids and Structures, 67, pp.340-352.

Jenq, Y. and Shah, S.P., 1985. Two parameter fracture model for concrete. Journal of engineering mechanics, 111(10), pp.1227-1241.

Jerjen, I., Poulikakos, L.D., Plamondon, M., Schuetz, P., Luethi, T. and Flisch, A., 2015. Drying of porous asphalt concrete investigated by X-ray computed tomography. Physics Procedia, 69, pp.451-456.

Kanellopoulos, A., Petrou, M.F. and Ioannou, I., 2012. Durability performance of self-compacting concrete. Construction and Building Materials, 37, pp.320-325.

Karamloo, M., Mazloom, M. and Payganeh, G., 2016. Effects of maximum aggregate size on fracture behaviors of self-compacting lightweight concrete. Construction and Building Materials, 123, pp.508-515.

Kazemi, M.T., Golsorkhtabar, H., Beygi, M.H.A. and Gholamitabar, M., 2017. Fracture properties of steel fiber reinforced high strength concrete using work of fracture and size effect methods. Construction and Building Materials, 142, pp.482-489.

Khalilpour, S., BaniAsad, E. and Dehestani, M., 2019. A review on concrete fracture energy and effective parameters. Cement and Concrete research, 120, pp.294-321.

Khaloo, A., Raisi, E.M., Hosseini, P. and Tahsiri, H., 2014. Mechanical performance of self-compacting concrete reinforced with steel fibers. Construction and building materials, 51, pp.179-186.

Klon, J., Sobek, J. and Veselý, V., 2017. Spatial Modeling of Wedge-Splitting Test on Cylindrical Specimens Using FEM Software. Procedia engineering, 190, 427-432.

Korte, S., Boel, V., De Corte, W. and De Schutter, G., 2014. Static and fatigue fracture mechanics properties of self-compacting concrete using three-point bending tests and wedge-splitting tests. Construction and Building Materials, 57, pp.1-8.

Linsbauer, H.N. and Tschegg, E.K., 1986. Fracture energy determination of concrete with cube-shaped specimens. Zement und Beton, 31(1), pp.38-40.

Loeffler, C.M., Qiu, Y., Martin, B., Heard, W., Williams, B. and Nie, X., 2018. Detection and segmentation of mechanical damage in concrete with X-Ray microtomography. Materials Characterization, 142, pp.515-522.

Löfgren, I., 2004. The wedge splitting test a test method for assessment of fracture parameters of FRC?. In Fracture Mechanics of Concrete Structures, Vol 2. Proceedings of the fifth international conference on fracture mechanics of concrete and concrete structures. In Vail, Colorado/USA/12-16 April 2004 (Vol. 2, pp. 1155-1162).

Löfgren, I., 2005. Fibre-reinforced Concrete for Industrial Construction-a fracture mechanics approach to material testing and structural analysis. Chalmers University of Technology.

Löfgren, I., Stang, H. and Olesen, J.F., 2005. Fracture properties of FRC determined through inverse analysis of wedge splitting and three-point bending tests. Journal of Advanced Concrete Technology, 3(3), pp.423-434.

Lublóy, É., Balázs, G.L., Kapitány, K. and Barsi, Á., 2017. CT analysis of core samples from fire-damaged concrete structures. Magazine of concrete research, 69(15), pp.802-810.

Madandoust, R., Ranjbar, M.M., Ghavidel, R. and Shahabi, S.F., 2015. Assessment of factors influencing mechanical properties of steel fiber reinforced self-compacting concrete. Materials & Design, 83, pp.284-294.

Magbool, H.M. and Zeyad, A.M., 2021. The effect of various steel fibers and volcanic pumice powder on fracture characteristics of Self-Compacting concrete. Construction and Building Materials, 312, p.125444.

Morgan, I.L., Ellinger, H., Klinksiek, R. and Thompson, J.N., 1980, January. Examination of concrete by computerized tomography. In Journal Proceedings (Vol. 77, No. 1, pp. 23-27).

Nallathambi, P. and Karihaloo, B.L., 1986. Determination of specimen-size independent fracture toughness of plain concrete. Magazine of Concrete Research, 38(135), pp.67-76.

Nikbin, I.M., Beygi, M.H.A., Kazemi, M.T., Amiri, J.V., Rahmani, E., Rabbanifar, S. and Eslami, M., 2014. Effect of coarse aggregate volume on fracture behavior of self compacting concrete. Construction and Building Materials, 52, pp.137-145.

NT Build 511 2005 'North Test BUILD 511 - Wedge splitting test method (WST): Fracture testing of fiber-reinforced concrete (Mode I)', Nord. METHOD. Oslo, Norway: Nordic Innovation Centre, 04032, 1–6.

Okamura, H. and Ouchi, M. 2003 'Self-Compacting Concrete', Journal of Advanced Concrete Technology, 1(1), 5-15.

Okamura, H. and Ozawa, K., 1994. Mix design method for self-compactable concrete. Doboku Gakkai Ronbunshu , 1994 (496), pp.1-8.

Østergaard, L., Lange, D. and Stang, H., 2004. Early-age stress–crack opening relationships for high performance concrete. Cement and Concrete Composites, 26(5), pp.563-572.

Pająk, M. and Ponikiewski, T., 2013. Flexural behavior of self-compacting concrete reinforced with different types of steel fibers. Construction and Building Materials, 47, pp.397-408.

Ponikiewski, T., Katzer, J., Bugdol, M. and Rudzki, M., 2015. X-ray computed tomography harnessed to determine 3D spacing of steel fibres in self compacting concrete (SCC) slabs. Construction and Building Materials, 74, 102-108.

Que, N.S. and Tin-Loi, F., 2002. Numerical evaluation of cohesive fracture parameters from a wedge splitting test. Engineering Fracture Mechanics, 69(11), 1269-1286.

Ramaswamy, K.P. and Santhanam, M., 2018. A study of deterioration of cement paste due to acid attack using X-ray computed micro-tomography. Advances in Cement Research, 30(3), pp.123-138.

Recommendations, R.D., 1985 50-FMC committee fracture mechanics of concrete. Materials and structures, 18(106), 285-290.

Rozière, E., Granger, S., Turcry, P. and Loukili, A., 2007. Influence of paste volume on shrinkage cracking and fracture properties of self-compacting concrete. Cement and concrete composites, 29(8), pp.626-636.

Shah, S.P., 1990. Size-effect method for determining fracture energy and process zone size of concrete. Materials and Structures, 23(6), pp.461-465.

Shah, S.P., 1997. An overview of the fracture mechanics of concrete. Cement, concrete and aggregates, 19(2), pp.79-86.

Siregar, A.P.N., Rafiq, M.I. and Mulheron, M., 2017. Experimental investigation of the effects of aggregate size distribution on the fracture behaviour of high strength concrete. Construction and Building Materials, 150, pp.252-259.

Sitek, M., Adamczewski, G., Szyszko, M., Migacz, B., Tutka, P. and Natorff, M., 2014. Numerical simulations of a wedge splitting test for high-strength concrete. Procedia Engineering, 91, 99-104.

Skarżyński, Ł., Marzec, I. and Tejchman-Konarzewski, A., 2019. Fracture evolution in concrete compressive fatigue experiments based on X-ray micro-CT images. International Journal of Fatigue, 122, pp.256-272.

Sonebi, M. and Bartos, P.J., 2002. Filling ability and plastic settlement of self-compacting concrete. Materials and structures, 35(8), pp.462-469.

Su, N., Hsu, K.C. and Chai, H.W., 2001. A simple mix design method for self-compacting concrete. Cement and concrete research, 31(12), pp.1799-1807.

Sucharda, O., Pajak, M., Ponikiewski, T. and Konecny, P., 2017. Identification of mechanical and fracture properties of self-compacting concrete beams with different types of steel fibres using inverse analysis. Construction and Building Materials, 138, 263-275.

Suzuki, T., Ogata, H., Takada, R., Aoki, M. and Ohtsu, M., 2010. Use of acoustic emission and X-ray computed tomography for damage evaluation of freeze-thawed concrete. Construction and Building Materials, 24(12), pp.2347-2352.

Tasdemir, M.A. and Karihaloo, B.L., 2001. Effect of aggregate volume fraction on the fracture parameters of concrete: a meso-mechanical approach. Magazine of Concrete Research, 53(6), pp.405-415.

Uysal, M. and Sumer, M., 2011. Performance of self-compacting concrete containing different mineral admixtures. Construction and Building materials, 25(11), pp.4112-4120.

Uysal, M. and Yilmaz, K., 2011. Effect of mineral admixtures on properties of self-compacting concrete. Cement and Concrete Composites, 33(7), pp.771-776.

Vicente, M.A., Mínguez, J. and González, D.C., (2019). Computed tomography scanning of the internal microstructure, crack mechanisms, and structural behavior of fiber-reinforced concrete under static and cyclic bending tests. International Journal of Fatigue, 121, 9-19.

Xiao, J., Schneider, H., Dönnecke, C. and König, G., 2004. Wedge splitting test on fracture behaviour of ultra high strength concrete. Construction and Building Materials, 18(6), pp.359-365.

Xu S, Reinhardt HW 1999 Determination of double-K criterion for crack propagation in quasi-brittle materials, part I: Experimental investigation of crack propagation. Int J Fract 98: 111–149.

Xu, S. and Zhang, X., 2008. Determination of fracture parameters for crack propagation in concrete using an energy approach. Engineering Fracture Mechanics, 75(15), pp.4292-4308.

Yang, S., Cui, H. and Poon, C.S., 2018. Assessment of in-situ alkali-silica reaction (ASR) development of glass aggregate concrete prepared with dry-mix and conventional wet-mix methods by X-ray computed micro-tomography. Cement and Concrete Composites, 90, 266-276.

Yang, Z., Ren, W., Sharma, R., McDonald, S., Mostafavi, M., Vertyagina, Y. and Marrow, T.J., 2017. In-situ X-ray computed tomography characterisation of 3D fracture evolution and image-based numerical homogenisation of concrete. Cement and Concrete Composites, 75, pp.74-83.

Yehia, S., Douba, A., Abdullahi, O. and Farrag, S., 2016. Mechanical and durability evaluation of fiber-reinforced self-compacting concrete. Construction and Building Materials, 121, pp.120-133.

Yu, Q., Le, J.L., Hoover, C.G. and Bažant, Z.P., 2010. Problems with Hu-Duan boundary effect model and its comparison to size-shape effect law for quasi-brittle fracture. Journal of engineering mechanics, 136(1), pp.40-50.

Yu, Q., Liu, H., Yang, T. and Liu, H., 2018. 3D numerical study on fracture process of concrete with different ITZ properties using X-ray computerized tomography. International Journal of Solids and Structures, 147, pp.204-222.

Yun, T.S., Kim, K.Y., Choo, J. and Kang, D.H., 2012. Quantifying the distribution of paste-void spacing of hardened cement paste using X-ray computed tomography. Materials characterization, 73, pp.137-143.

Zhang, J., Leung, C.K. and Xu, S., 2010. Evaluation of fracture parameters of concrete from bending test using inverse analysis approach. Materials and structures, 43(6), pp.857-874.

List of Standard Codes

ASTM C494 / C494M, 2016. Standard Specification for Chemical Admixtures for Concrete, ASTM International, West Conshohocken, PA, 2017, www.astm.org

IS: 12269-2013 specifications for 53 grade ordinary portland cement, Bureau of Indian Standards, New Delhi, India.

IS: 3812-2013 Specification for Pulverized Fuel Ash- part 1: for use as pozzolana in cement, cement mortar and concrete, Bureau of Indian Standards, New Delhi, India.

IS: 383-2016 Specification for coarse and fine aggregates from natural sources for concrete, Bureau of Indian Standards, New Delhi, India.

IS: 516-2013 Indian Standard Methods of Tests for Strength of Concrete, Bureau of Indian Standards, New Delhi, India.

IS: 5816-1999 Splitting Tensile Strength of Concrete - Method of Test, Bureau of Indian Standards, New Delhi, India.

IS: 2386 (Part-I to Part-VI)-1997, Method of test for Aggregates for Concrete, Bureau of Indian Standards, New Delhi, India.

PUBLICATIONS RELATED TO THE WORK

Journals

1. Raja Rajeshwari, B. Sivakumar, M.V.N. and Praneeth, P.H., "Visualization and quantification of aggregate and fiber in self-compacting concrete using computed tomography for wedge splitting test", ***Archives of Civil and Mechanical Engineering***, 2020, 20(4): 1-16. **(SCI)**
2. Raja Rajeshwari, B. and Sivakumar, M.V.N., "Influence of coarse aggregate properties on specific fracture energy of steel fiber reinforced self compacting concrete", ***Advances in concrete construction,*** 2020, *9*(2), 173-181. **(SCI)**
3. Raja Rajeshwari B, Sivakumar M.V.N, "Studies on effect of steel fiber and coarse aggregate on fracture properties of self compacting concrete using wedge splitting test", ***International Journal of Structural Integrity***, 2019, 11(6): 751-767. **(Scopus)**

Conferences

1. Raja Rajeshwari B, Sivakumar M.V.N, "A study on the fracture behaviour of fiber reinforced self compacting concrete using wedge split test", ***Structural Engineering Convention 2018***, 19^{th} – 21^{st} December 2018, Jadavpur University, page 38-43.
2. B Raja Rajeshwari, M.V.N Sivakumar, "Influence of Coarse Aggregate Size on Fracture Properties of Fibre Reinforced Self Compacting Concrete Using Wedge Split Test" The 2018 ***Structures Congress*** (Structures18) Songdo Convensia, Incheon, Korea, August 27 - 31, 2018, available on http://i-asem.org/structures18_publication.html.

APPENDIX – I

Nan Su Method of Mix Design

Max. Size of Aggregate		20.00	mm
Specific Gravity of C.A		2.80	
Bulk Density of C.A		1.49	g/cm^3
Specific Gravity of F.A		2.65	
Bulk Density of F.A		1.45	g/cm^3
Specific Gravity of Cement		3.10	
Specific Gravity of Fly Ash		2.11	
% Volume of F.A		50.00	
% Volume of C.A		50.00	
Specific Gravity of SP		1.10	
Packing Factor (Nan-Su, 2001)		1.063	
Water Cement Ratio(W/C)		0.35	
Water/Fly Ash(W/F)		0.45	
Step 1	**Determination of C.A & F.A content**		
	Weight of sand (W_s)=1450 x 1.063 x 0.50	771	kg/m^3
	Weight of coarse aggregate (W_a) =1450x 1.063 x 0.50	800	kg/m^3
Step 2	**Determination of Cement**		
	Weight of cement (W_c)= 70/0.14= 500	450.00	kg/m^3
Step 3	Determination of Water required		
	Weight of water (W_w)=0.4 x 450.00=180	190	kg/m^3
Step 4	**Determination of Fly Ash**		
	V_{pf} = 1 – [(771 / 1000 x 2.80) + (800 / 1000 x 2.65) + (450.00 / 1000 x 3.10) +(190 / 1000 x 1) + 0.01]	0.078	m^3
	Fly ash content W_f=[0.078 x 1000 x 2.11] / [(1+0.5) x 1.0]=109.97	150	kg/m^3
Step 5	**Determination of S.P dosage**		
	W_{sp}=0.008x(450.00+150.00) =4.8	4.6	kg/m^3

Nan Su Method of Mix Design

Max. Size of Aggregate		20.00	mm
Specific Gravity of C.A		2.80	
Bulk Density of C.A		1.46	g/cm^3
Specific Gravity of F.A		2.65	
Bulk Density of F.A		1.41	g/cm^3
Specific Gravity of Cement		3.10	
Specific Gravity of Fly Ash		2.11	
% Volume of F.A		55.00	
% Volume of C.A		45.00	
Specific Gravity of SP		1.10	
Packing Factor (Nan-Su, 2001)		1.08	
Water Cement Ratio(W/C)		0.35	
Water/Fly Ash(W/F)		0.45	
Step 1	**Determination of C.A & F.A content**		
	Weight of sand (W_s)=1410 x 1.08 x 0.55=837.54	835	kg/m^3
	Weight of coarse aggregate (W_a) =1460x 1.08 x 0.45	710	kg/m^3
Step 2	**Determination of Cement**		
	Weight of cement (W_c)= 70/0.14= 500	450.00	kg/m^3
Step 3	Determination of Water required		
	Weight of water (W_w)=0.4 x 450.00=180	190	kg/m^3
Step 4	**Determination of Fly Ash**		
	V_{pf} = 1 – [(835 / 1000 x 2.80) + (710 / 1000 x 2.65) + (450.00 / 1000 x 3.10) +(190 / 1000 x 1) + 0.01]	0.088	m^3
	Fly ash content W_f=[0.088 x 1000 x 2.11] / [(1+0.5) x 1.0]=123.78	150	kg/m^3
Step 5	**Determination of S.P dosage**		
	W_{sp}=0.008x(450.00+150.00) =4.8	4.6	kg/m^3

Nan Su Method of Mix Design

Max. Size of Aggregate		20.00	mm
Specific Gravity of C.A		2.80	
Bulk Density of C.A		1.43	g/cm^3
Specific Gravity of F.A		2.65	
Bulk Density of F.A		1.42	g/cm^3
Specific Gravity of Cement		3.10	
Specific Gravity of Fly Ash		2.11	
% Volume of F.A		60.00	
% Volume of C.A		40.00	
Specific Gravity of SP		1.10	
Packing Factor (Nan-Su, 2001)		1.11	
Water Cement Ratio(W/C)		0.35	
Water/Fly Ash(W/F)		0.45	
Step 1	**Determination of C.A & F.A content**		
	Weight of sand (W_s)=1420 x 1.11 x 0.60=945.72	945	kg/m^3
	Weight of coarse aggregate (W_a) =1430 x 1.11 x 0.40=634	630	kg/m^3
Step 2	**Determination of Cement**		
	Weight of cement (W_c)= 70/0.14= 500	450.00	kg/m^3
Step 3	Determination of Water required		
	Weight of water (W_w)=0.4 x 450.00=180	190	kg/m^3
Step 4	**Determination of Fly Ash**		
	V_{pf} = 1 – [(945 / 1000 x 2.80) + (630 / 1000 x 2.65) + (450.00 / 1000 x 3.10) +(190 / 1000 x 1) + 0.01]	0.079	m^3
	Fly ash content W_f=[0.079 x 1000 x 2.11] / [(1+0.5) x 1.0]=111.12	150	kg/m^3
Step 5	**Determination of S.P dosage**		
	W_{sp}=0.008x(450.00+150.00) =4.8	4.6	kg/m^3

Nan-Su method of mix design for non fibrous and fibrous self compacting concrete was used to arrive at initial trial mixes but then these mixes were modified accordingly as per EFNARC to achieve optimum mix proportions satisfying the fresh and hardened properties.